UNIVERSITY OF OKLAHOMA

GRADUATE COLLEGE

A SYSTEMATIC UPSCALING APPROACH TO PREDICT PRODUCTION PERFORMANCE OF TIGHT SHALE FORMATIONS

A THESIS

SUBMITTED TO THE GRADUATE FACULTY

in partial fulfillment of the requirements for the

Degree of

MASTER OF SCIENCE

By

WESLEY HERRON
Norman, Oklahoma
2017

A SYSTEMATIC UPSCALING APPROACH TO PREDICT PRODUCTION PERFORMANCE OF TIGHT SHALE FORMATIONS

A THESIS APPROVED FOR THE
MEWBOURNE SCHOOL OF PETROLEUM AND GEOLOGICAL ENGINEERING

BY

_____
Dr. Rouzbeh G. Moghanloo, Chair

_____
Dr. Chandra S. Rai

_____
Dr. Deepak Devegowda

Acknowledgements

I would like to express my sincere gratitude for the patience and dedication of Dr. Moghanloo, without whom this work would not have been possible. I would like to thank Dr. Rai, who has always been there for students in our department, and who helped me not get derailed by the unexpected. I would also like to thank the University of Oklahoma, the resources of which helped every step of the way.

Table of Contents

Acknowledgements iv

List of Tables ix

List of Figures x

List of Function xiii

Abstract xiv

Chapter 1: Introduction 1

The Shale Oil Boom 1

Decline Curve Analysis 2

Current Usage 3

Limitations 3

Limitations of existing models 4

Additional Considerations for more accurate Predictions 5

Minimize the chance of Human Error 5

Overfitting of models 7

Beyond the production itself 8

Thesis Organization 9

Chapter 2: Methodology 11

Simplified Model 11

Modeling Hydrocarbon Dispersion 13

Fourier Series Solution to Diffusion in a heated bar 14

Steady State Solution 14

Transient Solution 15

Bar with both ends kept at 0 degrees 16
Assumptions 21
Formation Compaction 21
Dispersion dominated fluid flow 22
Residual Water Saturation 22
Shared Volume Model 22
Pore size affecting fluid properties 23
Computer Program Workflow 23
The Program Controller 24
The Dispersion Code 25
Known Instabilities and Optimization Targets 27
Chapter 3: Possible Model Variations 29
Polynomial Approximation 29
Capillary Pressure 30
Basic Theory 31
The Approach Itself 32
Potential Cause of Failure 38
Unstimulated Volume Support 39
Cluster Efficacy and Fracture Efficiency 40
Three Dimensional Clusters 41
Time Offset cluster production 42
Initial Gas Saturation 42
Shut-in wells 43

EOR applications 43
Chapter 4: Results and Discussion 45
Full Run 45
Full Output 46
Summary of collection of runs 54
Recovery Factor 57
Sensitivity Analysis 58
Solution Gas Content 58
Timestep Resolution 59
Length Resolution 61
Dispersion Coefficient 63
Dispersion Decline Coefficient 64
Fracture Length 67
Bottom Hole Pressure 68
Total Runtime 70
Advantages of this model 71
Advantages over complex simulations 71
Advantages over Graphical Methods 72
Advantages over Type-Curve Matching 72
Limitations of this model 73
Chapter 5: Conclusion 74
Recommendations and Future Research 74
References 76

Appendix A: Nomenclature 79

Appendix B: Tables 81

Appendix C: Figures 90

Appendix D: Codes 97

List of Tables

Table 1: Shared Values 45

Table 2: Solution Gas Values 45

Table 3: Well Specific Information 45

Table 4: Runtimes 70

Table 5: Example Production data from well M47L6HRJ47 81

List of Figures

Figure 1: Predictions vs Results for drilled wells 6

Figure 2: Simplified Model schematic 11

Figure 3: Reciprocal Rate vs. Cumulative Production graph for Sample Well 10 12

Figure 4: Process Workflow 23

Figure 5: Oil Concentration with in-solution gas Boost vs. Pressure relationship 26

Figure 6: $P_{cap}(S_{oil},P_{oil})$ 34

Figure 7: $C_{gas}(S_{oil},C_{oil})$ 35

Figure 8: $M_{gas}(S_{oil},P_{oil})$ 36

Figure 9: $S_{oil}(C_{gas},C_{oil})$ 37

Figure 10: Sample Well 1's Production, with an initial dispersion start time, following convection dominated flow, that may need to be adjusted on a well by well basis 46

Figure 11: Sample Well 2's Production, with an initial dispersion start time, following convection dominated flow, that may need to be adjusted on a well by well basis 47

Figure 12: Sample Well 3's Production, with an initial dispersion start time, following convection dominated flow, that may need to be adjusted on a well by well basis 47

Figure 13: Sample Well 4's Production, with an initial dispersion start time, following convection dominated flow, that may need to be adjusted on a well by well basis 48

Figure 14: Sample Well 5's Production, with an initial dispersion start time, following convection dominated flow, that may need to be adjusted on a well by well basis 48

Figure 15: Sample Well 6's Production, with an initial dispersion start time, following convection dominated flow, that may need to be adjusted on a well by well basis 49

Figure 16: Sample Well 7's Production, with an initial dispersion start time, following convection dominated flow, that may need to be adjusted on a well by well basis 49
Figure 17: Sample Well 8's Production, with an initial dispersion start time, following convection dominated flow, that may need to be adjusted on a well by well basis 50
Figure 18: Sample Well 9's Production, with an initial dispersion start time, following convection dominated flow, that may need to be adjusted on a well by well basis 50
Figure 19: Sample Well 10's Production, with an initial dispersion start time, following convection dominated flow, that may need to be adjusted on a well by well basis 51
Figure 20: Sample Well 10 Oil Concentration over time 52
Figure 21: Sample Well 10 Oil Pressure over time 53
Figure 22: Sample Well 10 Gas Concentration over time 54
Figure 23: Permeability vs. Dispersion 55
Figure 24: Viscous Flow production dominates at higher permeability values 56
Figure 25: Dispersion Coefficients across the 10 sample well area 57
Figure 26: Sensitivity to increased Gas Content 58
Figure 27: Sensitivity to decreased Gas Content 59
Figure 28: Sensitivity to shorter timesteps 60
Figure 29: Sensitivity to longer timesteps 60
Figure 30: Sensitivity to much longer timesteps 61
Figure 31: Sensitivity to lower length resolution 62
Figure 32: Sensitivity to higher length resolution 62
Figure 33: Sensitivity to higher dispersion coefficient 63
Figure 34: Sensitivity to lower dispersion coefficient 64

Figure 35: Sensitivity to high dispersion exponent 65
Figure 36: Sensitivity to moderate dispersion exponent 65
Figure 37: Sensitivity to moderate negative dispersion exponent 66
Figure 38: Sensitivity to high negative dispersion exponent 66
Figure 39: Sensitivity to smaller fracture length 67
Figure 40: Sensitivity to larger fracture length 68
Figure 41: Sensitivity to lower BHP 68
Figure 42: Sensitivity to higher BHP 69
Figure 43: Sensitivity to much higher BHP 70
Figure C 1: Pore Size Distribution from IC^3 MICP Data 90
Figure C 2: Oil molarity beginning to destabilize 91
Figure C 3: Oil Pressure behaving as expected 91
Figure C 4: Oil Concentration behaving as expected 92
Figure C 5: Reasonable Gas Concentration behavior 92
Figure C 6: Increasingly unstable saturation behavior 93
Figure C 7: Saturation behavior has destabilized molar values entirely 93
Figure C 8: Oil Pressure still behaving perfectly 94
Figure C 9: Oil Concentration still behaving as expected 94
Figure C 10: Gas Concentration behaving as expected 95
Figure C 11: Gas Saturation has destabilized entirely, beyond any reasonable result 95
Figure C 12: Bulk Saving Output 96

List of Function

Function 1: FVF Controller 97

Function 2: FVF of saturated oil 97

Function 3: FVF of unsaturated oil 97

Function 4: Saturated Oil Compressibility 98

Function 5: Z Factor Calculation 98

Function 6: Efficient Function Controller 99

Abstract

This thesis presents a novel method to predict fluid flow in tight shale formations. Conventional Darcy models have proven valuable when working with conventional reservoirs, but cannot reliably relate microscopic dispersion behavior to field-scale production in tight shale formations. The aim of this paper is to provide an analytical method that allows for the effective upscaling of lab-scale results to the field-scale, and provides predictive power when working with additional wells in the same formation. We develop a microscopic mathematical model relating core and formation fluid properties to resulting production curves. The underlying calculations for this new approach are based on the Fourier transform solution of the Heat Conduction Equation. The release of gas from solution, the different rates of dispersion between the gas and liquid phases, and the effects of both on the pressure of the system are considered. An iterative numerical method is used, with the results from the previous time step acting as the initial condition for the current time step's Fourier solution, with boundary conditions being variable as bottom hole pressure data suggests. Underlying equations and assumptions are stated and explained. Results are compared and verified with a previously created macroscopic approach (Moghanloo et al, 2015).

A modeling tool using the above described microscopic method is developed for field applications. Production data from shale oil wells in the Niobrara formation are used to test and validate the simulation results. The advantages and limitations of this model are discussed, as well as the potential for further investigation and improvement.

The advantage of this method is that standard, readily available lab-scale data can be used to predict field production using analytical scaling techniques, allowing for

effective and realistic predictions to be made of well performance, using standard engineering level computer hardware.

Chapter 1: Introduction

The Oil and Gas industry is one of constant innovation, and constant uncertainty. Be it predicting new regulations, the price of oil, or even where the oil is in the first place, the winners and losers in our industry are often decided by the accuracy and precision of our predictions. Even when the regulations have been met, the price is good, the oil is found, and the well is drilled, we're still left with the simple uncertainty of how much oil we'll be able to produce. For nearly a century Decline Curve Analysis, in one form or another, has dominated this field of prediction. But despite the illusion of objectivity, given by decline coefficients and cumulative equations, not to mention precision to several decimal places of accuracy if we so wish, Decline Curve Analysis is little better than eyeballing what you've got, and hoping you know what you'll get. Without the ability to meaningfully ground existing production to laboratory and field data, we're left with little more than hopeful guesswork. What we're looking for in this thesis is a better way of doing things.

The Shale Oil Boom

The United States was once the oil production capital of the world. Yet after nearly a century of production, the US's oil throne was usurped by Saudi Arabia and a new generation of giant fields in the Middle East such as the Ghawar and Ahwaz fields. As the demand for gasoline and oil products continued to increase, and as fewer and fewer new fields were discovered throughout the US, the former king of oil found itself as the largest oil importer in the world, with a declining domestic industry.

Enter Shale. Once thought of as nothing more useful than a caprock for conventional reservoirs, the technological revolutions of horizontal drilling and water

fracturing turned massive formations, once thought of as unproducible, into the backbone of a new wave of domestic production, one significant enough to push the United States back up to accounting for 10% of global production (EIA, 2014). The great decline of US oil had come to an end, and the possibility of not only becoming a net producer, but a net producer of significance, had returned.

Decline Curve Analysis

Decline Curve Analysis began as the method by which future production was empirically or visually predicted using past data, and sometimes the performance of neighboring wells. Throughout time attempts were made to improve on this method, with different equations and declines being used to predict the long-term behavior, and reserves, of a given well. Much of this investigation culminated in the work of Arps (1945), who formalized the process, and cemented the place of hyperbolic and exponential declines in most common methods of decline curve analysis. The process and equations defined by Arps became the gold standard of decline curve analysis for decades to come.

Yet even then, the majority of Arp's work focused on graphical and empirical methods. Decline curve analysis itself remained, at its core, a solely empirical method, without a real basis in our scientific understanding of a reservoir and its behaviors. Eventually, Fektovich (1980) was able to unify decline curve analysis with an understanding of material balance and type curves, and present methods by which, in many cases, a unique and optimal solution could be found using objective methods, rather than the highly subjective graphical or type-curve based methods that had previously dominated the field. Fektovich's work finally grounded Decline Curve

Analysis in a scientific basis, but still depended on a host of assumptions about the characteristics and behaviors of wells, as well as simplifications to ensure the validity of the related models and comparisons.

Current Usage

To this day Decline Curve Analysis remains one of the most consistently used method of predicting production performance and ultimate reserves. Even with the advances made by Fektovich and many others towards a more consistent and objective approach to Decline Curve Analysis, actual implementation is often incomplete or incorrect, with modern methods mirroring those of engineers more than a half century ago, only with newer and faster computers to handle the calculations. A well's production may be viewed independently of its neighbors, missing out on valuable information, or real-world well behavior may be misunderstood or ignored, resulting in forecasts that don't properly take into account the diverse factors that may affect an individual well's behavior (Purvis, 2016).

Limitations

Wells regularly experience "unexpected" interruptions for which neither Arps nor Fektovich's models are well suited to handle. With Arp's model being primarily a graphical method, wells with interrupted production or that are experiencing changing conditions, such as due to nearby waterflooding, cannot be updated or tweaked to correct for changing circumstances in a consistent fashion. Even Fektovich's improvements still rely on a whole host of simplifications and assumptions, and result in a model that is not prepared to deal with interruptions or changes in production or wellbore characteristics.

Limitations of existing models

Over the decades a host of different models have been developed in order to predict the performance of oil and gas wells. Some the earliest of these were the decline and type curves developed by Arps (1945), which suffered from the basic issues of being graphical methods without a strong basis in scientific reality. But with rapid improvements in computing power have come new innovations with regards to models requiring mountains of calculations that far exceeded reason before modern computing. Models with thousands of gridblocks and hundreds or thousands of timesteps have now become a common part of many companies attempts to understand their assets. Each of these models, despite their improvements on previous iterations or methods, come with their own limitations or issues.

Modern graphical methods are the simplest example of this, where wells no longer need to be manually fit to a type-curve, but can be automatically fit using a number of different approaches (Kanfar and Wattenbarger, 2012). This approach has many advantages, namely its speed and the minimal amount of well information required, and the introduction of computers and standardized models certainly limits both the time requirements and subjectivity of this approach, yet it is still essentially an empirical method, and it can't automatically respond to known changes in reservoir behavior. Some modern versions of what are still essentially graphical models can even account for their own uncertainty ranges (Rotondi et al., 2006).

Other models use vast arrays of gridblocks, sophisticated numerical modeling, and sizeable amounts of computing time (Wang et al., 1993), but are still limited by their inability to gather enough input data, or to meaningfully take into account existing

production. Even when values of a sort are present, many models do not meaningfully quantify their own uncertainty, leaving the user unsure of how sensitive the program might be to their different inputs, which each have their own ranges of certainty. More recent research has attempted to mitigate some of these issues, and to quantify the uncertainty resulting from 3D modeling (Yemez et al., 2014). Still other models attempt to incorporate the best of both worlds, taking into account existing production data and using it to supplement 3D information to form more comprehensive gridblock based models, all the while taking into account uncertainties inherent in their information (Portellaand and Prais, 1999).

The model presented in this thesis cannot hope to account so thoroughly for spatial differences and for all the precise heterogeneity that some 3D models are capable of. Nor is it quite as fast as a simple matching program. But by attempting to take into account key reservoir and fluid parameters, while also not performing a full 3D analysis, this model can hopefully make sizeable improvements on the accuracy and scientific grounding of production matching methods, while improving significantly on the speed of standard gridblock based models.

Additional Considerations for more accurate Predictions

It is important to understand that even models that are based on sound science can easily be used to produce inaccurate predictions. These different biases and mistakes need to be understood in order for their effects to be minimized or prevented entirely.

Minimize the chance of Human Error

It is said that many skills are more art than science. While there certainly seems to be a case for this when interpreting geological data, it has become clear that

production forecasting can generally benefit from a bit more science. Despite the importance of production forecasts, which affect not just our understanding of the economic viability of an individual well, but also long-term company decision making, a company's ability to meet contract requirements, and our reputation as engineers, production forecasts regularly overshoot the actual performance of a well (Boomer, 1995). It should be noted that almost any analysis of the quality of well production predictions in practical applications will likely be similar to Boomer's results in 1995, as shown below:

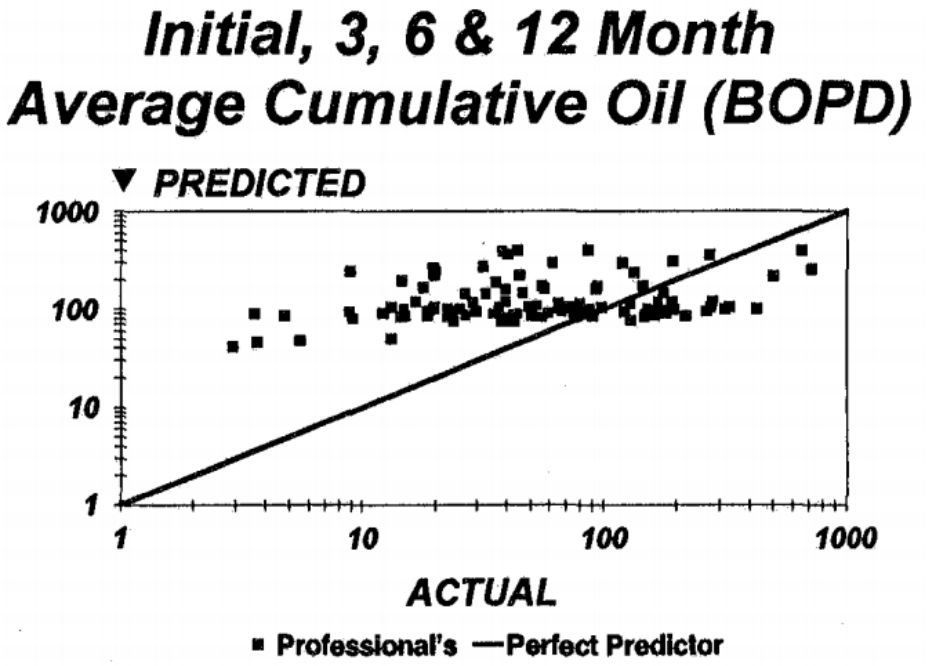

Figure 1: Predictions vs Results for drilled wells

These results are seen throughout the industry, as wells whose production is overpredicted are drilled, while those that are underpredicted are not, so their "actual" production is never found. As such solving this issue, the issue of poor production prediction, is not simply one of assuming our wells won't produce as much as we think they will, which would be a reasonable solution if we were simply overpredicting. The

solution instead is that we must improve the accuracy of our predictions, as the wells that we overpredict cost us money, and the wells we under predict cost us opportunity.

Causes of this are as diverse as our capacity for making mistakes. From unconscious over-optimism about a project's potential, to pressure from management to produce exciting prospects, to losing sight of variables that affected the performance of previous wells, production forecasting often suffers from a host of oft-repeated mistakes and errors (Rajvanshi et al, 2012). To minimize these mistakes, and to apply a level of consistency that will make identifying errors easier, we must minimize human interaction with production forecasting.

There will always be intricacies that cannot be easily pre-programmed into a model. Be it allocation errors in the production data of neighboring wells, or downtime, or changes in geology, or changes in our understanding of the reservoir, there will always be a need for someone to keep an eye on things and apply changes where necessary. These changes need to be standardized and quantified whenever possible. By making use of production models, like the one proposed here, we can do away with personal fudge factors, and begin working with more controlled methods that can be improved over time as our understanding of our models and the physical realities that we're working with improves.

Overfitting of models

The concept of overfitting generally pertains to statistical models, but is a relevant concern in any situation where a collection of input parameters is being used to predict or correlate with some outcome. In the case of production models such as the one discussed in this thesis, there are a whole host of variables and parameters that can act

as inputs or assumptions for the model. Every additional factor that is taken into account can improve a match, which makes considering additional parameters tempting. Yet in cases where additional parameters take the form of assumed values that are determined primarily by whether they improve the quality of a match, overfitting is almost guaranteed. Each additional factor will improve the match with the given data, while often providing no meaningful predictive power, and possibly sabotaging what may have actually been a more accurate model when less parameters were included (Cook and Ranstam, 2016).

Beyond the production itself

Any discussion of production prediction needs to also consider the real world limitations that surround the production of hydrocarbons. Even a model that could perfectly predict the production capabilities of a well won't prevent a project from underperforming those predictions if additional factors are not considered.

Beyond the human bias that often directly affects the production forecast itself, production forecasts, which should be representing the production potential of a well, are often taken to represent the actual, realistic production of that well. The implicit assumption here is that no downtime, slipups, or execution errors of any kind will occur, an assumption that regularly proves itself to be a poor one. Therefore any model, such as the one presented here, must be understood as the performance of a well under ideal circumstances. There should be a number of a wells in a field that perform at the level predicted by the model, if the drilling, completion, and production of those wells are executed perfectly.

However, the chance of slipups during any of those operations, as well as the production or economic ramifications of those mistakes must be considered in any model that seeks to accurately predict the average production of new wells. Therefore, it is recommended that any program outputs be tempered with data on the success rate of different well operations, so that the resulting economic predictions are as accurate as possible. Fortunately, due to the speed of the program presented in this thesis, sensitivity analysis can be performed in a relatively short period of time, allowing for the multiple possible scenarios to be run on each individual well, or type of wells, without significant computing costs.

Thesis Organization

This thesis was designed in such a manner as to try to walk the reader through the intent, approach, and results of this research in a clear, logical manner. So far we have already explored the background of production prediction, as well as discussed the necessity of more consistent methods that have a strong grounding in the physical, and ideally measurable, world. The following chapters seek to clarify what was done, what limitations exist in the model's predictive power, the methods that were employed, and what steps need to be taken to further the research or to implement it in a working scenario.

- Chapter 2 discusses methodology of the model generated during the course of this research, the mathematics underlying that model, as well as many of the assumptions used. There is also a discussion of the structure of the MATLAB program that runs the model.

- Chapter 3 discusses a number of model variations. As discussed previously in this introduction, overfitting is a serious concern when generating models that are meant to have predictive power, especially when real data is limited, but potential factors and adjustable terms are numerous. The model variations discussed in Chapter 3 could significantly improve the accuracy of the model, if reliable, well-specific data is available, but are essentially an exercise in overfitting without it.
- Chapter 4 discusses the results of the research and includes a sensitivity analysis of many of the programs options. It also discusses some of the advantages of the model when compared to other approaches at predicting production.
- Chapter 5 includes the primary conclusions of this thesis, as well as recommendations for future research.

Chapter 2: Methodology

Simplified Model

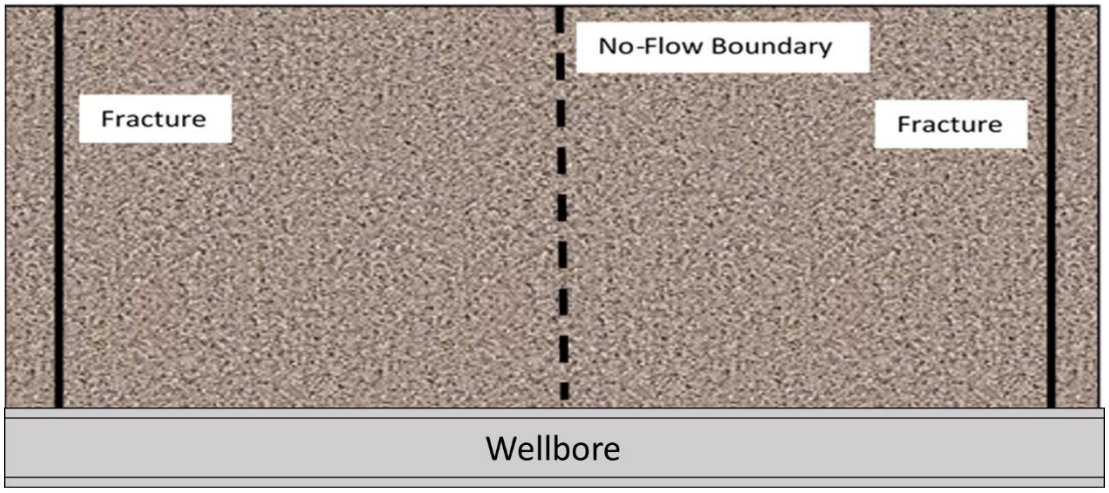

Figure 2: Simplified Model schematic

Our model focuses on the volume between two identical, perfectly thin, circular fractures in a homogenous section of a fractured shale reservoir. The left and right fractures, acting as our boundaries, are assumed to have infinite conductivity. The No-Flow Boundary is defined as the point of symmetry between the two fractures, across which no flow or transfer occurs. The No-Flow Boundary is assumed to be a flat surface, equidistant from and parallel to the two fractures.

Our model begins with initial reservoir conditions existing between the two fractures. As the fractures are produced and reach a pseudo-steady state, the reservoir matrix experiences a concentration drawdown at its boundaries, which are assumed to maintain a specific oil and gas concentration resulting from fluid properties and the well's specific BHP. This concentration drawdown becomes the primary driver of production after initial fracture production has ended.

If adequate BHP data is available, the matrix contribution towards production can be found from the first day of production. In that case, initial matrix production volumes would be quite small, as during the early days of production the well would be producing primarily from the fractures. Initial and early production is viscous flow dominated, and while the reservoir matrix would be contributing to this early production, the contribution would be minimal. Once the hydraulic fractures reach a pseudo-steady state, after a duration of two hundred days or so, varying from well to well, the matrix contribution to production becomes dominant, and should begin matching existing production values. The onset of pseudo-steady state in the fractures can be approximated by observing the change in behavior of the well's production on a reciprocal rate vs. cumulative graph, as shown below.

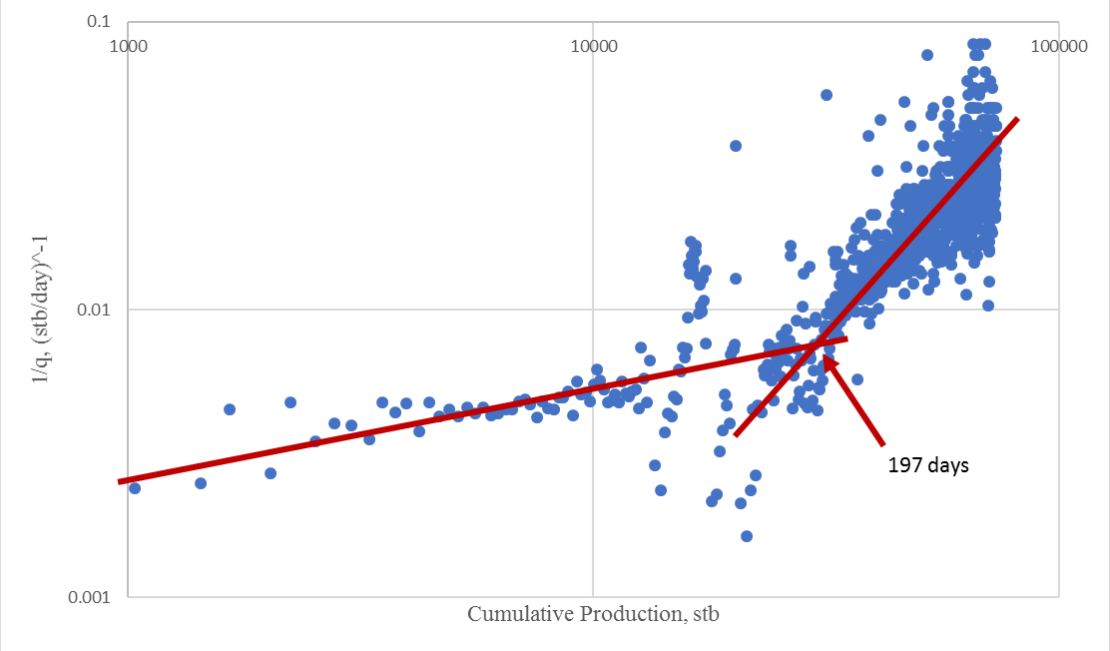

Figure 3: Reciprocal Rate vs. Cumulative Production graph for Sample Well 10

The BHP data available for this thesis was calculated using production data. The resulting BHP's were below 1000psi from the first day of production, for each of the ten

test wells. While completely unreasonable, these were the values that were available, and as such are the ones that have been used throughout the results and sensitivity analysis sections.

Modeling Hydrocarbon Dispersion

Dispersion, for the purposes of this thesis, is defined as the rate at which a substance disperses, encapsulating the effects of permeability, as well as other effects on fluid flow such as diffusion, while not taking the form of a conventional convection based mass-transport (Warren and Skiba, 1964). In particular numerous papers have explored the ways in which Darcy flow assumptions no longer hold in nanoscale pores, underestimating actual production behavior by a significant margin (Wang and Marongiu-Porcu, 2015). Factors such as diffusion, Knudsen number, gas pressure, and a long list of others have all been been explored, and all limit the applicability of the Darcy flow equation at this scale (Swami et al., 2012). In this thesis the Dispersion Coefficient "D" is assumed to encapsulate the majority of these effects, with the remaining effects being minor enough to not drastically affect results.

The dispersion coefficient "D" is related to diffusivity and convection based flow by the following equation:

$$D = \frac{D_{diff}}{\tau} + \frac{D_{disp} u^{1.2}}{\varphi S} \qquad \text{eqn. 1}$$

At higher permeability values the second term dominates fluid flow, allowing Darcy flow to adequately explain production, but at lower permeability values, such as those in the nano-Darcy range, the first term becomes significant enough that it must be taken into account to accurately predict production (Lake, 1989),

The dispersion of hydrocarbons is modeled using a variation of the Heat Diffusion equation "$\alpha u_{xx} = u_t$", which is commonly used to describe the temperature change of a thin rod with both ends kept at arbitrary temperatures. For a given timestep the dispersion of the oil and gas are assumed to be constant and uniform, with the dispersion of the gas set to five times that of the oil. Across timesteps the solution to the diffusion equation is re-solved with the new initial and boundary conditions, allowing for changes in boundary conditions, changes in dispersion of the oil and gas phases, and for simulating equilibrium between the two phases.

It is assumed that at initial reservoir conditions the reservoir is fully saturated with oil, and that the oil is fully saturated with in-solution gas. As the concentration of oil drops each timestep, its pressure is recalculated and gas is released from solution and begins dispersing.

Fourier Series Solution to Diffusion in a heated bar

For the case of a metal bar with two ends kept at arbitrary temperatures, the solution can be found by employing the Fourier Series Solution, which takes the form of a steady state solution $v(x)$, which describes the solution without respect to time, as well as a transient solution $w(x,t)$, which incorporates the effects of time.

Steady State Solution

Differential Equation**:**

$\alpha u_{xx} = u_t$ with $0 < x < L$ and $t > 0$ eqn. 2

Boundary Conditions:

$\mathrm{u}(0,t) = T_1$ and $u(L,t) = T_2$ eqn. 3

Initial Condition:

$$u(x,0) = f(x)$$ eqn. 4

To begin the problem, we will break the final solution into two parts, the steady state $v(x)$ and transient $w(x,t)$ solutions:

$$u(x,t) = w(x,t) + v(x)$$ eqn. 5

The steady state solution $v(x)$ is not a function of time, therefore using the heat conduction equation we note that,

$$\alpha v_{xx} = 0$$ eqn. 6

The solution of which can be quickly found using integration with respect to x to be:

$$v(x) = Ax + B$$ eqn. 7

By rewriting the boundary conditions using v we find that:

$$u(0,t) = v(0) = A\times 0 + B = B$$ eqn. 8

$$u(L,t) = v(L) = A\times L + B$$ eqn. 9

The first of which implies that $B = T_1$ which can then be used with the second equation to show that $A = \frac{T_2 - T_1}{L}$, which can then be used to show that:

$$v(x) = Ax + B = \frac{T_2 - T_1}{L}x + T_1$$ eqn. 10

Transient Solution

For the transient solution, recall that our final solution $u(x,t) = v(x) + w(x,t)$ will describe the entirety of the model, including the boundaries, and as such the boundaries can be rewritten in the form of our steady state and boundary conditions like so:

$$u(0,t) = v(0) + w(0,t) = T_1$$ eqn. 11

$$u(L,t) = v(L) + w(L,t) = T_2$$ eqn. 12

Which tells us that:

$$w(0,t) = T_1 - v(0) \qquad \text{eqn. 13}$$

$$w(L,t) = T_2 - v(L) \qquad \text{eqn. 14}$$

Since our boundary conditions for the transient solution are constants with respect to time and the steady state solution v(x) describes the portion of the final solution that is constant with respect to time by definition, we know that:

$$w(0,t) = 0 = w(L,t) \qquad \text{eqn. 15}$$

Therefore the initial condition $u(x,0) = f(x)$ can be converted to the form:

$$w(x,0) = f(x) - v(x) \qquad \text{eqn. 16}$$

Using the heat conduction equation, eqn. 2, our new boundary conditions eqn. 15, and our new initial condition eqn. 16, we have a simpler problem when solving $w(x,t)$; that of a bar with both ends kept at a temperature of 0.

Bar with both ends kept at 0 degrees

This solution is quite a bit more straightforward. In summary our current problem for solving the transient solution $w(x,t)$ depends on the following conditions:

$$w(0,t) = 0 = w(L,t)$$

$$\alpha w_{xx} = w_t$$

$$w(x,0) = f(x) - v(x)$$

Now we'll apply separation of variables, and assume that the solution takes the form:

$$w(x,t) = \varphi(x)G(t) \qquad \text{eqn. 17}$$

Plugging this into our IC we get:

$$\alpha\varphi_{xx}(x)G(t) = \varphi(x)G_t(t) \qquad \text{eqn. 18}$$

$$w(0,t) = \varphi(0)G(t) = 0 \qquad \text{eqn. 19}$$

$$w(L,t) = \varphi(L)G(t) = 0 \qquad \text{eqn. 20}$$

Noting that $G(t) = 0$ for all t is the trivial solution, we look for a non-trivial solution using the boundary conditions:

$$\varphi(0) = \varphi(L) = 0 \qquad \text{eqn. 21}$$

By reorganizing the IC:

$$\frac{\varphi_{xx}(x)}{\varphi(x)} = \frac{G_t(t)}{\alpha \times G(t)} \qquad \text{eqn. 22}$$

We then note that the left and right sides of the equation must be equal to a constant, since they are dependent on separate variables yet remain equivalent. For ease of notation, we will assume that this constant is "$-\lambda$". From there our two equations can be reorganized to:

$$G_t(t) = -\alpha\lambda G(t) \qquad \text{eqn. 23}$$

And

$$\frac{\varphi_{xx}(x)}{\varphi(x)} + \lambda\varphi(x) = 0 \qquad \text{eqn. 24}$$

Knowing this we can limit our possible solutions for $\varphi(x)$ to three potential scenarios, depending on the value the eigenvalue "λ" takes:

$\boldsymbol{\lambda > 0}$ case

It can be shown (Haberman, 2004) that the eigenfunction in this case takes the form:

$$\varphi(x) = c_1 \cos\left(\sqrt{\lambda}x\right) + c_2 \sin\left(\sqrt{\lambda}x\right) \qquad \text{eqn. 25}$$

And by applying eqn. 21 we find that:

$$\varphi(0) = c_1 \cos\left(\sqrt{\lambda}\times 0\right) + c_2 \sin\left(\sqrt{\lambda}\times 0\right) = 0 \qquad \text{eqn. 26}$$

Which suggests that $\varphi(0) = c_1 \cos\left(\sqrt{\lambda}\times 0\right) = 0$, thus $c_1 = 0$, which tells us that

$$\varphi(L) = 0 * \cos\left(\sqrt{\lambda}\times L\right) + c_2 \sin\left(\sqrt{\lambda}\times L\right) = 0 \qquad \text{eqn. 27}$$

And therefore $\varphi(L) = c_2 \sin(\sqrt{\lambda}\times L) = 0$, meaning that $\sqrt{\lambda}\times L = n\times\pi$ where n is a positive integer. Reassembling this solution we find that:

$$\lambda_n = \left(\frac{n\times\pi}{L}\right)^2, \quad \varphi_n(x) = c_2 \sin\left(\frac{n\times\pi\times x}{L}\right), \quad n = 1,2,3 \ldots \qquad \text{eqn. 28}$$

$\boldsymbol{\lambda < 0}$ *case*

It has been shown (Haberman, 2004) that for negative eigenvalues in our case the solution takes the form:

$$\varphi(x) = c_1 \cosh(\sqrt{-\lambda}\times x) + c_2 \sinh(\sqrt{-\lambda}\times x) \qquad \text{eqn. 29}$$

By applying the boundary condition eqn. 21 we can show that:

$$\varphi(0) = c_1 \cosh(\sqrt{-\lambda}\times 0) + c_2 \sinh(\sqrt{-\lambda}\times 0) = 0 \qquad \text{eqn. 30}$$

therefore $c_1 = 0$, as well as that:

$$\varphi(L) = 0 * \cosh(\sqrt{-\lambda}\times L) + c_2 \sinh(\sqrt{-\lambda}\times L) \qquad \text{eqn. 31}$$

and since we are assuming $\lambda < 0$ for this case,

$$\sinh(\sqrt{-\lambda}\times L) \neq 0 \qquad \text{eqn. 32}$$

So $c_2 = 0$, which is the trivial solution, so the eigenvalue for this problem is not $\lambda < 0$.

$\boldsymbol{\lambda = 0}$ *case*

This solution is fortunately fairly short. It is known (Haberman, 2004) that the solution for this eigenvalue takes the form $\varphi(x) = c_1 + c_2\times x$, and by applying the boundary conditions in eqn. 21 we find that,

$$\varphi(0) = c_1 + c_2\times 0 = 0 \qquad \text{eqn. 33}$$

thus $c_1 = 0$, and that,

$$\varphi(L) = 0 + c_2\times L = 0 \qquad \text{eqn. 34}$$

thus $c_2 = 0$, which is the trivial solution, so $\lambda = 0$ is not an eigenvalue in our case.

Eigenfunction for $\varphi(x)$

As we now know that $\lambda > 0$ and that our eigenvalue takes the form:

$$\lambda_n = \left(\frac{n\times\pi}{L}\right)^2, n = 1,2,3 \ldots \quad \text{eqn. 35}$$

And that our eigenfunction takes the form:

$$\varphi_n(x) = c_2 \sin\left(\frac{n\times\pi\times x}{L}\right), n = 1,2,3 \ldots \quad \text{eqn. 36}$$

Going back to the time equation eqn. 23,

$$G_t(t) = -\alpha\lambda G(t)$$

After noting that the equation is separable, it is fairly easy to find the solution in the exponential form:

$$G(t) = c_1 * \exp(-\alpha\lambda t) \quad \text{eqn. 37}$$

Therefore:

$$w(x,t) = c_2 \sin\left(\frac{n\times\pi\times x}{L}\right) * c_1 * \exp\left(-\alpha\left(\frac{n\times\pi}{L}\right)^2 \times t\right), n = 1,2,3 \ldots \quad \text{eqn. 38}$$

Though it should be noted that the constants vary with each n, and that any linear combination of solutions will themselves be solutions, so the full solution should be written as:

$$w(x,t) = \sum_{n=1}^{\infty} B_n \times \sin\left(\frac{n\times\pi\times x}{L}\right) \times \exp\left(-\alpha\left(\frac{n\times\pi}{L}\right)^2 \times t\right) \quad \text{eqn. 39}$$

Combining the Steady State and Transient Solutions

By combining the steady state solution eqn. 10, and the transient solution eqn. 39, we can solve the initial equation eqn. 5, resulting in our final solution:

$$u(x,t) = \sum_{n=1}^{\infty}\left[B_n \times \sin\left(\frac{n\times\pi\times x}{L}\right)\exp\left(-\alpha\left(\frac{n\times\pi}{L}\right)^2 t\right)\right] + \frac{T_2 - T_1}{L}x + T_1, \quad n = 1,2,3 \ldots \qquad \text{eqn. 40}$$

Using the initial condition eqn. 4 we know that

$$u(x,0) = \sum_{n=1}^{\infty} B_n \times \sin\left(\frac{n\times\pi\times x}{L}\right)\times 1 + \frac{T_2 - T_1}{L}\times x + T_1 = f(x) \qquad \text{eqn. 41}$$

Fourier Sine Series Coefficients

To determine the coefficients B_n we'll want to simplify eqn. 41 to:

$$\sum_{n=1}^{\infty} B_n \times \sin\left(\frac{n\times\pi\times x}{L}\right) = f(x) - \mathrm{v(x)} \qquad \text{eqn. 42}$$

And then multiply both sides of the equation by $\sin\left(\frac{m\times\pi\times x}{L}\right)$, where m is a fixed, arbitrary positive integer, resulting in:

$$\sum_{n=1}^{\infty} B_n \times \sin\left(\frac{n\times\pi\times x}{L}\right)\sin\left(\frac{m\times\pi\times x}{L}\right) = \left(f(x) - \mathrm{v(x)}\right)\times \sin\left(\frac{m\times\pi\times x}{L}\right) \qquad \text{eqn. 43}$$

Then integrate both sides from $x = -L$ to $x = L$ and factor B_n out of the integral:

$$\sum_{n=1}^{\infty} B_n \int_{-L}^{L} \sin\left(\frac{n\times\pi\times x}{L}\right)\times \sin\left(\frac{m\times\pi\times x}{L}\right) dx = \int_{-L}^{L}\left(f(x) - \mathrm{v(x)}\right)\times \sin\left(\frac{m\times\pi\times x}{L}\right) dx \qquad \text{eqn. 44}$$

It has been shown (Haberman, 2004) that $\int_{-L}^{L} \sin\left(\frac{n\times\pi\times x}{L}\right)\times \sin\left(\frac{m\times\pi\times x}{L}\right) dx = \begin{Bmatrix} L \; if \; n = m \\ 0 \; if \; n \neq m \end{Bmatrix}$, therefore for the left side the only integral from the summation that will

not equal 0 occurs when $m = n$, therefore the result of the single non-zero integral throughout the entire infinite summation must be L:

$$B_n L = \int_{-L}^{L} \big(f(x) - \mathrm{v(x)}\big) \times \sin\left(\frac{m \times \pi \times x}{L}\right) dx \qquad \text{eqn. 45}$$

And after dividing both sides by L, and noting that we're integrating by two odd functions, making the integral itself even, we have solved for all the terms of our Fourier Sine series:

$$B_n = \frac{2}{\mathrm{L}} \int_0^L \big(f(x) - \mathrm{v(x)}\big) \times \sin\left(\frac{m \times \pi \times x}{L}\right) dx \quad ,m = 1,2,3 \ldots \qquad \text{eqn. 46}$$

Giving us a final solution, using concentrations C in place of Temperatures T and a dispersion factor "D" instead of the diffusivity constant α, of:

$$u(x,t) = \sum_{n=1}^{\infty} \left[B_n \times \sin\left(\frac{n \times \pi \times x}{L}\right) \exp\left(-D\left(\frac{n \times \pi}{L}\right)^2 t\right)\right] + \frac{C_2 - C_1}{L} x + C_1 \qquad \text{eqn. 47}$$

Where,

$$B_n = \frac{2}{\mathrm{L}} \int_0^L \big(f(x) - \mathrm{v(x)}\big) \times \sin\left(\frac{n \times \pi \times x}{L}\right) dx, \quad n = 1,2,3 \ldots \qquad \text{eqn. 48}$$

Assumptions

Formation Compaction

For the purposes of the model it was assumed that formation compaction occurred at the exact required to maintain a single fluid phase during the entire course of production. No considerations were made for how this compaction would affect dispersion or production. The works of Davudov et al. (2017) and Lan et al. (in press) discuss the effects of formation compressibility throughout the productive life of a shale oil well,

both in terms of the initial improvements to production as well as the long-term conductivity effects of accessible pore closure.

Dispersion dominated fluid flow

We hypothesize that the flow of oil and gas in shale reservoirs is dominated by dispersion, rather than the more traditional flow regimes and convection displayed in conventional reservoirs. Gas and oil flow in fractures is assumed to be essentially instantaneous, with any dispersion into the fractures resulting in immediate production, with the exception of residual concentrations of oil and gas that act as boundary conditions for the dispersion equation, as calculated using the BHP.

Residual Water Saturation

It is assumed that the only water existing in the system is irrevocably bound to the surface of the grains within the formation, and at no point will participate in, or influence, fluid flow within the model. It is assumed that any effects of this residual water saturation are accounted for with the dispersion coefficient "D". Residual water is treated as a uniform decrease in porosity, such that 25% water saturation results in a 25% decrease in porosity. No water production is calculated, and no diffusion of water takes place in this model.

Shared Volume Model

For the purposes of this model gas released from solution at pressures below bubble-point pressure is assumed to be generated uniformly throughout the oil volume, and to disperse following the same model that governs the oil dispersion. It is assumed that no distinct gas saturation develops, and that the gas is perfectly miscible with the oil phase. This assumption is much more reasonable at higher pressures, such as those

above 4,000 psi, and if assuming a gas composition with larger, reasonably high percentages of C_{2+}, such as values in excess of 30% (Rao and Lee, 2003)

Pore size affecting fluid properties

It is understood that at very small pore sizes, such as those common in the sort of reservoirs this model focuses on, that many fluid properties are affected by the pore sizes and pore size distributions (Zhang, 2016). For the sake of simplicity in this model, an idealized case, in which fluid properties mirror their lab values, has been assumed. The Vasquez and Beggs method for calculating FVF has been used throughout the program, and gas is assumed to release from solution fully upon the completion of each timestep. No consideration is given for how the pore size distribution might affect the Dispersivity constant, the FVF calculations, or the release of gas from solution. The FVF is calculated using Function 1, located in the Appendix.

Computer Program Workflow

The general behavior of the model follows the below flowchart:

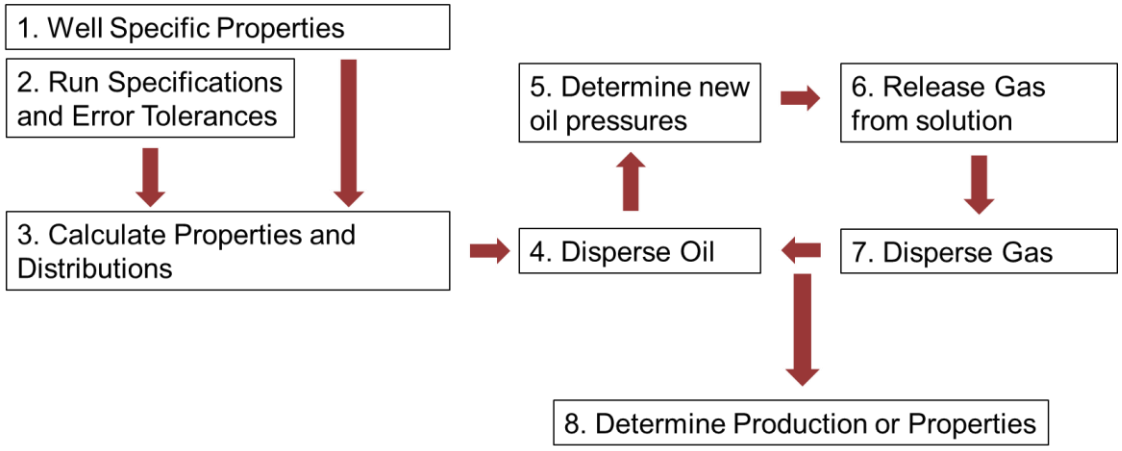

Figure 4: Process Workflow

This process may need to be adjusted or expanded to implement additional or different functionality. The below sections discuss the actual implementation of the process. The

program controller handles the process of iterating through the different collections of inputs and handles program outputs, while the dispersion code itself performs the primary calculations, and can be called any number of times by the controller, depending on the wells and values being tested.

The Program Controller

1. Initiate User Settings and constants

Well or field specific rock and fluid properties, as well as run settings and potential sensitivity analysis values, are defined by the user.

2. Initiate Primary Loop

The Dispersion Code is run with the prescribed settings. A detailed explanation is provided in the following section.

3. Perform Production fit check

Production values resulting from the Dispersion Code are automatically matched to the well's production data. If an efficiency value is provided no scaling will occur, and only an error value will be returned. If no efficiency value is provided, or if an upper and lower bound value are provided, the program will determine the best match between the Dispersion Code's output and the actual production data, accounting for both the oil and gas match simultaneously. An error scaling value can be provided to give additional weight to errors where theoretical production is below actual production, and an initial window of half weighted errors can be provided so that initial decline behavior from the Dispersion Code does not overly influence the matching process.

4. Bulk Saving

In the event of a sensitivity analysis or range of tested values, the production results of each individaul run will be labeled and saved in auto-generated, labeled folders for the well that was run. Once all test values have been run the program will save a file containing all run outputs, as well as scaling values and errors. The filename will indicate which of the runs resulted in the best match, as shown in Figure C 12.

The Dispersion Code

1. Define Run Specifications and calculated values

Additional run specifications are defined, as well as internal constants. Properties are converted to metric units, and property distributions are calculated where relevant.

2. Solve the Dispersion Equation for oil

Following the description of the Dispersion Equation's solution provided on page 21, and using the boundary concentration derived from the bottomhole pressure data provided for the well, dispersion for the oil section occurs.

3. Determine the new oil pressure

Oil pressure is then determined using the new oil concentrations. The calculation is accomplished by interpolating from a Pressure vs. Concentration distribution that was generated by a taking a distribution of pressures, determining the in-solution molar gas content of a given mole of oil, and dividing this "boosted" oil concentration by the volume of the oil at that pressure, which is found using the molar volume of the oil at standard conditions and the oil's FVF (formation volume factor) at the given pressures. The FVF was determined using Vasquez and Beggs correlations for FVF. An example distribution is provided below, with the distribution for a given well depending on its specific fluid properties.

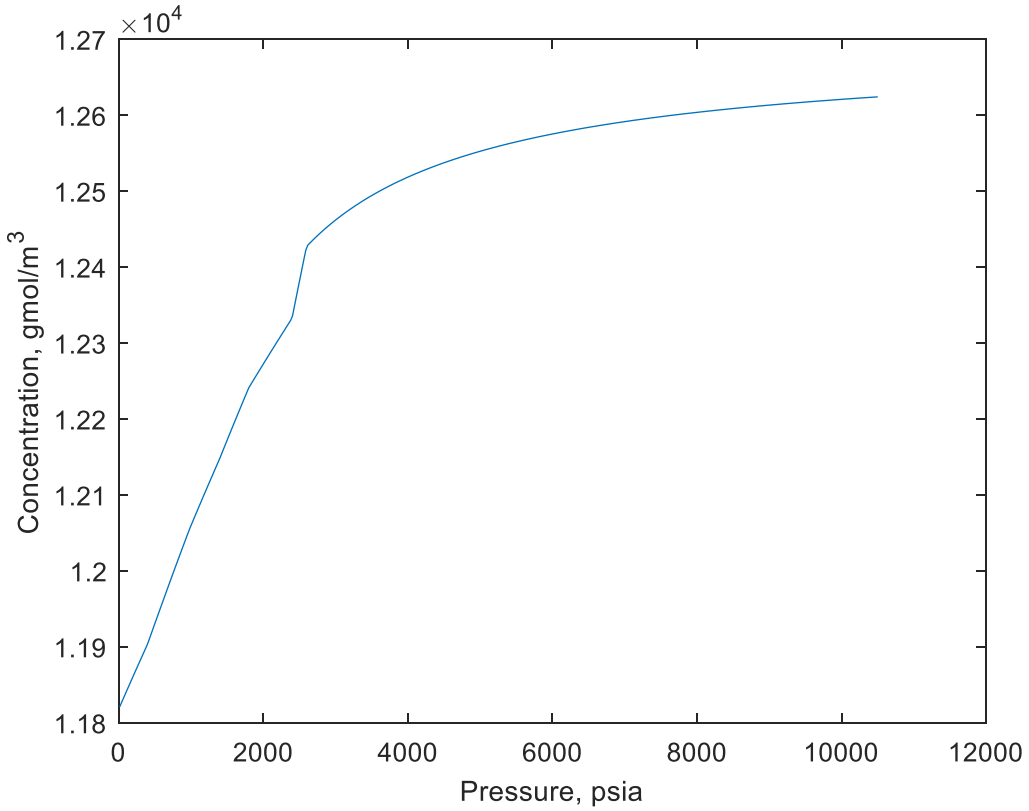

Figure 5: Oil Concentration with in-solution gas Boost vs. Pressure relationship

4. Add released gas to existing, dispersed gas

The pressure drop resulting from concentration drops near the boundary fractures results in gas release from solution found using RS data for the well. This is summed with the gas that has previously been released and experienced dispersion.

5. Disperse the gas concentrations

Using the same algorithm as the one used for the oil concentrations, gas concentrations are dispersed using a dispersion factor five times that of the oil dispersion factor.

6. Determine production

The difference in the integral of the initial and final concentrations for gas and oil give us the amount of gas and oil produced, once we account for the volume of gas that comes out of solution from the oil as it is produced, assuming a dry gas.

7. Convert output values to STB, MSCF, and days

Program calculations are all handled in SI units, notably moles/m^3 for concentrations of oil and gas, and seconds for time. The final step of the Dispersion Code is to convert all related values to surface conditions and to days, for ease of comparison with conventional production data.

Known Instabilities and Optimization Targets

The primary sources of instability in the program are also ideal locations for optimization. The first potential instability is due to the calculation of the integral in eqn. 48 in the dispersion solution. This is done using Simpson's Rule and is the by far the most called function in the program, as it must be run "Approximately Infinity" times, twice every timestep. For a standard run, such as the default with 500 x-values and a dispersion constant of 10^{-6}, this runs just fine. But as the dispersion constant drops orders of magnitude the error inherent in the approximation begins to exceed the amount of dispersion that occurs in an individual timestep by a significant margin, and anomalous behavior begins to occur.

In particular the program has produced dispersion in the wrong direction and several orders of magnitude too large. This problem can always be remedied by increasing the number of x-values, but a linear increase in runtime should be expected, so being able to relate the number of x-values with the dispersion constant would be ideal.

The second primary source of instability is inherent in the Fourier transform method itself, which by definition should involve the summation of an infinite series of sines. Using too few terms results in diffused data that has visible waves, as well as completely inaccurate boundary values, while using too many terms linearly increases

runtimes and becomes meaningless due to rounding error. “Too many” or “too few” depends on the values given to equations eqn. 47 and eqn. 48, as the exponential term in the infinite series will cause additional terms to gradually drop orders of magnitude. By reorganizing the equations that define the additional terms, and setting an upper bound on the value of the last summed term, an optimized value for “Approximate Infinity” can be dynamically calculated with any set of inputs and any arbitrarily chosen accuracy value. For all simulation runs an accuracy, or maximum final term, value of 10^{-20} was used, with the equation shown below:

$$ApproxInfinity = \frac{L}{\pi} \times \sqrt{\frac{ln\left(\frac{MaxError}{2} \times \frac{L}{\int_0^L f(x) - v(x)\,dx}\right)}{-D \times t}} \qquad \text{eqn. 49}$$

It should be noted that changes in the dispersion constant, affecting both the value of approximate infinity as note above, and the required number of x-values through some less explicit relationship, have a rather significant impact on runtimes. In particular order of magnitude decreases in the dispersion constant result in nearly order of magnitude increases in runtimes.

Chapter 3: Possible Model Variations

In the course of this research a large number of alternate methods and improvements were attempted. Many methods were successful, and have been implemented in the final version of the program discussed throughout this thesis. A number of modifications were not successful, and some of those are discussed here.

Polynomial Approximation

In order to bypass the need for an approximate integral function, such as by using Simpson's rule, the instability of which was previously discussed, and to potentially improve runtimes by removing the need for repeated solving of the Dispersion equation, a polynomial approximation approach was attempted. Rather than using a numerical solution to the Dispersion equation using Simpson's Rule to approximate the integral of $f(x)$ using a collection of points, a high order polynomial was used to attempt and approximate all solutions to the Dispersion equation. Using this method the constants to the polynomial approximation, as well as any changed conditions, would act as inputs for a function generated by applying the *matlabFunction* command to the symbolic solution of the Dispersivity equation where all input values had been replaced with symbolic placeholders. This would prevent the need for constant recalculation of the solution, while also providing an integral as accurate as the polynomial approximation itself.

This approach was eventually abandoned. While this method did provide a speed benefit, as the solution could be derived a single time and then reloaded across different simulations, or rerun within the same simulation, it was determined that the polynomial approximation itself ventured between inadequate and unstable. Approximation orders

exceeding 16th order or so displayed increasingly unstable behavior, especially near the boundaries. Approximation orders that displayed a greater deal of stability all suffered from an inability to adequately approximate a straight line, namely the concentrations of the unaffected regions of the reservoir. Especially when dealing with smaller time steps or smaller dispersivity constants the inaccuracies in the approximation became significant when compared to the dispersion occurring during a single timestep, and anomalous results became a regularity. In particular gas or oil concentrations shifting earlier than reasonable, such as before dispersion effects had even reached them, occurred regularly. Smoothing functions, manual corrections of unreasonable behavior, and a number of other methods were experimented with in order to correct this behavior, but eventually it was determined that any potential runtime or integral accuracy benefits were far outweighed by the instability issues, and the approach was abandoned.

Capillary Pressure

The ability to accurately calculate capillary pressure within the system is required in order to determine volumetric changes between the gas and oil phase over time. The theory discussed here was used in multiple attempts to implement a volumetric calculation section in order to better model oil and gas concentrations, as well as their dispersion. After several months we were unable to create any stable solutions, but this section includes a discussion of the underlying science of the attempt, as well as how the problem was approached. In particular, reasonable oil and gas volumes could be found upon each timestep, but if those volumes were used in the

iterative calculations to act as inputs for the following timesteps, instability would inevitably arise.

Basic Theory

In order to properly understand the conditions of the oil and gas phases in the reservoir a capillary pressure must be determined. This Capillary Pressure represents the pressure offset between the two fluids in the form $P_{cap} = P_{gas} - P_{oil}$. MICP (Mercury Injection Capillary Pressure) data provided by the University of Oklahoma's Integrated Core Characterization Center (IC^3) lab was used to determine a pore throat size distribution, dependent on the oil saturation of the well, as shown in Figure C 1 in the Appendix. The pore throat sizes are then used to calculate the capillary pressure experienced at the oil-gas interfaces using the Young-Laplace equation:

$$P_{cap} = \frac{2 \times \sigma \times \cos(\theta)}{r_{cap}} \times .1 \frac{Pa}{dyne/cm^2} \qquad \text{eqn. 50}$$

With the surface tension in dyne/cm being determined by the Ramey (1973) correlation:

$$\sigma = \left[Par_o \times \left(x_o \frac{\rho_o}{M_{og}} - y_o \frac{\rho_g}{M_{go}} \right) - Par_g \times \left(x_g \frac{\rho_o}{M_{og}} - y_g \frac{\rho_g}{M_{go}} \right) \right]^4 \qquad \text{eqn. 51}$$

With,

$$x_o = \frac{RS_{moles}}{1 + RS_{moles}}, \qquad y_o = \frac{1}{1 + RS_{moles}},$$

$$M_{og} = x_o M_o + x_g M_g, \qquad M_{go} = y_o M_o + y_g M_g$$

$$\rho_g = \frac{C_{gas} \times M_{go}}{10^6}, \qquad \rho_o = \frac{C_{oil} \times M_{og}}{10^6}$$

$$C_{gas} = \frac{P_{gas}}{Z \times R \times T}, \qquad C_{oil} = \frac{1 + RS_{moles}}{V_{oilmolar_{STP}} \times FVF}$$

With the Parachors being calculated using equations designed by Whitson and Brulé (2000),

$$Par_o = (2.376 + .0102\gamma_{API}) \times M_o \quad \text{eqn. 52}$$

$$Par_g = 25.2 + 2.86M_g \quad \text{eqn. 53}$$

The Approach Itself

This final model uses a "Shared Volume" approach to calculating oil and gas concentrations. The concentration of any existing amount of oil or gas, measured in gmol/m^3, is found by dividing the number of moles of that substance by the total volume. In essence, no distinct saturation is being recognized. Oil and gas are free to intermingle and disperse past one another, without them being relegated to specific areas, zones, or flowpaths.

This is a rather significant simplification of real phenomena, and as such a great deal of effort was put into bypassing this assumption, and meaningfully tracking the oil and gas saturations throughout the course of production. The attempts were ultimately unsuccessful, but hopefully this discussion of the final approach will aid future attempts.

Step 1: Disperse the Oil Phase and calculate oil pressure

Dispersion of the oil phase results in a new set of oil concentrations (including in-solution gas support). This distribution can then be used to calculate oil pressures at any concentration, as shown in Chapter 2.

Step 2: Diffuse Gas and then determine the number of Moles of Gas in the system

Gas is diffused using the same methodology as the oil phase, and then this new concentration and the old gas volume are used to determine the number of moles of gas post diffusion. This amount is then summed with gas released from solution using the new and old oil pressures, as well as the old oil volumes to find the number of moles of gas for the new timestep.

Step 3: Determine the Oil Saturation

Using the pore size to oil saturation distribution included in Figure C 1 and the equations for calculating capillary pressure, a distribution of capillary pressures can be found across the full range of oil saturations and possible oil pressures. Generating this distribution requires testing different assumed capillary pressures with the provided oil pressure and oil saturation information, in order to find the related gas pressure and gas density, which is required for the capillary pressure calculation. Once this process has occurred with any of a number of root finding methods, a stable distribution, where the assumed capillary pressure is equivalent to the resulting one, can be found. This only needs to be done at the beginning of the program once fluid properties are known. An example is shown below:

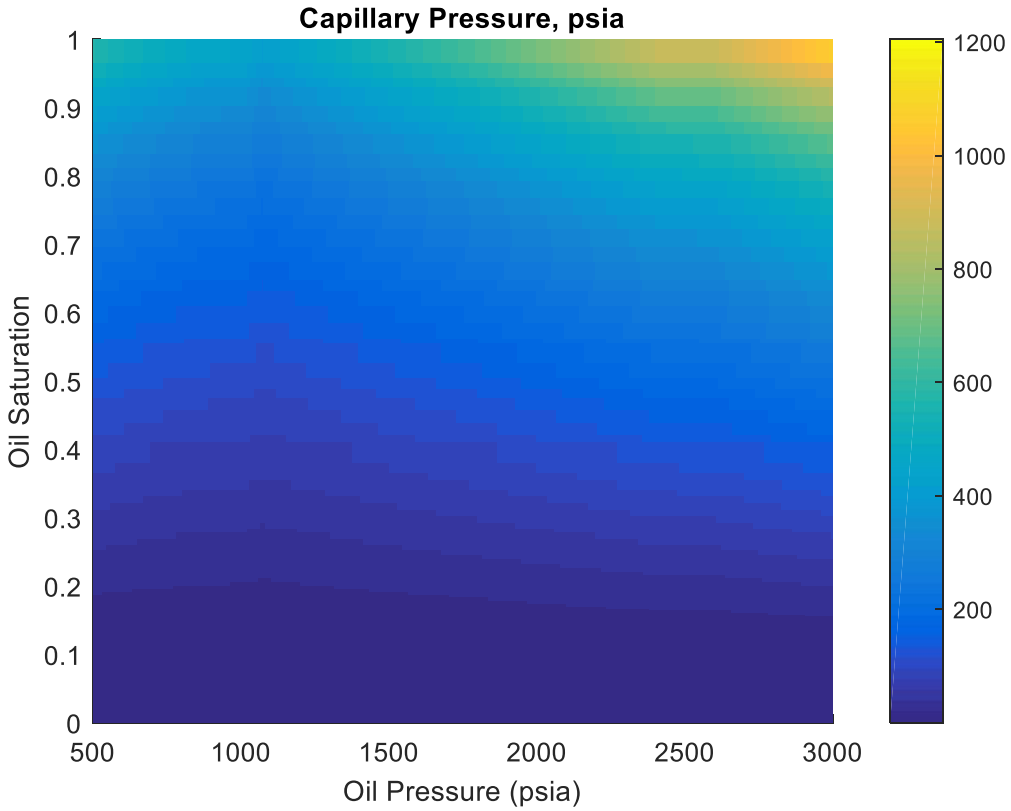

Figure 6: $P_{cap}(S_{oil},P_{oil})$

Since capillary pressure and oil pressure values are known throughout the distribution, gas pressure can be found, and from that a gas concentration distribution with respect to

oil pressure and saturation, as shown below:

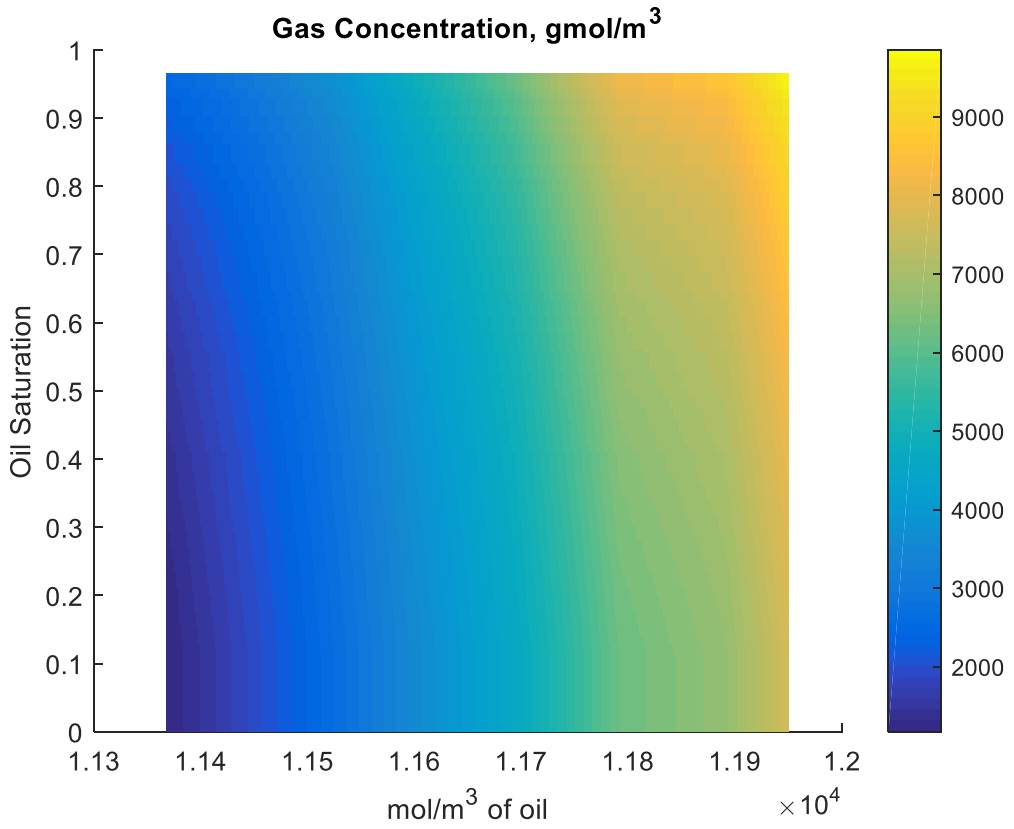

Figure 7: $C_{gas}(S_{oil},C_{oil})$

Then with the gas concentration information, knowing the total volume of the system, and noting the oil saturation in the y-axis, we can generate a surface describing the number of moles of gas present in the system for any oil saturation and oil pressure, as shown below:

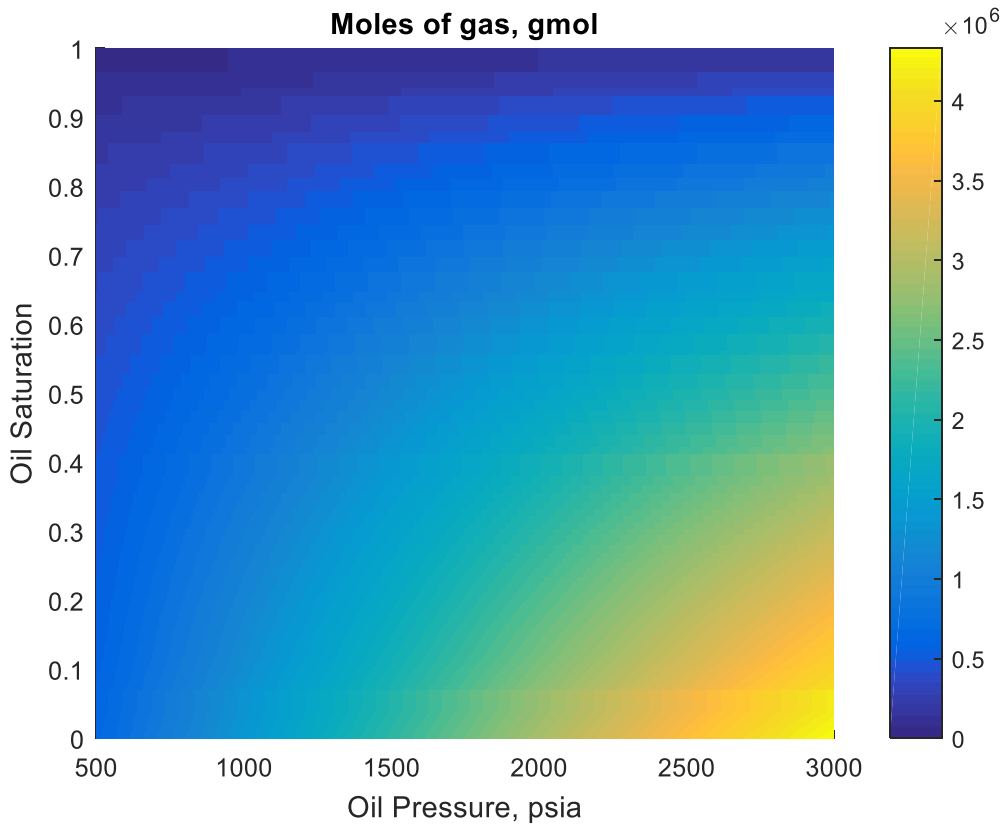

Figure 8: $M_{gas}(S_{oil},P_{oil})$

Then using MATLAB's *scatteredInterpolant* function with the information from the above figure, we can generate a function that will determine the oil saturation at any given combination of oil and gas concentrations:

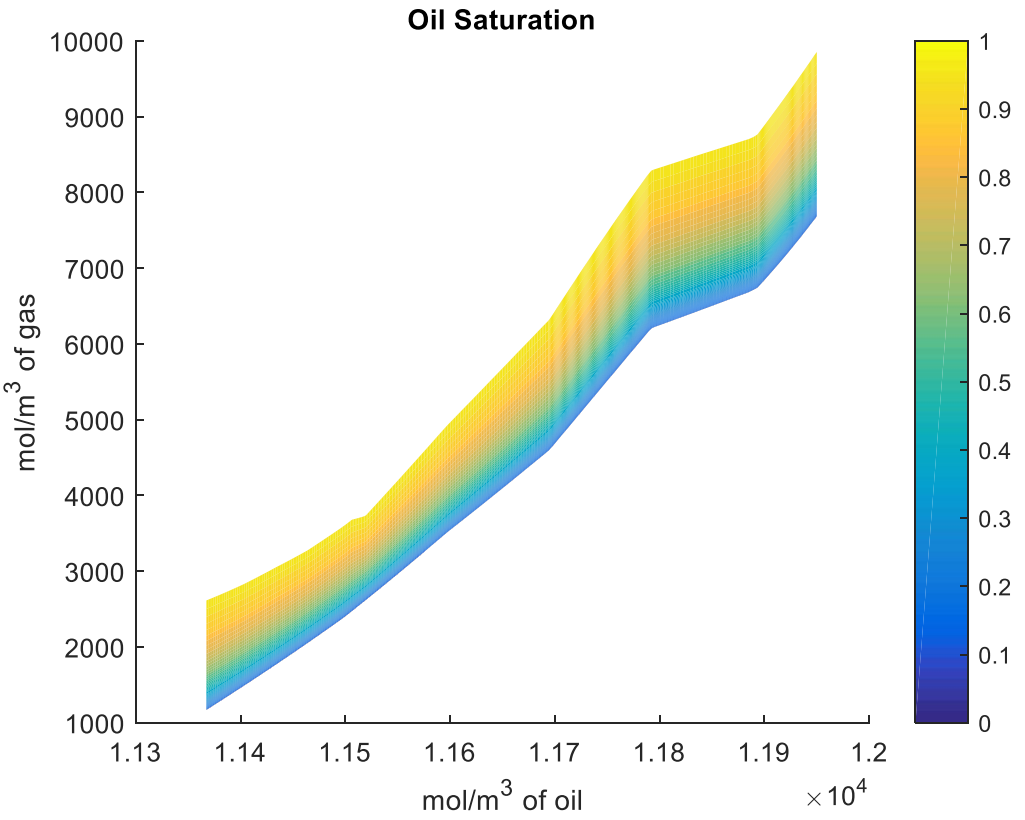

Figure 9: $S_{oil}(C_{gas},C_{oil})$

Knowing the oil saturation from step 1, and the moles of gas due to step 2, we then test values of oil saturation until we reach one that stabilizes with a correct gas concentration/oil saturation combination using Figure 9.

Step 4: Calculate the Gas Concentration

Knowing the oil saturation and the moles of gas, we can then determine the gas concentration.

Step 5: Continue to the next timestep

In the standard approach, after calculating the new gas concentration, production volumes were found, and the next timestep began.

Alternate Method

An alternate method was attempted, where the last timestep's number of moles of gas was used to calculate oil saturation, the gas release was determined with this new oil saturation, then gas was diffused. A distribution from the *scatteredInterpolant* function was then used to find the new oil concentration, which was used in the following timestep after production volumes had been found.

Smoothing functions were tested in order to handle any anomalous results, iterative processes were used to test a result before it was accepted in order to try to find a more stable solution, and different calculation direction and dependencies were explored. The end results were all more or less the same; the gas or oil saturations would destabilize resulting in 100% saturation in an unrealistic area. In addition the oil production volumes resulting from this method far exceeded those of actual production data, even more than the current method which often requires efficiency factors from 5-15% to justify. Figure C 2 through Figure C 11 in the appendix follow this destabilization process. Of note is that the oil concentrations and pressures behaved in a perfectly reasonable manner, consistent with the final model. This suggests that the instability must be in the calculation process for the saturations, rather than anything to do with the concentrations or pressure, but I was unable to find a solution.

Potential Cause of Failure

The inability of the program to stabilize at any reasonable equilibrium using the capillary pressure and density based approach discussed above is likely due to many of the same characteristics that make this dispersion based model necessary in the first place. In particular the inaccuracy of many conventional models and theories in the nanoscale, as well as this model's limited approach with regards to pressure based flow,

likely contributed to destabilization of the simulation. Theories and methodologies more accurate than those presented here would likely be required to approach this problem, as many of the basic equilibrium requirements don't hold true at the nanoscale (Sigal et al., 2015).

Unstimulated Volume Support

Despite the majority of production in a fractured reservoir resulting from the fractures themselves, early on, and followed by the matrix between the fractures later on, a third contributor to reservoir production exists. While certainly a small contributor during initial production, the unstimulated portion of the reservoir will invariably contribute an ever more significant amount of production to a stimulated well. This tri-linear flow model, follows many of the same basic assumptions as the model used for the dispersion model discussed in this thesis, and helps explain the long-term decline plateau experienced by shale wells (Zheng et al., 2016). The basic theory behind this unstimulated volume support is that a slowly expanding "tank" of oil, the result of the pressure disturbance caused by production expanding into the fractured reservoir, provides support for the stimulated region (Moghanloo et al., 2015).

From an implementation perspective there are two primary routes to modeling the unstimulated zone support. The first is using a combination of the dispersion model discussed here, as well as the work of Zheng et al. (2016), to account for the current size of the dynamic drainage volume (DDV). With this approach the DDV, found using Zheng et al.'s methodology, provides the length in a false symmetrical system, which expands each timestep, allows the differential equations that govern the fluid flow in the stimulated zone to model the fluid flow in the unstimulated zone. Production from the

unstimulated zone is assumed to enter the stimulated zone in such a way as for the increase in concentration to be linearly related to the missing concentration in that area. Ie, areas near the fractures get more unstimulated support than areas near the center due to the lower concentration and pressure in that area. The unstimulated region is assumed to have fluid properties identical to the initial properties of the stimulated region, as well as a dispersion coefficient $1/10^{th}$ of that seen in the stimulated region, and the boundary conditions used for the unstimulated region are the mean concentrations of oil and gas in the stimulated zone.

The second possible approach is to use the work of Yuan et al. (2016) to both control the expansion of the DDV over time, as well as to account for the production of that volume. The second approach benefits from internally consistent assumptions between the size of the DDV, and its production rates. While the first approach both accounts for the DDV, but also maintains the production mechanisms and assumptions of the core dispersion model.

In either case, after flow from the unstimulated region joins with the existing volumes and concentrations in the stimulated region, their properties, such as sGOR, are reconciled appropriately, and the next timestep begins. Dispersion into specific areas of the stimulated zone is determined by linearly distributing new fluids wherever existing concentrations are lowest.

Cluster Efficacy and Fracture Efficiency

Any fractured reservoir experiences a degree of underperformance depending on the difference between the ideal cluster behavior and the reality. Not only are some clusters physically smaller than would be expected, but there is also the risk that overly close

clusters will inhibit the production performance of neighboring clusters, decreasing their cluster efficacy (Ran and Kelkar, 2015). This model does not differentiate between any cluster pair, with equal performance being assumed from any given pair. The model itself assumes perfectly circular, 2D clusters, or fractures, with each pair being evenly spaced throughout the lateral length of the well, and the reality. Final production values from the model use an assumed "Fracture Efficiency" scaling factor, which acts as a corrective factor between the ideal model and reality. This scaling factor, which was set to 10% for all wells, encapsulates both the effects of cluster efficacy as well as differences between real cluster shape and the circular shape that has been assumed.

If additional information were available with regards to cluster efficacy on a well by well basis that information could be easily incorporated into the dispersion model. This variation of the current model would treat cluster efficacy and shape information as a program input on a well or field basis, and an assumed fracture efficiency value would not be necessary. Mean fracture dimensions could be used, with a single cluster efficiency multiplier scaling the simulation outputs to find the production of the system. As this information was not available, and any values used would have to be assumed or determined by viewing their effect on the production match, the Fracture Efficiency term was used to act as a crude, but uniform assumption, which would minimize the risk of overfitting.

Three Dimensional Clusters

In the existing models fracture clusters are treated as circular surfaces of infinite conductivity. This causes an overestimation of the distance between fracture clusters that is dispersion dominated. If detailed cluster information is available, the model can

be easily modified such that only the volume outside of the clusters is dispersion dominated. Separate modeling would then be required to account for production from within each individual cluster, but this change would improve the accuracy of early predictions.

Time Offset cluster production

The current model assumes that all production throughout the well occurs simultaneously. In particular it assumes that the pressure in all fractures are equivalent. This results in an excessively large spike of initial production. By analyzing information on the delays between different fractures beginning to produce, and their individual BHP, would allow the model to bring individual fracture pairs online at the correct time, or even assume unequal boundary conditions for a given fracture pair. This would more accurately model the behavior of an actual reservoir, and would also result in a more realistic early production phase.

Initial Gas Saturation

The current model takes a "Shared Volume" approach to oil and gas saturations, essentially assuming miscibility between oil and gas at all pressures. From that perspective the existing model is actually perfectly capable of using an initial concentration of gas to represent existing free gas. But in order to model an actual gas saturation the issues with the capillary pressure and oil saturations discussed earlier in this chapter must be resolved. In addition any approach that generates an actual gas saturation needs to account for how additional gas joins the gas phase. One possible form this could take would be a sort of vapor pressure approach where any gas that is released instantly joins the gas phase, as if it were coming out of solution at the oil-gas

boundary. A second possible approach would make use of the miscibility assumption used in the existing model, but with dispersion occurring in the direction of the fractures and in the direction of the gas phase. This would require a dispersion coefficient for the miscible gas as well as a separate coefficient for the gas phase.

Shut-in wells

Well production is almost never as easy as "complete the hole, make money." Interruptions to production take many forms, but one form of interruption this model is particularly well suited for is a shut-in well. While the existing model only employs the constant boundary condition version of the heat diffusion equation, the insulated boundary form of the equation is actually even simpler to solve. If a well was shut-in, and the timing of that shut-in was known, the model could take that process into account when determining its production estimates. The shut-in period would give the concentrations in the reservoir matrix time to equalize, resulting in a sizeable increase in near-boundary concentrations, which would result in a production spike when production resumed. This change has value both in determining dispersion coefficients of existing production wells, as it can account for the spikes they experience post shut-in, as well as in predicting the effects of a shut-in on future production.

EOR applications

As this model is focused on concentration driven production, as well as how in-solution gas helps drive oil production by boosting oil concentrations, it has several potential applications in relation to CO_2 or ethane based EOR. Not only does the model relate oil pressures and concentrations to distance from fractures, but it also has mechanisms by which the presence of gas can improve or generate production of oil. That being said,

the existing model only uses in-solution gas to boost oil concentrations, not miscible gas, and adjustments may need to be made in order to predict how the presence of injected gas affects the production of gas through dispersion. A number of analytical solutions are available for understanding the behavior of CO_2 based EOR, through the work of Moghanloo (2012), which would allow for this dispersion model to interpret the effects of CO_2 injection program.

Chapter 4: Results and Discussion

Full Run

Table 1: Shared Values

Res. Temp. (F)	118
API Gravity	46
Gas Gravity	0.8377
Porosity (fraction)	0.075
Initial Press. (psia)	7010
Initial Sw (fraction)	.26
Fracture Efficiency (fraction)	.1

Table 2: Solution Gas Values

Pressure	RS
psia	SCF/STB
14.7	0
400	90
600	150
980	265
1400	380
1800	500
2400	625
2600	760

Table 3: Well Specific Information

Sample Well	Fracture Half Length	Fracture Spacing	Number of Fractures	Gas Multiplier	Dispersion Coefficient
-	ft	ft	-	-	m^2/s
1	223	83.40	48	2.5	1.05E-06
2	201	64.86	69	1.75	1.78E-06
3	236	54.42	74	1.75	4.05E-07
4	234	39.68	157	1.75	1.50E-07
5	224	60.95	57	1.75	4.05E-07
6	243	80.00	80	2.25	7.11E-07
7	247	28.57	140	2.5	1.50E-07
8	214	59.19	74	1.5	8.63E-07
9	212	72.84	57	2	8.63E-07
10	233.2	65.52	75	1.5	1.02E-06

Fracture Half Length was calculated using the OU Well Evaluation Software (2017). Number of clusters and number of fractures is used interchangeably, as in this model a cluster is modeled as a single, two dimensional circle with infinite conductivity, or essentially as single super fracture. Gas Multiplier values were found on a well by well basis by determining the multiplier on the base distribution that resulted in the correct GOR.

Full Output

Using the shared values and sample values listed above, the following production matches were found for the 10 Niobrara wells used in this research. It should be noted that the match for the first 200 days of production may not accurately represent the initiation of matrix dominated flow, and may need to be adjusted on a well by well basis:

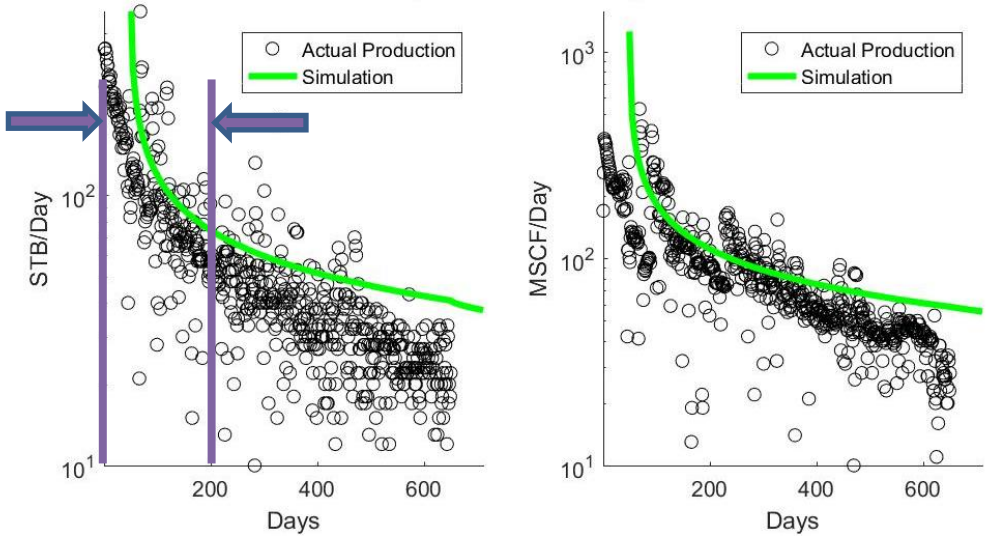

Figure 10: Sample Well 1's Production, with an initial dispersion start time, following convection dominated flow, that may need to be adjusted on a well by well basis

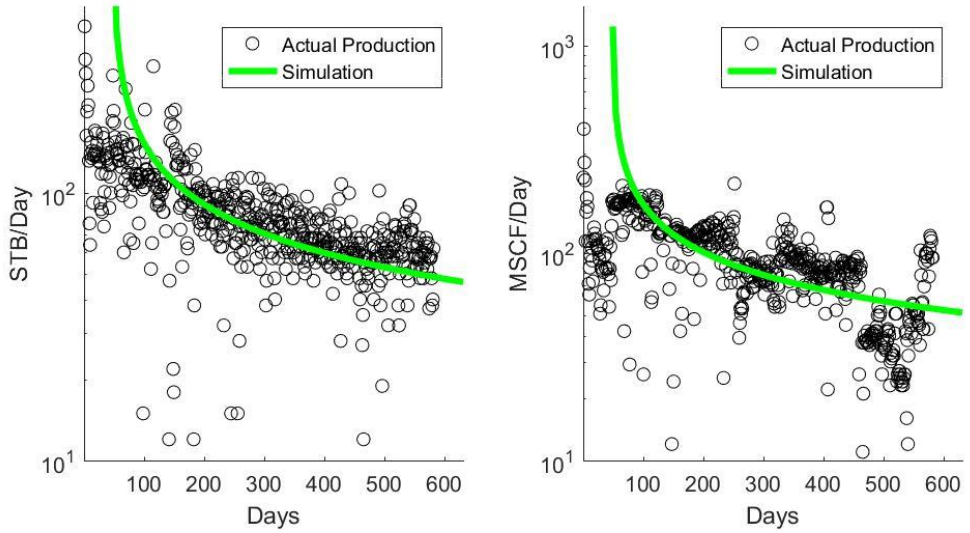

Figure 11: Sample Well 2's Production, with an initial dispersion start time, following convection dominated flow, that may need to be adjusted on a well by well basis

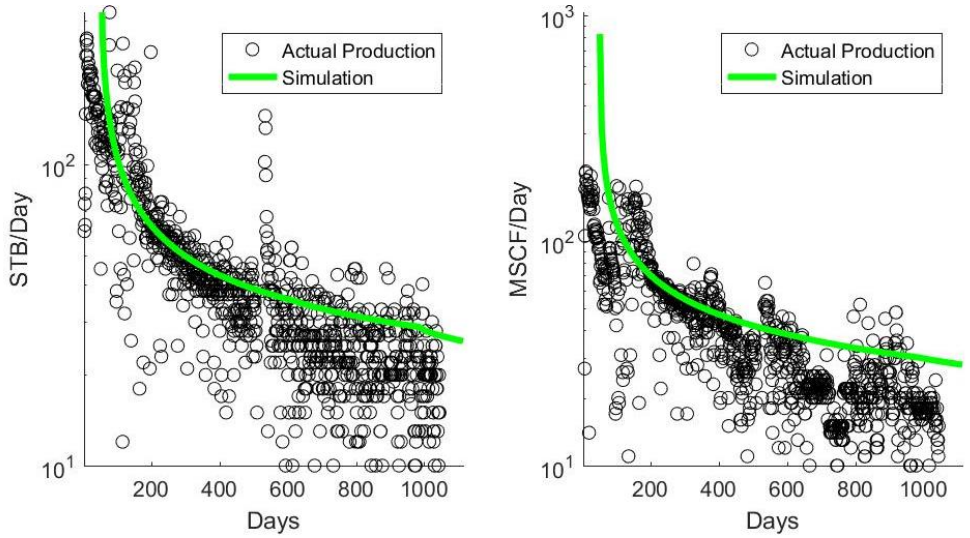

Figure 12: Sample Well 3's Production, with an initial dispersion start time, following convection dominated flow, that may need to be adjusted on a well by well basis

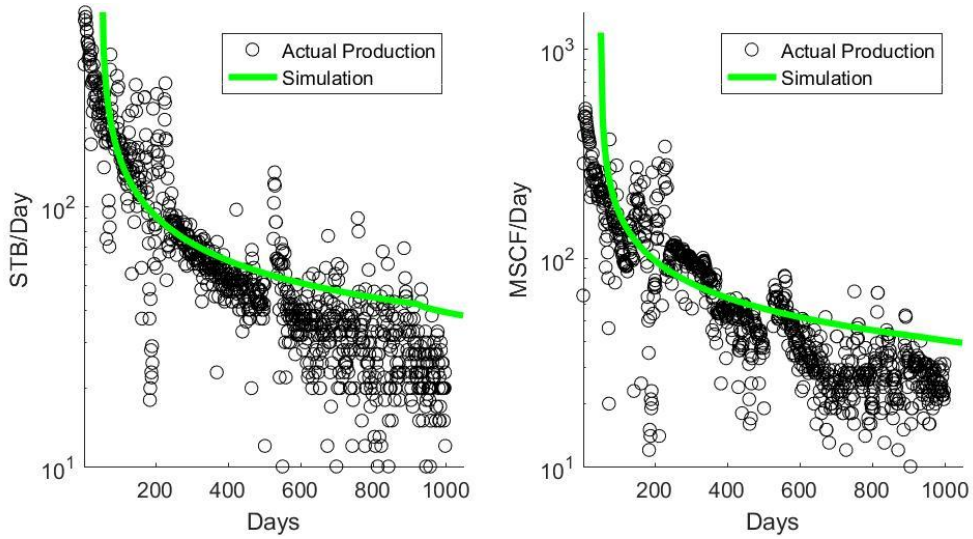

Figure 13: Sample Well 4's Production, with an initial dispersion start time, following convection dominated flow, that may need to be adjusted on a well by well basis

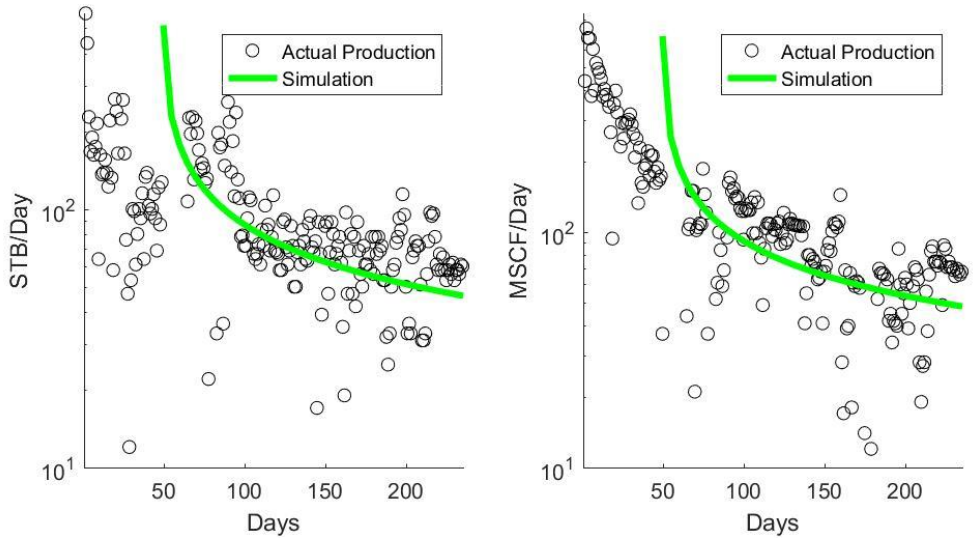

Figure 14: Sample Well 5's Production, with an initial dispersion start time, following convection dominated flow, that may need to be adjusted on a well by well basis

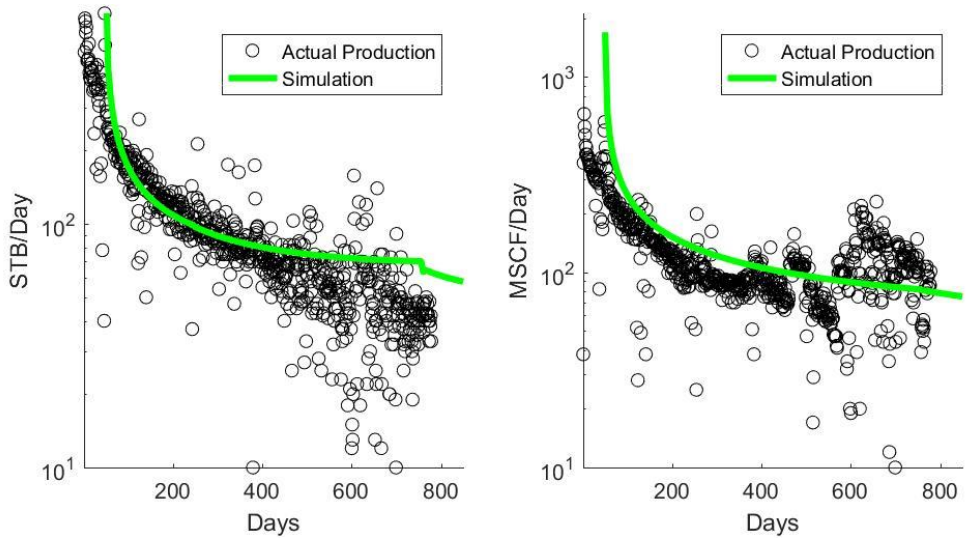

Figure 15: Sample Well 6's Production, with an initial dispersion start time, following convection dominated flow, that may need to be adjusted on a well by well basis

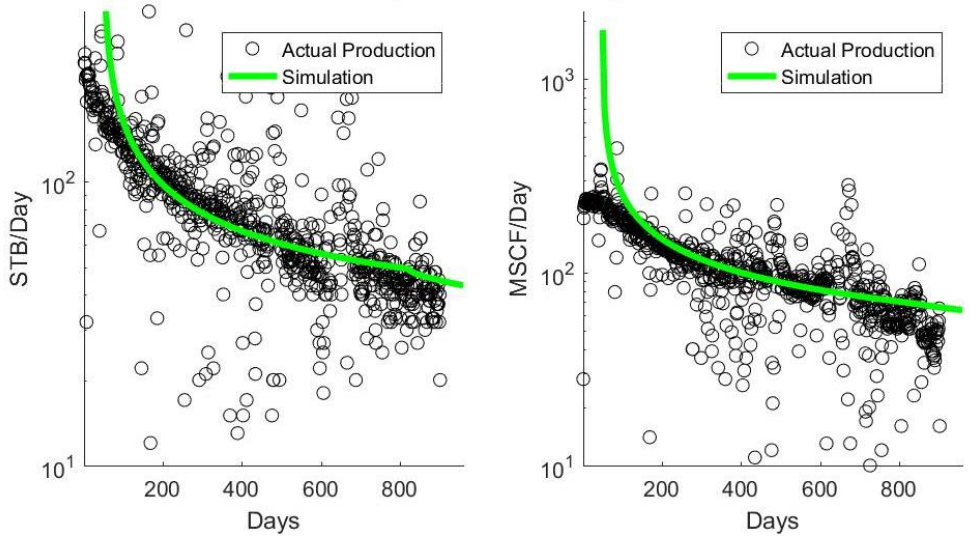

Figure 16: Sample Well 7's Production, with an initial dispersion start time, following convection dominated flow, that may need to be adjusted on a well by well basis

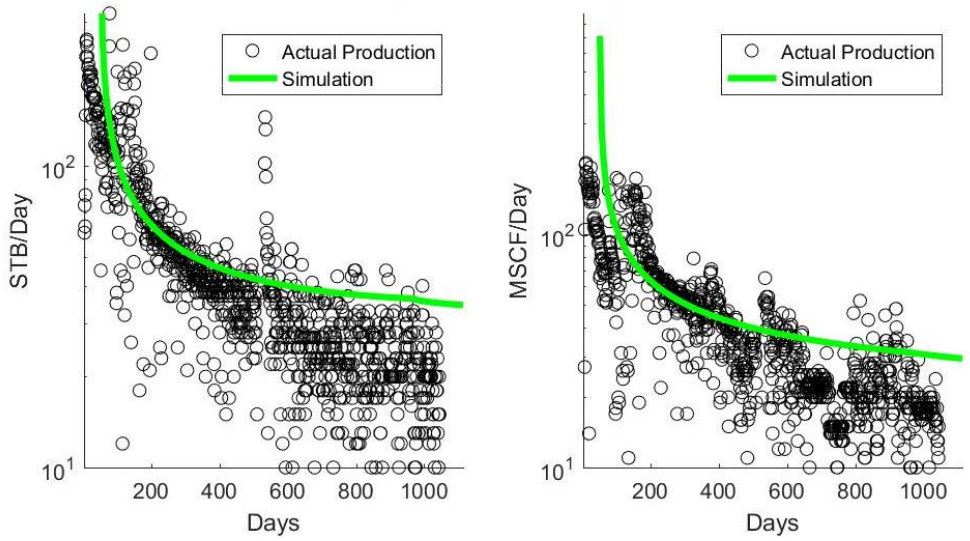

Figure 17: Sample Well 8's Production, with an initial dispersion start time, following convection dominated flow, that may need to be adjusted on a well by well basis

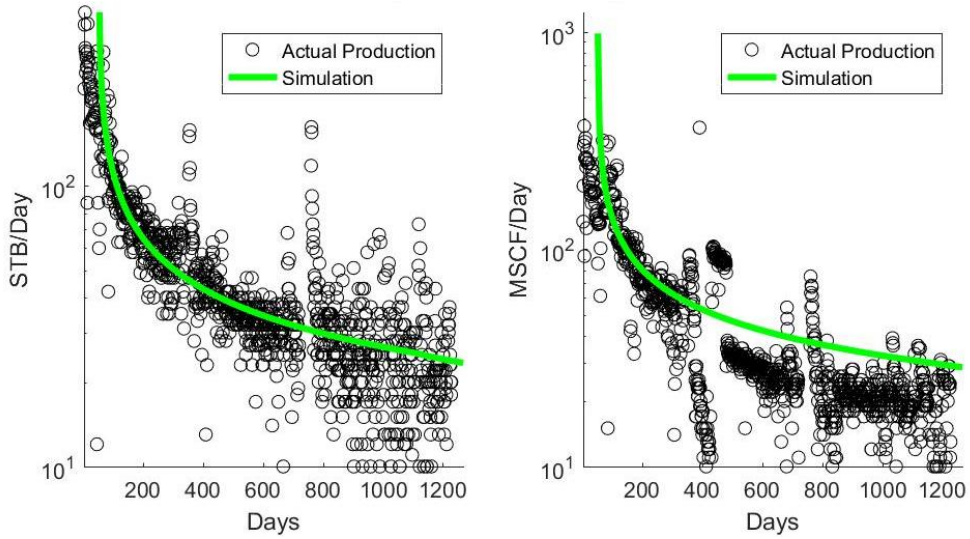

Figure 18: Sample Well 9's Production, with an initial dispersion start time, following convection dominated flow, that may need to be adjusted on a well by well basis

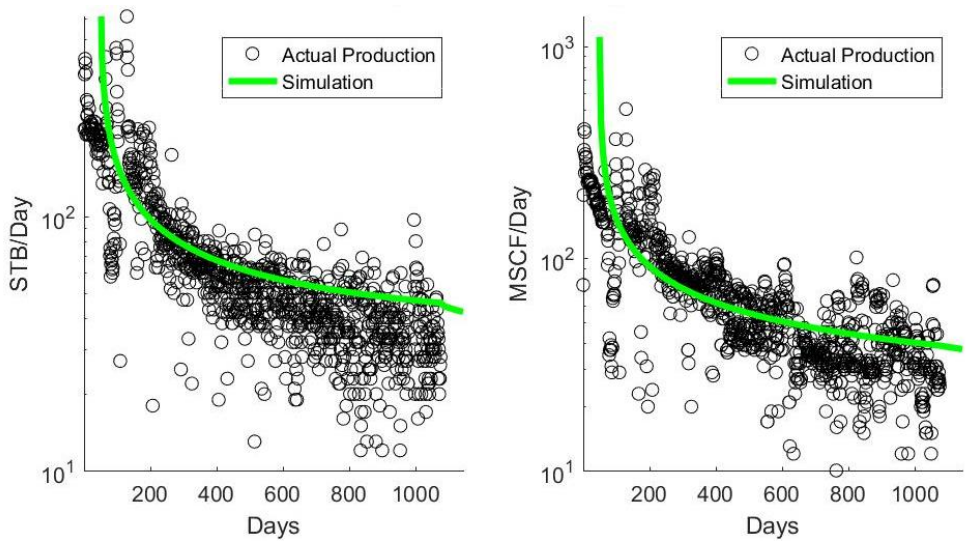

Figure 19: Sample Well 10's Production, with an initial dispersion start time, following convection dominated flow, that may need to be adjusted on a well by well basis

Each of the 10 sample wells shown above has its own gas concentration, oil concentration, and oil pressure distributions. While they do very from well to well depending on the related dispersion rates, cluster spacing, and fluid compositions, their general behavior is the same, and as such only a single example of each is shown below. Oil Concentration over time, accounting for the moles of in-solution gas as a "boost" to concentration, behaves as expected, with the boundaries experiencing a rapid dropoff in concentration due to the low boundary concentrations at the fractures, with a more gradual decline experienced near the central No-Flow boundary:

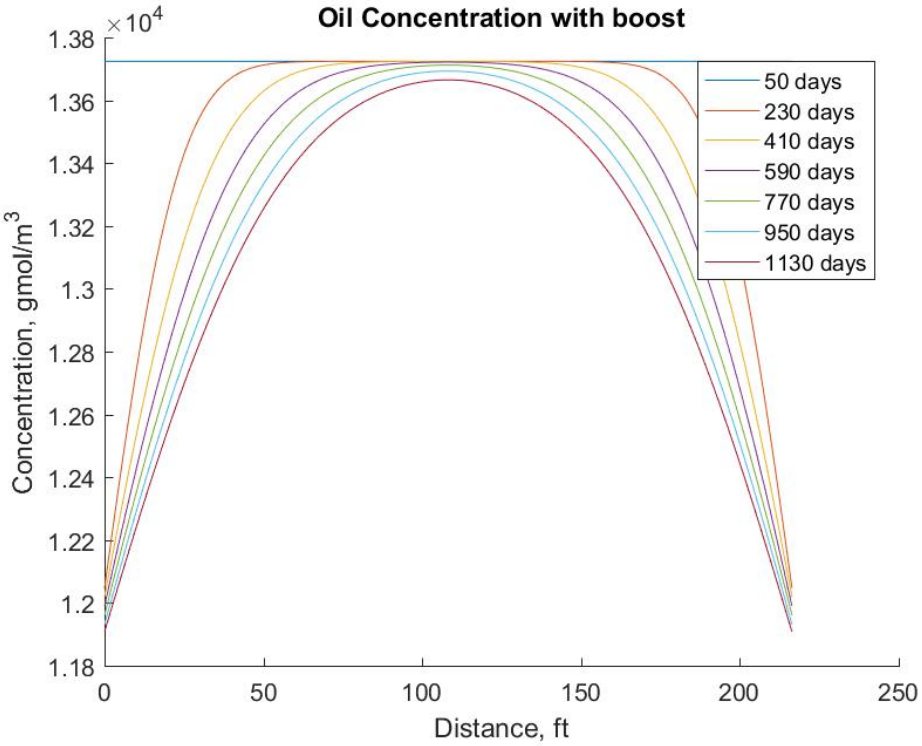

Figure 20: Sample Well 10 Oil Concentration over time

Oil pressures also behave as expected, dropping with the concentrations of oil. These drops are more pronounced above bubblepoint pressure, and the seemingly anomalous behavior at approximately 2500psi is due to the bubblepoint pressure being passed, and gas being subsequently released from solution.

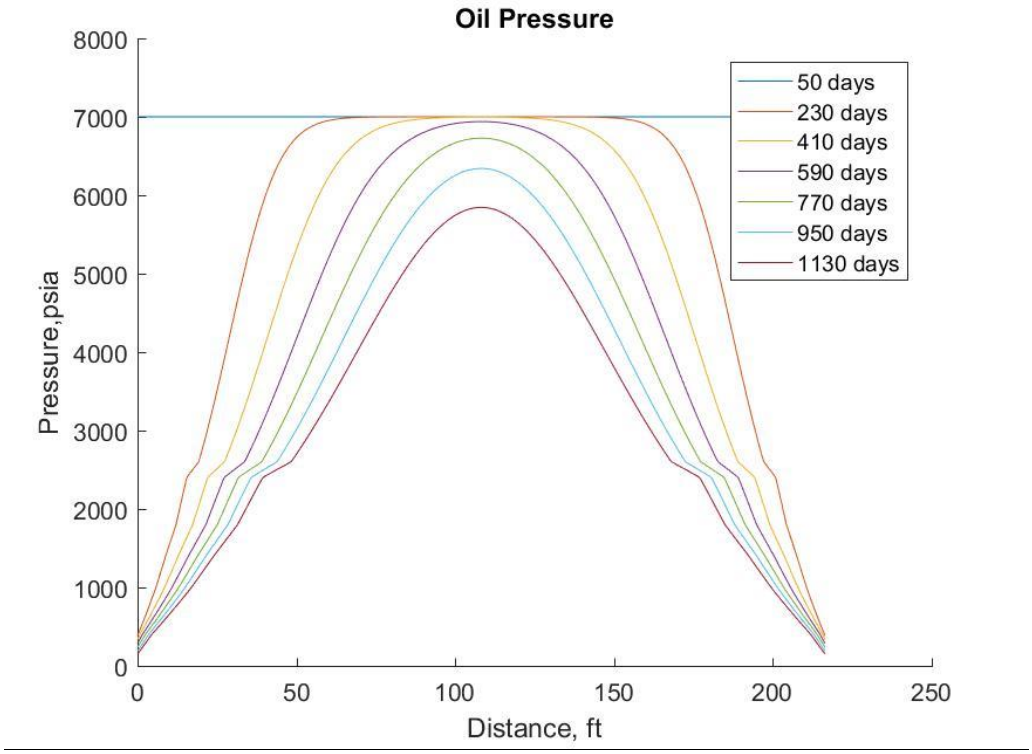

Figure 21: Sample Well 10 Oil Pressure over time

Gas concentrations originate in areas where the oil has dropped below bubble-point, but using our Shared Volume model they are able to disperse into above bubble-point regions:

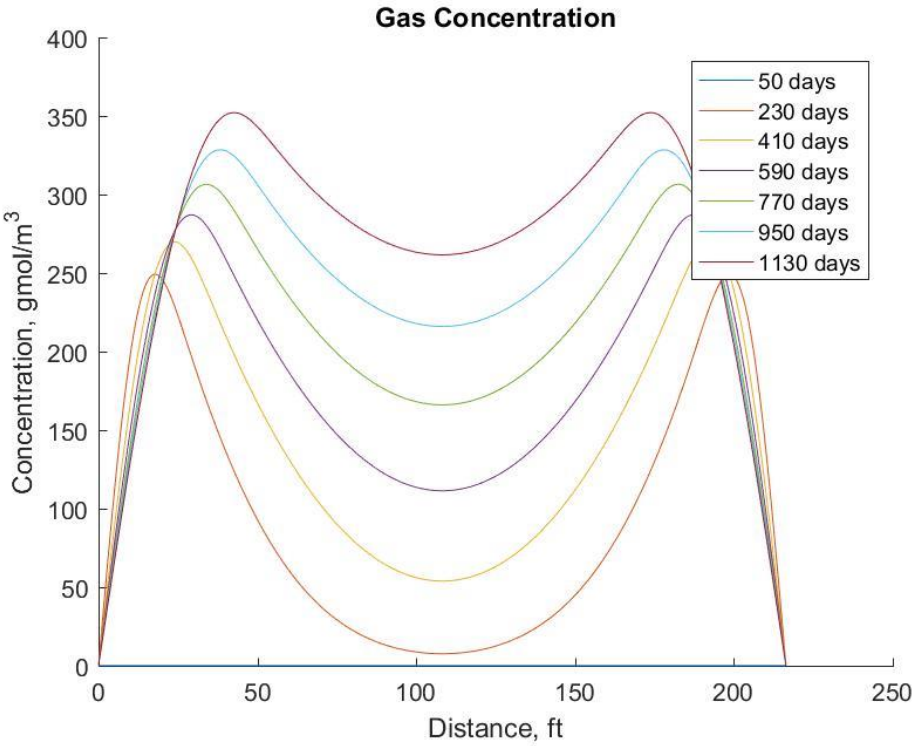

Figure 22: Sample Well 10 Gas Concentration over time

A false No-Flow boundary model was generated where areas above bubble-point could be insulated from gas diffusion without causing unreasonable behavior on the part of the gas, but it was decided that when assuming miscibility and a Shared Volume it was more reasonable for the gas to be able to disperse into high pressure areas, as shown above.

Summary of collection of runs

The simulation was run, and an ideal dispersivity constant found, for 10 wells in the Niobrara formation. Their production results were shown in the previous section, and the relationship between their dispersion coefficient and effective permeability, as calculated by the OU Well Evaluation Software (2017), is below:

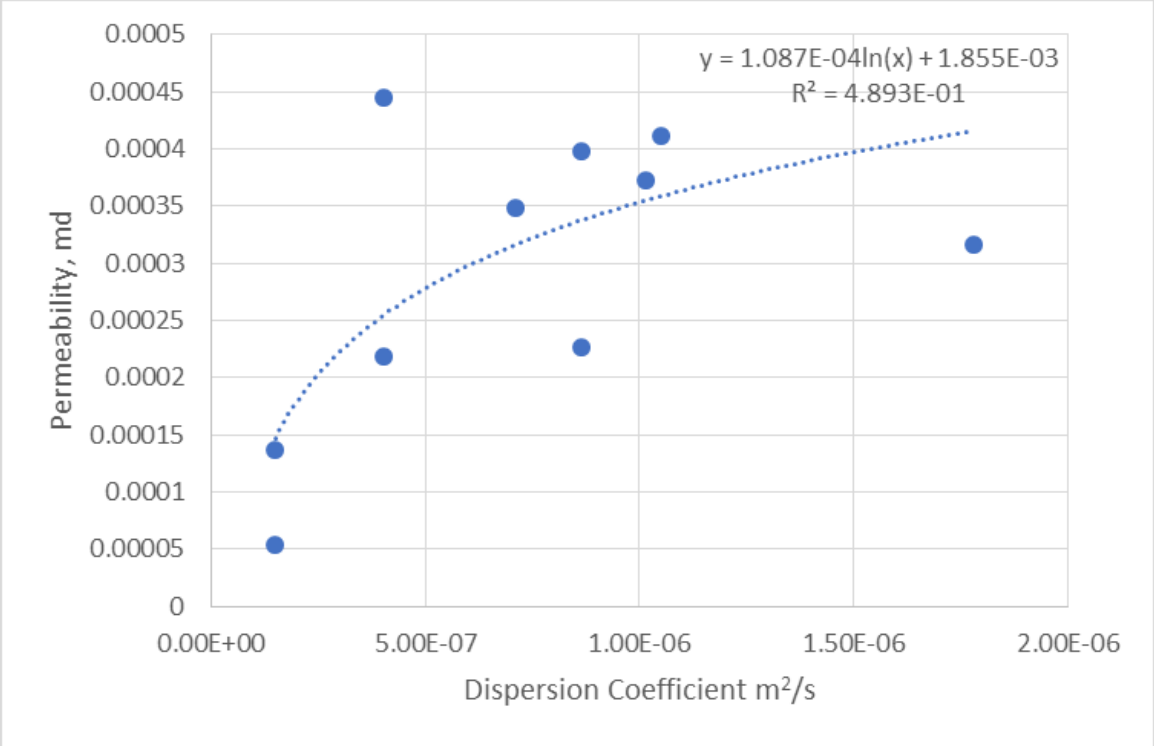

Figure 23: Permeability vs. Dispersion

This suggests that in order to justify the production rates seen at higher permeability values, an absurdly large dispersion coefficient would be required. As fluid flow at higher permeability's are convection dominated rather than dispersion dominated, this makes sense, as dispersion alone can no longer account for the fluid flow seen at those rates, as represented in the figure below.

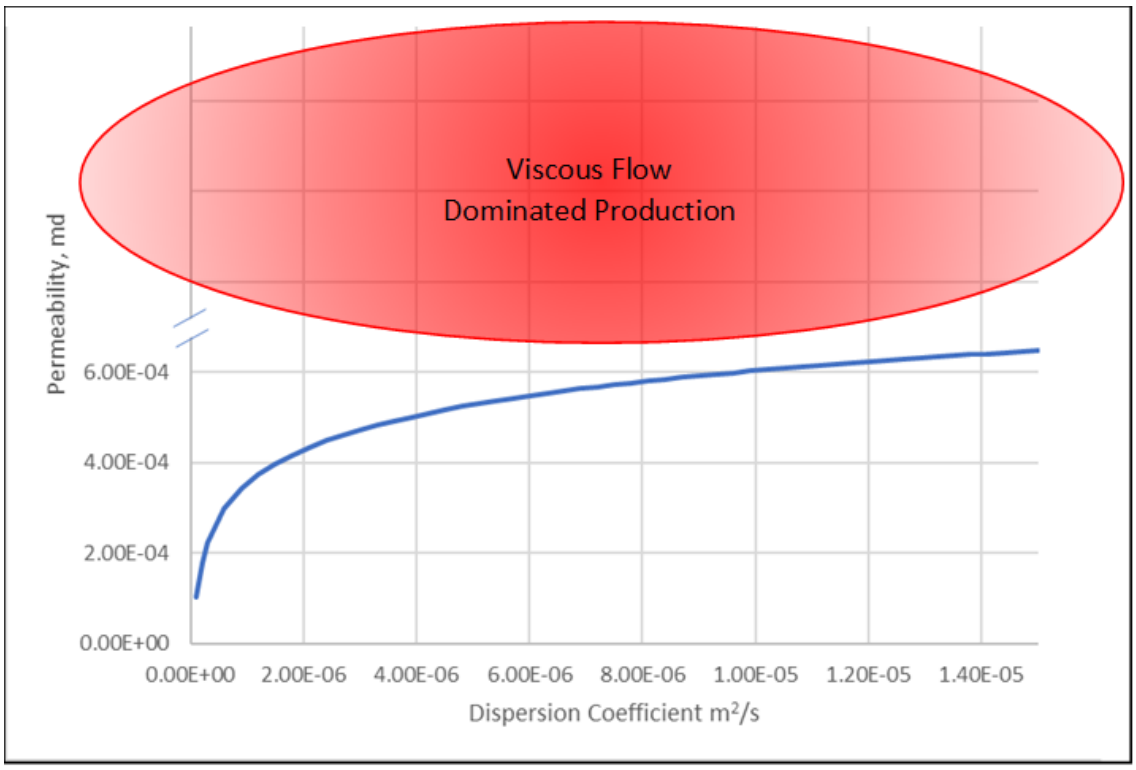

Figure 24: Viscous Flow production dominates at higher permeability values

An additional potential application of this method is determining geologic distributions of reservoir rock quality, as measured by the dispersion coefficient. In areas that already have existing production dispersion coefficients can be found for all existing wells, allowing an aerial map of reservoir quality to be determined:

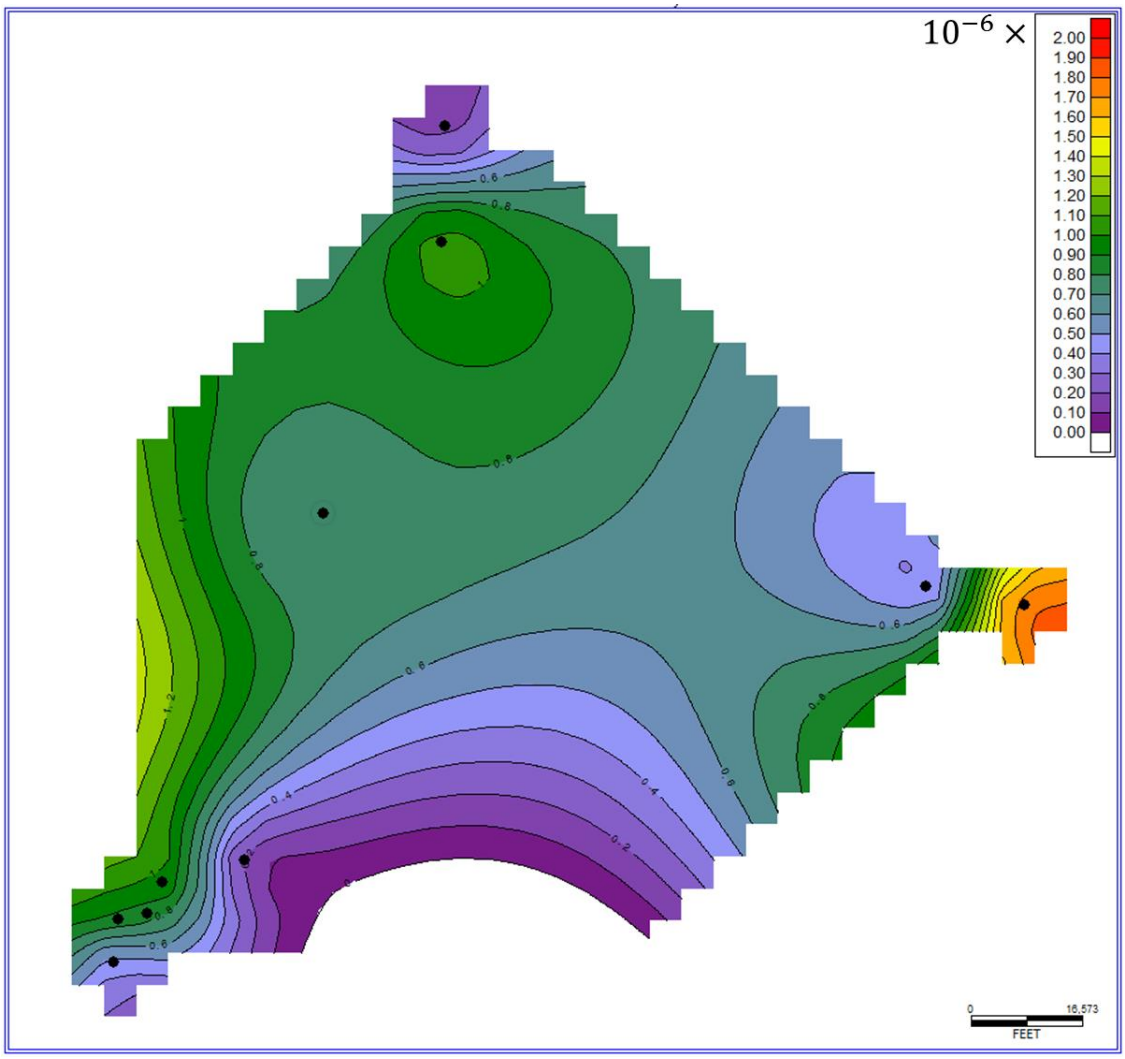

Figure 25: Dispersion Coefficients across the 10 sample well area

Recovery Factor

An additional point of interest that results from this model is a theoretical limit on the recovery factor. The maximum recovery factor for each well is limited by the possible concentration change. For the wells in the sample, maximum possible recovery factors ranged from 12-18%, assuming perfect cluster efficacy. This value would be decreased to real cluster efficacy values, but increased by corrections to the dimensions of the cluster itself, where dispersion flow would not be dominant.

Sensitivity Analysis

The measure of any new model can often be found in observing how it behaves under different conditions. In particular observing whether changes to input parameters create reasonable changes in outputs is a strong indication of a potentially useful model, and helps limit the risk of relationships and behaviors that were developed due to overfitting, rather than due to sound scientific principles. The following discussions on the programs sensitivity to different inputs and controls were all performed using Sample Well 10.

Solution Gas Content

Using the multiplier for the solution gas content discussed in the "Full Run" section earlier in this chapter, multipliers in addition to these values were applied to check sensitivity to increases or decreases in gas content.

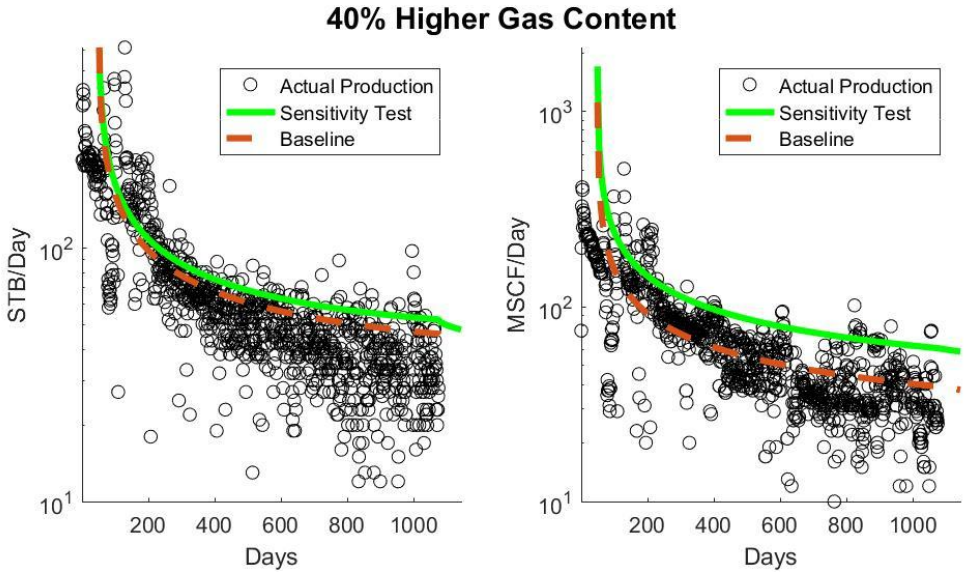

Figure 26: Sensitivity to increased Gas Content

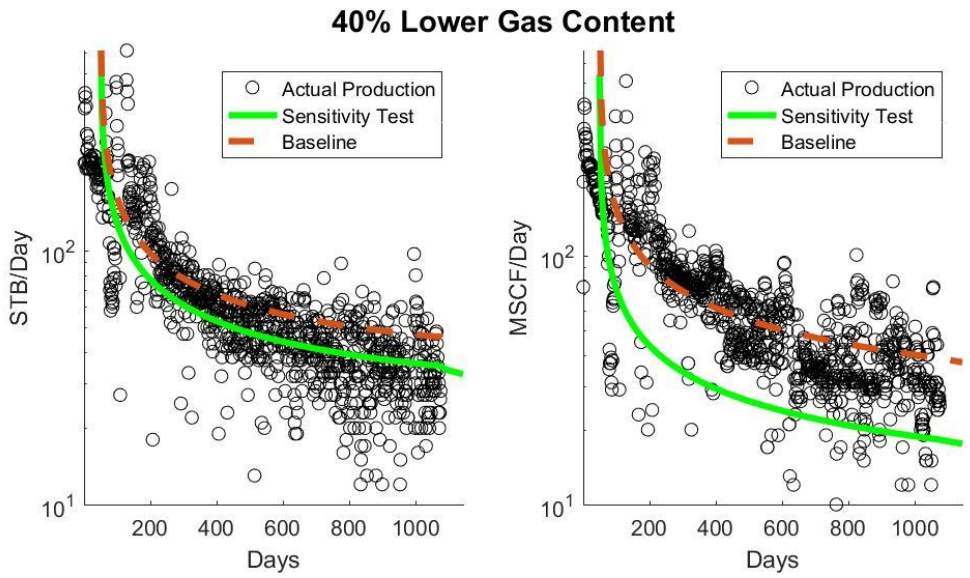

Figure 27: Sensitivity to decreased Gas Content

As expected changes to gas content have a sizeable impact on the amount of gas produced by the system. In addition, as in-solution gas content acts as a boost the oil concentration for dispersion purposes, changes to the gas content actually decrease both the oil production rate, and the ultimate recoverable reserves under dispersion based flow.

Timestep Resolution

Changing the number of timesteps is a significant contributor to overall runtimes, as discussed later in this section. Significantly higher numbers of timesteps also risk estimation errors and imperfect approximations. As such a sweetspot of runtime efficiency, minimal errors, and accurate simulation results is desired. For the purposes of applying BHP data or shut-in information a timestep resolution similar to the resolution of input data is ideal, while resolution exceeding that is unnecessary unless additional, time dependent terms are added to the simulation. By default the simulation uses a timestep of five days.

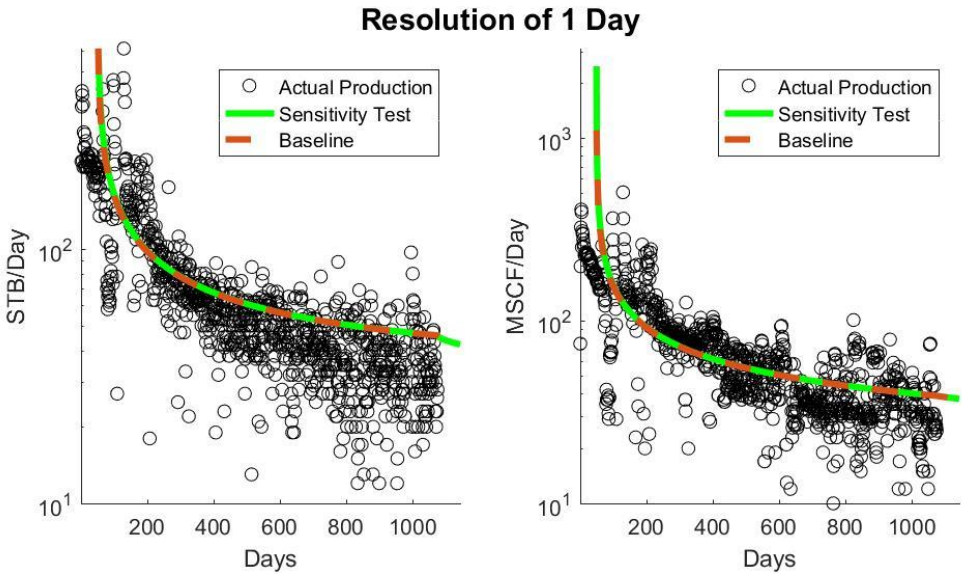

Figure 28: Sensitivity to shorter timesteps

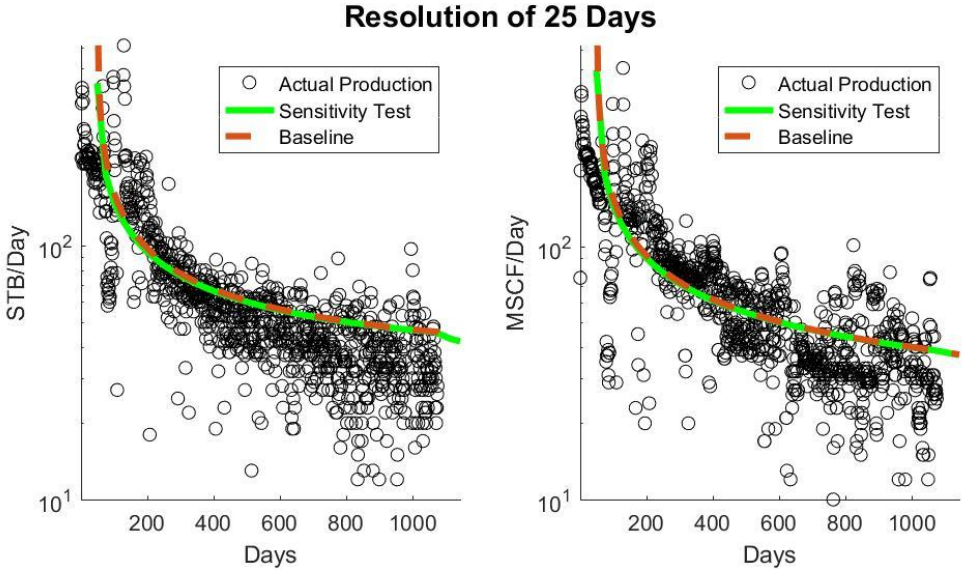

Figure 29: Sensitivity to longer timesteps

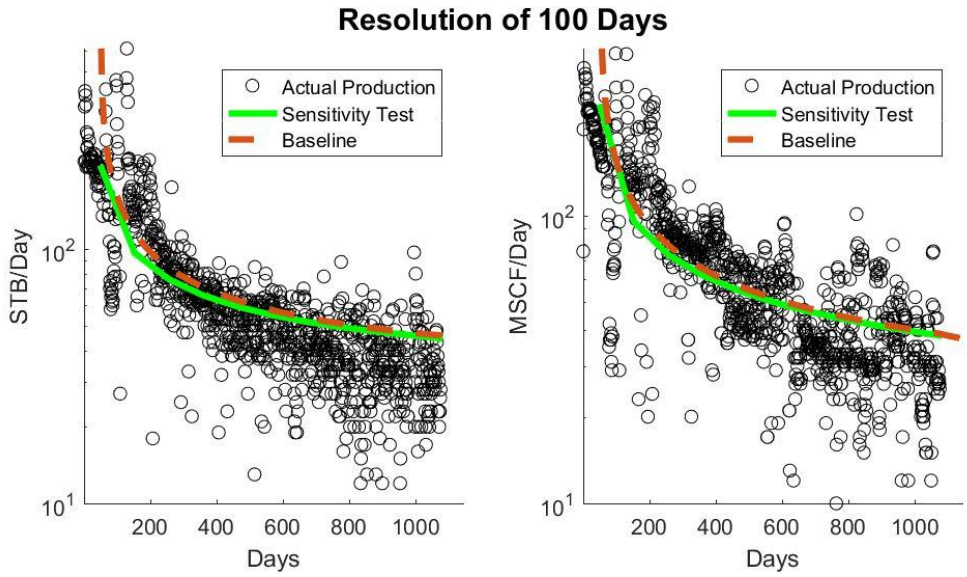

Figure 30: Sensitivity to much longer timesteps

Increasing the resolution of the simulation with respect to time simply increases runtimes, while decreasing resolution limits sensitivity to BHP changes, and eventually makes it difficult to generate a reasonable match with daily production data. The default time resolution of 5 days seems to be an ideal mix of decreasing runtimes while providing adequate resolution with respect to time. A time resolution of 1 day or lower would necessary in the event of well shut-in.

Length Resolution

As discussed later in this section, changes to the length resolution of the simulation have a noticeable, but manageable, effect on runtimes. They, however, has surprisingly little impact on the quality of results.

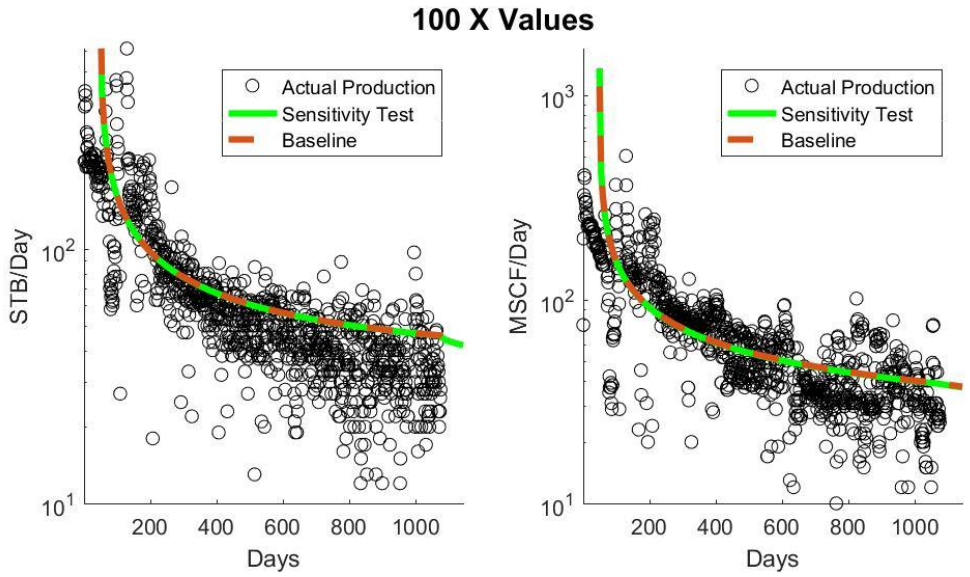

Figure 31: Sensitivity to lower length resolution

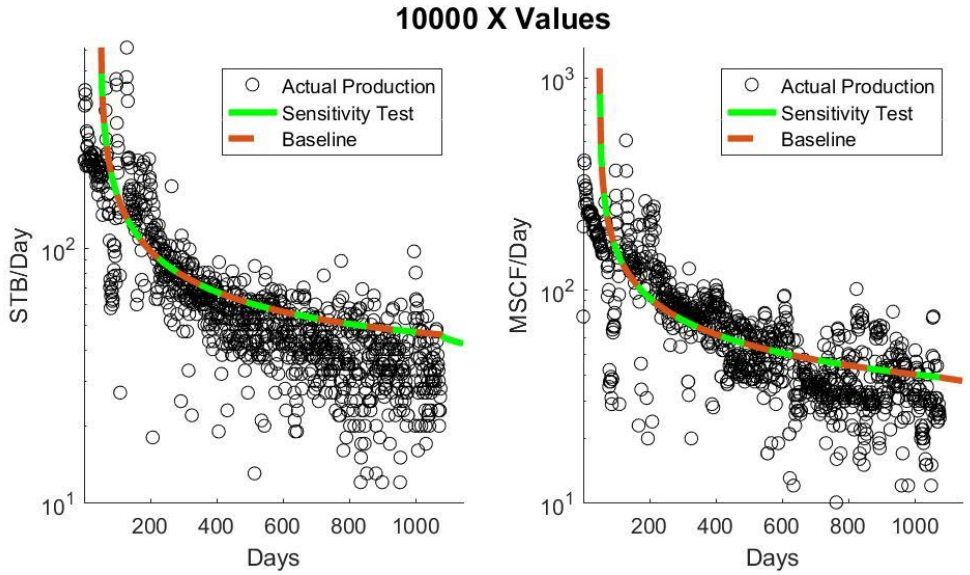

Figure 32: Sensitivity to higher length resolution

The default value actually used in the simulation is a length resolution of 2000 points. This value was chosen so that runs with significantly lower dispersion coefficients would be stable. In this case, with Sample Well 10's dispersion coefficient of 1.02E-6 m^2/s allows the simulation to remain stable until somewhere between fifty and one

hundred points, where the dispersion behavior collapses. Usage of Simpson's Rule is effective enough that the change from a length resolution of 100 to 10,000 points creates no appreciable difference in results with the current settings.

Dispersion Coefficient

The dispersion coefficient itself is the driving factor for the rate of production. While it has no effect on the ultimately recoverable reserves, as it primarily stretches production out with time, it is nonetheless very important for economic purposes.

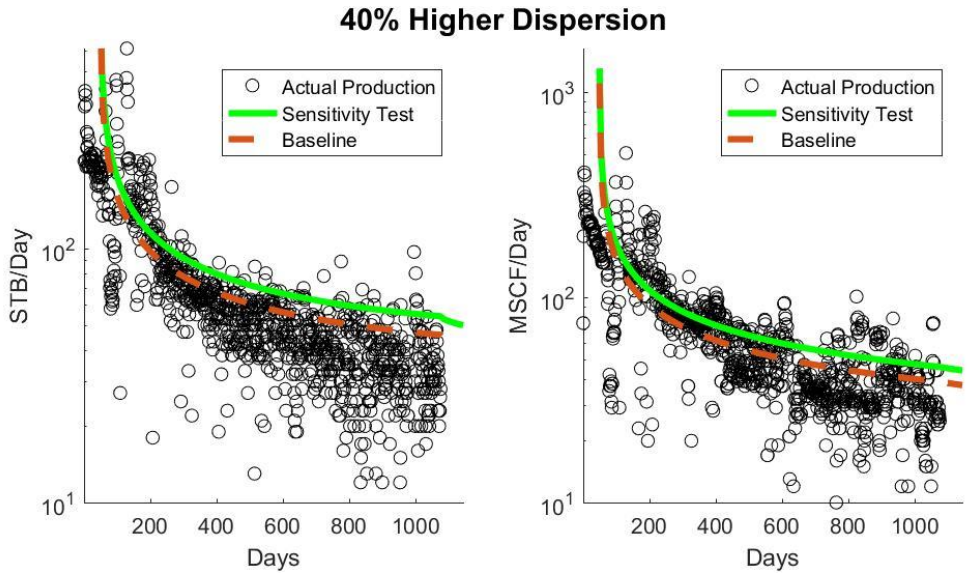

Figure 33: Sensitivity to higher dispersion coefficient

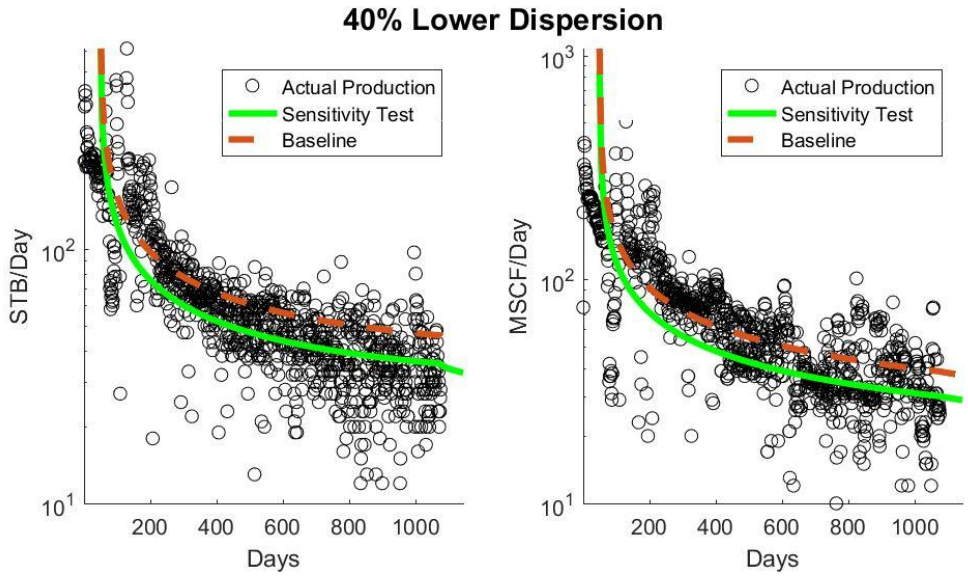

Figure 34: Sensitivity to lower dispersion coefficient

As would be expected, higher dispersion coefficients result in greater production rates, while smaller coefficients result in smaller production rates.

Dispersion Decline Coefficient

In the course of a simulation run, the dispersion coefficient is assumed to be constant. This is likely not true, due to pore throat closures and fluctuations in fluid properties that occur with declining pore pressure. In addition compression of the formation could result in increased production, that is currently being accounted for with the dispersion coefficient. A pressure dependent dispersion coefficient was experimented with, which would use the mean oil pressure of the system to change the dispersion coefficient on each timestep using the following equation:

$$D = D_{base} * exp(-D_{exponent} * (1 - \frac{P_{mean}}{P_{base}})) \quad \text{eqn. 54}$$

Resulting in a gradual decrease in the dispersion coefficient as pressure drops, assuming a positive dispersion decline exponent. This change affects the entire production decline, and additional research will need to be done in order to use it correctly, and to

prevent overfitting. In the base simulation this dispersion decline exponent is set to 0, resulting in a constant dispersion coefficient value.

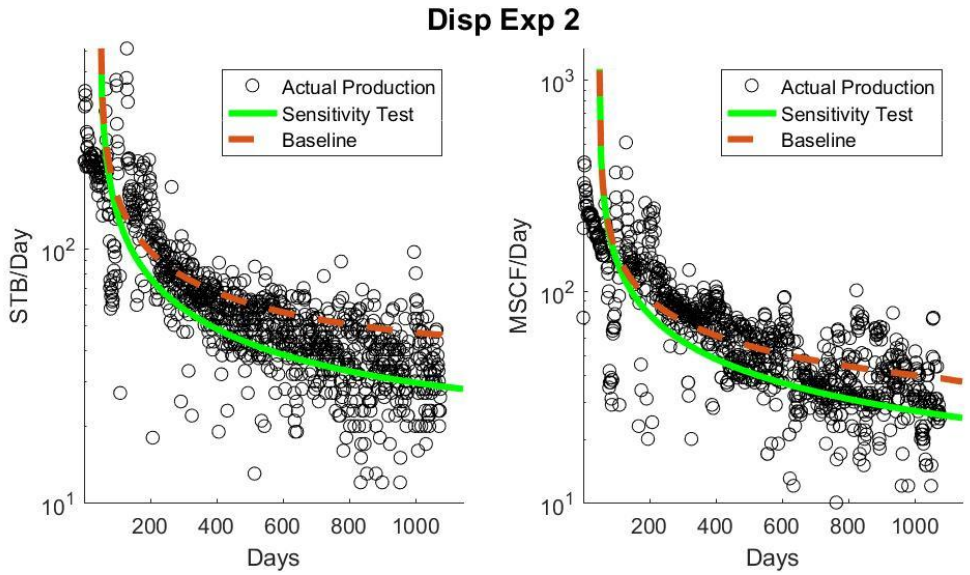

Figure 35: Sensitivity to high dispersion exponent

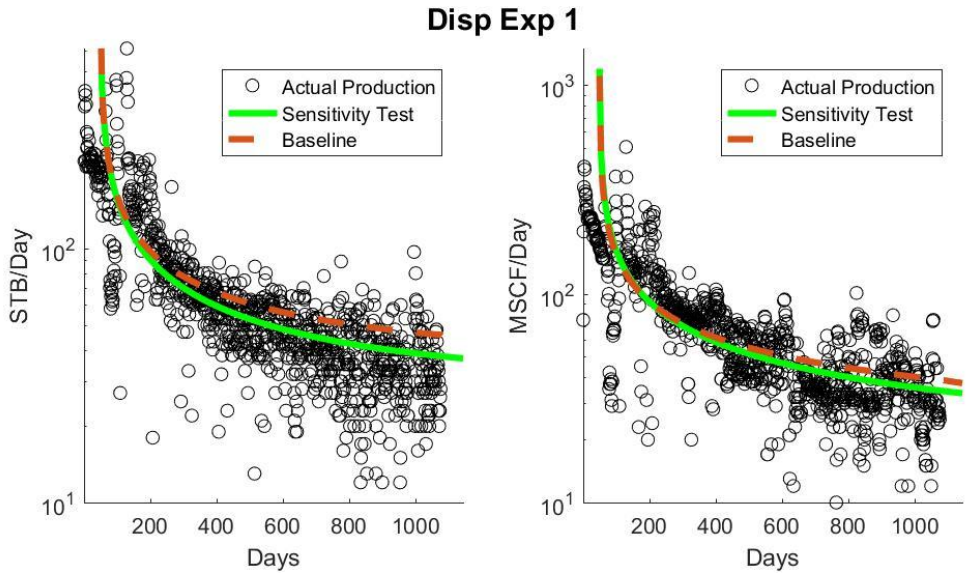

Figure 36: Sensitivity to moderate dispersion exponent

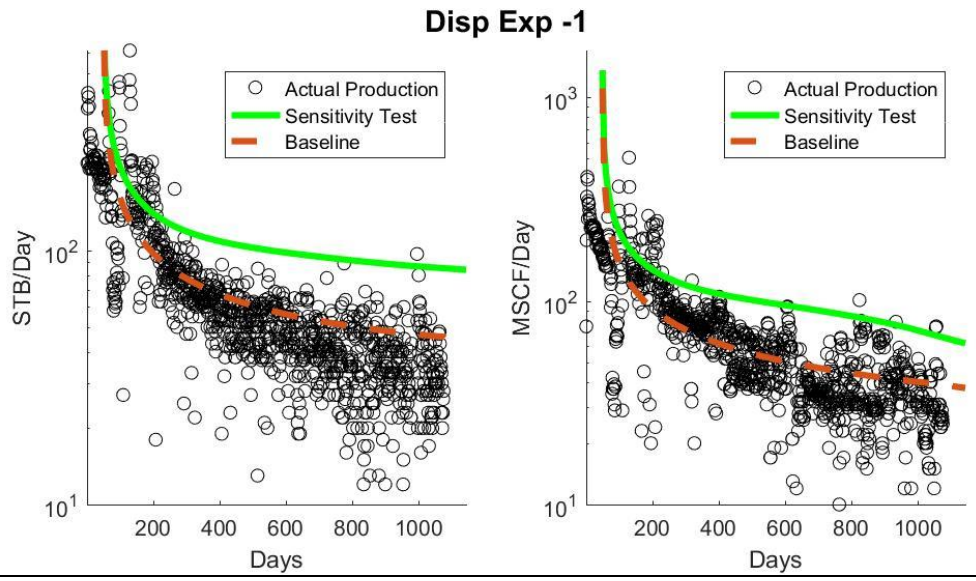

Figure 37: Sensitivity to moderate negative dispersion exponent

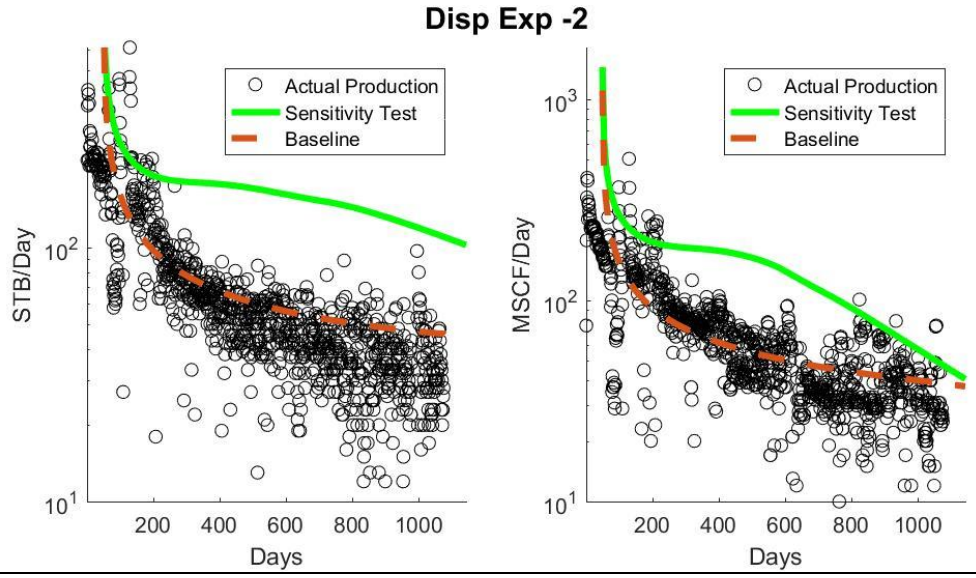

Figure 38: Sensitivity to high negative dispersion exponent

As the dispersion decline exponent just affects the dispersion coefficient it doesn't actually result in changes to the amount of oil and gas that can be produced, it instead affects how rapidly that production. In the case of positive decline exponents production results in ever lower amounts of production, simply slowing the production process. In the case of negative decline exponents there is a significant increase in production as the reservoir pressure drops, reaching the point where the formation rapidly becomes

depleted, and despite the larger dispersion coefficients, there simply isn't enough concentration remaining in the formation matrix to support such high production rates, and the production rates begin to collapse.

Fracture Length

Fracture length acts only as a means to calculate the cross-sectional area of the production zone. This value was calculated on a well by well basis using the OU Well Evaluation Software (2017). As expected, higher and lower lengths simply scale production accordingly:

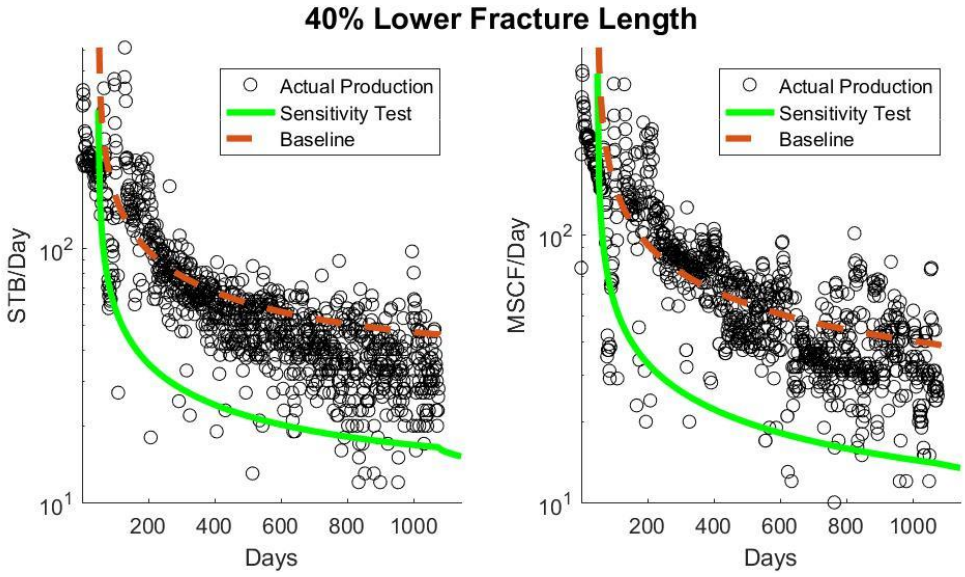

Figure 39: Sensitivity to smaller fracture length

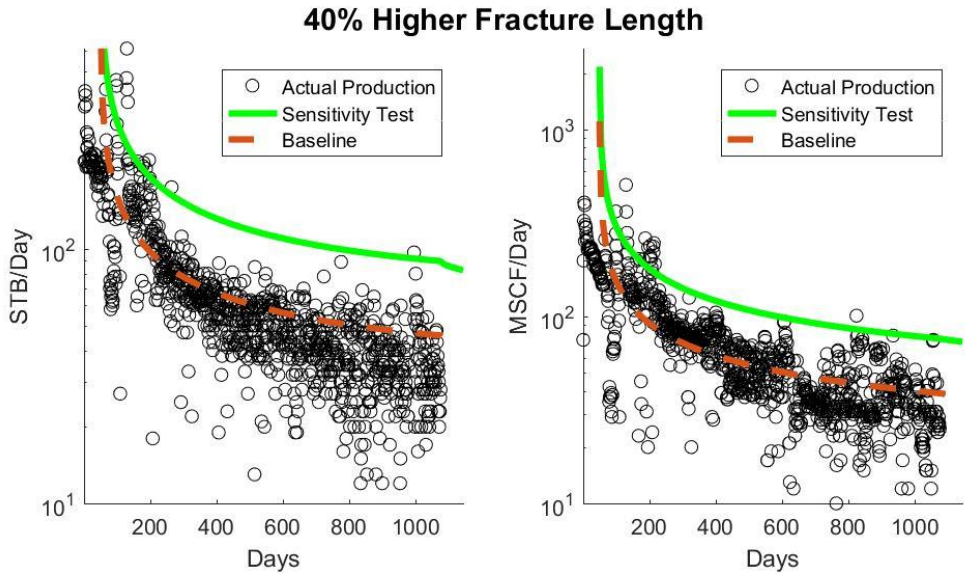

Figure 40: Sensitivity to larger fracture length

Bottom Hole Pressure

BHP is one of the driving forces of production. In situations where BHP is equivalent to formation pressure, no production is expected. For this dispersion based model, BHP primarily determines the boundary concentrations the drive production.

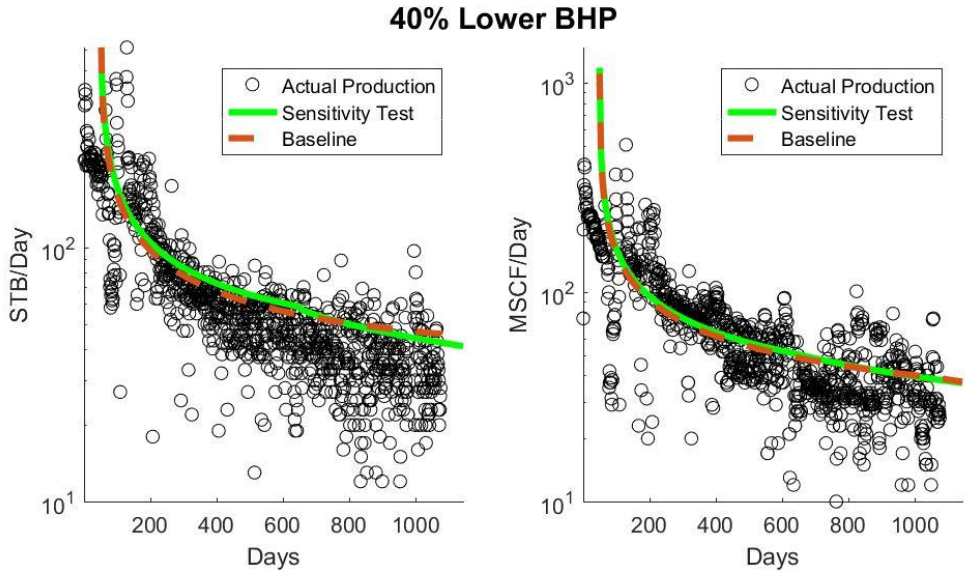

Figure 41: Sensitivity to lower BHP

As there is no support from unstimulated regions to provide additional production, a lower BHP results in draining the formation more quickly. In addition, lower BHP values increase the volume of gas that is released inside of rock matrix, no longer providing a boost to oil concentrations.

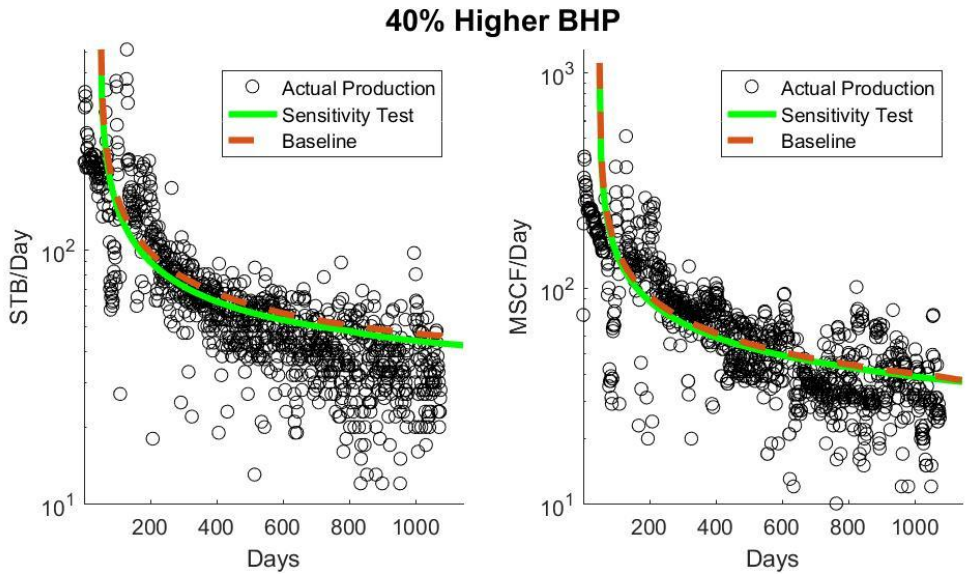

Figure 42: Sensitivity to higher BHP

Slightly higher BHP increase the concentration of oil at the boundary conditions, resulting in a weaker pull from the central regions, and decreased production.

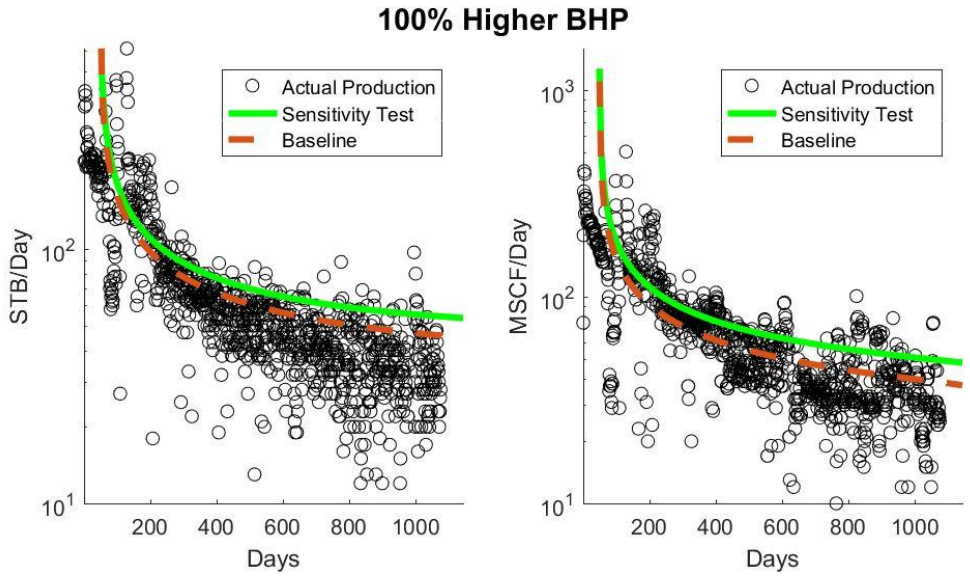

Figure 43: Sensitivity to much higher BHP

Much higher BHP's, which for this well normally range from 440 to 150psi, but in this sensitivity analysis range from 880 to 300 psi, result in less oil production being lost due to the release of gas in the reservoir. As this gas still comes out of solution in the wellbore the net effect is actually higher oil and gas production, despite the higher BHP.

Total Runtime

For any simulation or prediction algorithm runtimes become particularly important as they grow large. A simulation with perfect predictive power that takes a supercomputer a day to run per well, while intellectually interesting, is not particularly useful. While a rather coarse approximation can be more than adequate in certain applications if the computations involved are quick and simple enough. The following runtimes are for running all ten sample wells with their unique well-specific information, using a standard engineering quality desktop computer.

Table 4: Runtimes

X Values	Infinite term size	Time step	Dispersion multiplier	Run Duration

# of points	-	days	-	seconds
2000	10^-20	5	1	86.4
500	10^-20	5	1	64
6000	10^-20	5	1	137.4
2000	10^-25	5	1	84.3
2000	10^-15	5	1	84.4
2000	10^-20	1	1	476.4
2000	10^-20	25	1	44.5
2000	10^-20	5	0.5	100.9
2000	10^-20	5	2	75.5

Advantages of this model

Adopting any new modeling system requires the time of busy professionals, who must learn the intricacies of the given model, as well as its interface. In many cases licenses must also be purchased, software changes must be made, and other tasks must be temporarily set aside. Comparisons must be made between the new model and previous models the company may have employed, and in many cases information must be converted to a new format. In short, there is a burden associated with adopting a new model, so it is important that the change is worthwhile.

Advantages over complex simulations

This model, at its core based on a single dispersivity equation, runs far faster than complex reservoir models. Individual wells can be simulated fast enough for entire sets of different input variables to be explored in a reasonable time, without the need for engineering level hardware. Changes to a simulation can be made essentially “on-the-fly”, in the course of a meeting, or in bulk to consider a whole host of different possibilities, such as to perform a Monte-Carlo analysis. This adds flexibility, and makes it much easier to consider alternate possible scenarios.

Advantages over Graphical Methods

Graphical methods, especially graphical Decline Curve Analysis, while a valuable tool before computers became dominant, is lacking in many areas. The manual adjustment of decline parameters in order to generate a curve that seems to match existing production, or even to predict the performance of new wells, makes it impossible to generate an objective or unique solution, especially when the process is approached by different engineers. It also becomes very difficult to incorporate gradual changes and differences between wells, such as those that may be gleaned by understanding changes in the local geology, or through core analysis.

This method not only allows for the incorporation of additional, well-specific data, such as from a field gradient or core data, but also generates unique, repeatable solutions from a given set of inputs.

Advantages over Type-Curve Matching

Many computer models for generating type curves exist. By allowing a computer to perform matching calculations, a unique, repeatable solution can often be found, and found in a rapid, automated fashion, without the need for direct engineer intervention and regular, manual updating. Yet since these models are, at their core, graphical models, they do not have the ability to accurately predict the effects of changes in reservoir parameters. A temporary shut-in, a better understanding of the reservoir's dimensions or characteristics, or adjustments made to the drilling or fracturing of the well cannot be used to improve a type-curve model, especially when any changes do not match situations for which previous type curves exist.

This model, if implemented correctly, allows for a prediction that is responsive to changes in your understanding of the reservoir, as well as changes in the completion regime of the well. Additionally, due to the model's iterative nature, changes in reservoir parameters can be scheduled into the simulation itself, allowing for a model that accounts for expected occurrences, such as a shut-in.

Limitations of this model

Several limitations exist for this model. While its speed of calculation is exceptional, this is made possible by not accounting for the effects of 3D geometry and reservoir heterogeneity, which many modern simulators consider. While standard decline curve analysis is limited by being a primarily graphical approach, this dispersion model considers both production information, as well as BHP, formation, and fluid information. Any inaccuracy or incorrect assumptions in these inputs will result in inaccuracies in the final result any derived dispersion coefficients. Many effects on fluid properties in the nanoscale are also not accounted for in this model.

Chapter 5: Conclusion

The outcome of this thesis is a new approach for predicting fluid flow in shales. This novel approach for predicting fluid flow in tight shale formations moves beyond many of the limitations of conventional Darcy flow models, and relates microscopic dispersion behavior to field-scale production. The model relates core and fluid properties to resulting production curves, and can account for BHP information when determining either production or the dispersion coefficient associated with the well. The developed modeling tool uses readily available lab-scale data to predict field production using analytical scaling techniques, allowing for realistic predictions to be made of well performance. A simple collection of inputs are required, and the physics of the problem and of shale reservoirs is taken into account. The resulting production information is useful for economic forecasts, while the concentration profiles generated by the model could prove invaluable when considering different EOR applications, as long as the applied BHP information is accurate.

Recommendations and Future Research

This research, and the computer code that explored it, were designed to act as a proof of concept. On multiple occasions changes that would be valuable for a field implementation, when adequate data would be available, were set aside to avoid the risk of overfitting, which would likely be the result of the matching that would be required to pick many of these values. Future research should focus on exploring EOR applications, and how the concentration distribution generated by the program can inform the viability of a well as a potential EOR project. The relationship between permeability and the dispersion coefficient used in the program should also be

investigated, as well as a way to separately account for the effects of Darcy and diffusion based flow.

References

Arps, J. J. (1945, December 1). Analysis of Decline Curves. Society of Petroleum Engineers. doi:10.2118/945228-G

Boomer, R. J. (1995, January 1). Predicting Production Using a Neural Network (Artificial Intelligence Beats Human Intelligence). Society of Petroleum Engineers. doi:10.2118/30202-MS

Cook, J. A. and Ranstam, J. (2016), Overfitting. Br J Surg, 103: 1814. doi:10.1002/bjs.10244

Davudov, D., Moghanloo, R. G., Lan, Y., & Vice, D. (2017, February 15). Investigation of Shale Pore Compressibility Impact on Production with Reservoir Simulation. Society of Petroleum Engineers. doi:10.2118/185059-MS

EIA (2014, March) Tight oil production pushes U.S. crude supply to over 10% of world total, https://www.eia.gov/todayinenergy/detail.php?id=15571

Fetkovich, M. J. (1980, June 1). Decline Curve Analysis Using Type Curves. Society of Petroleum Engineers. doi:10.2118/4629-PA

Haberman, R. (2004). Heat Equation with Zero Temperatures at Finite Ends. In Applied partial differential equations: With Fourier series and boundary value problems. 5th edition, Chap. 2.3.4., 38-43. Upper Saddle River, N.J: Pearson Prentice Hall.

Kanfar, M., & Wattenbarger, R. (2012, January 1). Comparison of Empirical Decline Curve Methods for Shale Wells. Society of Petroleum Engineers. doi:10.2118/162648-MS

Lan, Y., Moghanloo, R. G., & Davudov, D.. Pore Compressibility of Shale Formations. SPE Journal (In Press)

Lake, Larry W. (1989) Enhanced oil recovery. Englewood Cliffs, N.J.: Prentice Hall.

Moghanloo, R.G., Yuan, B., Ingraham, N., Krampf, E., Arrowooda, J., Dadmohammadi, Y. (2015, November). Applying macroscopic material balance to evaluate interplay between dynamic drainage volume and well performance in tight formations, Journal of Natural Gas Science and Engineering, Volume 27, Part 2, Pages 466-478, ISSN 1875-5100, http://doi.org/10.1016/j.jngse.2015.07.047.

Moghanloo, R.G. (2012). Modeling the Fluid Flow of Carbon Dioxide through Permeable Media (Doctoral Dissertation). Retrieved from https://repositories.lib.utexas.edu/handle/2152/ETD-UT-2012-05-4813

OU Well Evaluation Software. (2017), OTD Invention No. 2017-043, University of Okalhoma

Portellaand, R. C. M., & Prais, F. (1999, January 1). Use of Automatic History Matching and Geostatistical Simulation to Improve Production Forecast. Society of Petroleum Engineers. doi:10.2118/53976-MS

Purvis, D. C. (2016, May 10). The Practice of Decline Curve Analysis. Society of Petroleum Engineers. doi:10.2118/179979-MS

Rajvanshi, A. K., Gmelig Meyling, R., & Ten Haaf, D. (2012, January 1). Instilling Realism in Production Forecasts: Dos and Don. Society of Petroleum Engineers. doi:10.2118/155443-MS

Ramey, H.J. Jr. 1973. Correlations of Surface and Interfacial Tensions of Reservoir Fluids. Paper SPE-4429-MS available from SPE, Richardson, Texas.

Ran, B., & Kelkar, M. (2015, July 20). Fracture Stages Optimization in Bakken Shale Formation. Unconventional Resources Technology Conference. doi:10.15530/URTEC-2015-2154796

Rao, D., & Lee, J., Determination of gas–oil miscibility conditions by interfacial tension measurements, Journal of Colloid and Interface Science, Volume 262, Issue 2, 15 June 2003, Pages 474-482, ISSN 0021-9797, http://doi.org/10.1016/S0021-9797(03)00175-9.

Rotondi, M., Nicotra, G., Godi, A., Contento, F. M., Blunt, M. J., & Christie, M. (2006, January 1). Hydrocarbon Production Forecast and Uncertainty Quantification: A Field Application. Society of Petroleum Engineers. doi:10.2118/102135-MS

Sigal, R. F., Devegowda, D., & Civan, F. (2015, August 10). On the Equilibrium State of Shale Gas Reservoirs. Society of Petrophysicists and Well-Log Analysts.

Swami, V., Clarkson, C. R., & Settari, A. (2012, January 1). Non-Darcy Flow in Shale Nanopores: Do We Have a Final Answer? Society of Petroleum Engineers. doi:10.2118/162665-MS

Wang, B., Markitell, B. N., & Huang, W. S. (1993, January 1). Case Studies of Horizontal Well Design and Production Forecast. Society of Petroleum Engineers. doi:10.2118/25567-MS

Wang, H., & Marongiu-Porcu, M. (2015, November 1). Impact of Shale-Gas Apparent Permeability on Production: Combined Effects of Non-Darcy Flow/Gas-Slippage, Desorption, and Geomechanics. Society of Petroleum Engineers. doi:10.2118/173196-PA

Warren, J. E., & Skiba, F. F. (1964, September 1). Macroscopic Dispersion. Society of Petroleum Engineers. doi:10.2118/648-PA

Whitson, C.H. and Brulé, M.R. 2000. Phase Behavior, No. 20, Chap. 3. Richardson, Texas: Henry L. Doherty Monograph Series, Society of Petroleum Engineers.

Yemez, I., Singh, V., Orellana, N. H., & Izaguirre, E. (2014, December 10). Factors Contributing to Uncertain Production Forecasts: 3D Reservoir Modelling Perspectives. International Petroleum Technology Conference. doi:10.2523/IPTC-18196-MS

Yuan, B., Zheng, D., & Ghanbarnezhad Moghanloo, R. (2016, August 24). Integrated Production Analysis Using the Concept of Dynamic Drainage Volume: Modelling, Simulation and Field Applications. Society of Petroleum Engineers. doi:10.2118/181781-MS

Zhang, K., Dong, X., Li, J., Lv, J., Wu, K., Kusalik, P., & Chen, Z. (2016, August 1). Effect of Nanoscale Pore Confinement on Multi-Component Phase Equilibrium. Unconventional Resources Technology Conference.

Zheng, D., Moghanloo, R. G., Yuan, B., & Dong, X. (2016, August 24). Modeling Dynamic Drainage Volume for Multi-Stage Fractured Wells in Composite Shale Systems: New Analytical Solution for Transient Linear Flow. Society of Petroleum Engineers. doi:10.2118/181875-MS

Appendix A: Nomenclature

C_{gas}	Concentration of gas, gmol/m^3
C_{oil}	Concentration of oil with in-solution gas contribution, gmol/m^3
D_{diff}	Diffusion coefficient, m^2/s
D_{disp}	Dispersivity, m^2/s
D_{lab}	Dispersion coefficient at the lab-scale, m^2/s
D_{SRV}	Dispersion coefficient of the SRV, m^2/s
F_t	Time scaling factor, s/s
FVF	Formation Volume Factor (res vol/standard vol)
IC^3	Integrated Core Characterization Center
L_{REV}	Length of the REV, m
L_{SRV}	Length of the SRV, m
MICP	Mercury Injection Capillary Pressure
M_{og}	Molecular weight of oil with in-solution gas, g/gmol
M_{og}	Molecular weight of gas with in-solution oil, g/gmol
σ	Interfacial Tension, dynes/cm
φ	Porosity, p.u.
S	Fluid Saturation
τ	Tortuosity coefficient
u	Fluid velocity, m/s
x_g	Mole fraction of gas in the oil phase
x_o	Mole fraction of oil in the oil phase

y_g	Mole fraction of gas in the gas phase
y_o	Mole fraction of oil in the gas phase

Appendix B: Tables

Table 5: Example Production data from well M47L6HRJ47
Headers are Time (day), Oil Production (stb/day), and Gas Production (Mscf/day)

Time Days	Q_oil STB	Q_gas MSCF	BHP psia	Time Days	Q_oil STB	Q_gas MSCF	BHP psia	Time Days	Q_oil STB	Q_gas MSCF	BHP psia
1	0	14	440.8	360	63	68	343.9	719	43	28	247.0
2	31	75	440.6	361	66	77	343.6	720	35	33	246.7
3	221	199	440.3	362	63	72	343.4	721	43	32	246.4
4	363	325	440.0	363	80	74	343.1	722	45	31	246.2
5	418	407	439.8	364	73	96	342.8	723	33	27	245.9
6	402	394	439.5	365	50	104	342.6	724	38	39	245.6
7	222	253	439.2	366	57	66	342.3	725	78	36	245.4
8	370	310	439.0	367	58	75	342.0	726	32	38	245.1
9	210	301	438.7	368	65	75	341.8	727	47	36	244.8
10	288	298	438.4	369	60	90	341.5	728	45	55	244.6
11	249	279	438.1	370	63	68	341.2	729	40	35	244.3
12	252	265	437.9	371	69	79	340.9	730	42	41	244.0
13	282	255	437.6	372	63	95	340.7	731	27	45	243.7
14	210	253	437.3	373	67	66	340.4	732	40	34	243.5
15	228	229	437.1	374	50	81	340.1	733	0	28	243.2
16	212	227	436.8	375	63	91	339.9	734	45	19	242.9
17	266	235	436.5	376	80	57	339.6	735	50	29	242.7
18	210	236	436.3	377	47	89	339.3	736	58	31	242.4
19	235	232	436.0	378	77	56	339.1	737	35	63	242.1
20	223	229	435.7	379	43	81	338.8	738	33	32	241.9
21	236	227	435.4	380	67	89	338.5	739	52	30	241.6
22	219	233	435.2	381	65	56	338.2	740	37	48	241.3
23	230	230	434.9	382	50	66	338.0	741	39	34	241.0
24	219	235	434.6	383	73	74	337.7	742	56	31	240.8
25	233	234	434.4	384	53	76	337.4	743	30	53	240.5
26	229	233	434.1	385	62	87	337.2	744	33	42	240.2
27	222	231	433.8	386	67	54	336.9	745	50	38	240.0
28	222	222	433.6	387	55	79	336.6	746	32	45	239.7
29	209	215	433.3	388	67	60	336.4	747	33	27	239.4
30	205	206	433.0	389	48	77	336.1	748	27	38	239.2
31	213	203	432.7	390	40	29	335.8	749	48	44	238.9
32	237	214	432.5	391	72	74	335.5	750	40	25	238.6
33	208	188	432.2	392	68	85	335.3	751	40	32	238.3
34	221	215	431.9	393	43	56	335.0	752	43	36	238.1
35	223	216	431.7	394	72	28	334.7	753	43	43	237.8
36	202	203	431.4	395	72	83	334.5	754	33	43	237.5
37	202	204	431.1	396	50	83	334.2	755	33	31	237.3

38	192	200	430.9	397	76	68	333.9	756	35	23	237.0
39	233	199	430.6	398	71	88	333.7	757	41	30	236.7
40	178	190	430.3	399	55	94	333.4	758	42	38	236.5
41	198	180	430.0	400	62	83	333.1	759	27	33	236.2
42	194	179	429.8	401	63	86	332.8	760	48	29	235.9
43	208	183	429.5	402	60	105	332.6	761	23	32	235.6
44	182	184	429.2	403	69	95	332.3	762	39	33	235.4
45	162	180	429.0	404	53	100	332.0	763	41	26	235.1
46	176	178	428.7	405	55	94	331.8	764	35	26	234.8
47	190	184	428.4	406	65	91	331.5	765	35	10	234.6
48	210	187	428.2	407	54	98	331.2	766	40	16	234.3
49	207	182	427.9	408	19	83	331.0	767	38	36	234.0
50	198	169	427.6	409	88	78	330.7	768	60	51	233.8
51	210	165	427.3	410	55	85	330.4	769	35	65	233.5
52	178	163	427.1	411	63	85	330.1	770	22	66	233.2
53	196	172	426.8	412	53	75	329.9	771	47	0	232.9
54	200	165	426.5	413	65	83	329.6	772	62	61	232.7
55	192	161	426.3	414	60	85	329.3	773	50	59	232.4
56	190	159	426.0	415	48	57	329.1	774	22	32	232.1
57	220	159	425.7	416	32	64	328.8	775	30	23	231.9
58	135	153	425.5	417	53	67	328.5	776	0	23	231.6
59	174	148	425.2	418	38	39	328.3	777	89	33	231.3
60	211	148	424.9	419	42	39	328.0	778	30	17	231.1
61	150	148	424.6	420	70	62	327.7	779	25	26	230.8
62	2	148	424.4	421	63	52	327.4	780	26	26	230.5
63	0	148	424.1	422	58	74	327.2	781	64	45	230.2
64	0	148	423.8	423	75	55	326.9	782	28	32	230.0
65	0	148	423.6	424	53	67	326.6	783	40	41	229.7
66	0	0	423.3	425	67	79	326.4	784	16	32	229.4
67	348	161	423.0	426	67	52	326.1	785	53	31	229.2
68	425	259	422.8	427	50	70	325.8	786	35	31	228.9
69	268	211	422.5	428	57	58	325.6	787	28	42	228.6
70	229	207	422.2	429	62	82	325.3	788	37	33	228.4
71	235	199	421.9	430	67	63	325.0	789	55	61	228.1
72	201	178	421.7	431	45	73	324.7	790	32	30	227.8
73	205	169	421.4	432	62	79	324.5	791	37	30	227.5
74	162	146	421.1	433	72	54	324.2	792	50	31	227.3
75	164	129	420.9	434	23	73	323.9	793	18	32	227.0
76	136	93	420.6	435	41	37	323.7	794	52	45	226.7
77	147	121	420.3	436	47	36	323.4	795	35	32	226.5
78	137	131	420.1	437	57	66	323.1	796	47	38	226.2
79	107	100	419.8	438	58	36	322.9	797	23	33	225.9
80	70	35	419.5	439	43	63	322.6	798	35	33	225.7
81	75	42	419.2	440	45	38	322.3	799	38	34	225.4
82	58	37	419.0	441	60	52	322.0	800	35	39	225.1

83	65	37	418.7	442	53	57	321.8	801	37	46	224.8
84	72	37	418.4	443	57	44	321.5	802	58	50	224.6
85	67	37	418.2	444	62	68	321.2	803	30	49	224.3
86	68	39	417.9	445	42	42	321.0	804	20	31	224.0
87	62	31	417.6	446	57	46	320.7	805	47	38	223.8
88	60	29	417.4	447	62	68	320.4	806	55	60	223.5
89	63	38	417.1	448	38	42	320.2	807	25	33	223.2
90	77	38	416.8	449	81	48	319.9	808	50	38	223.0
91	103	65	416.5	450	38	65	319.6	809	2	32	222.7
92	82	63	416.3	451	50	44	319.3	810	35	42	222.4
93	97	67	416.0	452	67	61	319.1	811	46	28	222.1
94	102	76	415.7	453	44	48	318.8	812	45	23	221.9
95	78	68	415.5	454	73	46	318.5	813	28	31	221.6
96	93	67	415.2	455	42	66	318.3	814	23	41	221.3
97	131	78	414.9	456	67	41	318.0	815	40	32	221.1
98	73	87	414.7	457	58	54	317.7	816	35	48	220.8
99	462	204	414.4	458	42	71	317.5	817	20	30	220.5
100	438	365	414.1	459	50	43	317.2	818	48	31	220.3
101	310	278	413.8	460	62	61	316.9	819	55	22	220.0
102	264	239	413.6	461	52	49	316.6	820	30	31	219.7
103	198	207	413.3	462	66	47	316.4	821	33	36	219.4
104	215	184	413.0	463	43	66	316.1	822	32	49	219.2
105	248	167	412.8	464	55	44	315.8	823	25	31	218.9
106	143	152	412.5	465	60	75	315.6	824	37	35	218.6
107	138	142	412.2	466	42	39	315.3	825	48	35	218.4
108	138	131	412.0	467	45	45	315.0	826	54	101	218.1
109	132	116	411.7	468	52	49	314.8	827	48	78	217.8
110	78	95	411.4	469	52	50	314.5	828	32	70	217.6
111	27	29	411.1	470	57	40	314.2	829	57	71	217.3
112	0	0	410.9	471	57	72	313.9	830	42	80	217.0
113	0	0	410.6	472	39	41	313.7	831	20	65	216.7
114	0	0	410.3	473	73	70	313.4	832	32	33	216.5
115	0	0	410.1	474	45	40	313.1	833	58	67	216.2
116	0	0	409.8	475	65	48	312.9	834	3	33	215.9
117	0	0	409.5	476	40	59	312.6	835	58	16	215.7
118	0	0	409.3	477	48	42	312.3	836	12	17	215.4
119	0	0	409.0	478	59	68	312.1	837	15	31	215.1
120	0	0	408.7	479	52	41	311.8	838	17	22	214.9
121	0	0	408.4	480	62	43	311.5	839	23	29	214.6
122	0	0	408.2	481	45	70	311.2	840	45	32	214.3
123	0	0	407.9	482	53	41	311.0	841	69	73	214.0
124	0	0	407.6	483	50	69	310.7	842	52	51	213.8
125	0	0	407.4	484	43	39	310.4	843	50	73	213.5
126	0	0	407.1	485	75	47	310.2	844	47	76	213.2
127	0	0	406.8	486	51	61	309.9	845	45	70	213.0

128	0	0	406.6	487	33	48	309.6	846	23	45	212.7
129	0	0	406.3	488	63	68	309.4	847	3	27	212.4
130	470	153	406.0	489	38	37	309.1	848	17	15	212.2
131	614	506	405.7	490	43	43	308.8	849	20	18	211.9
132	424	363	405.5	491	62	65	308.5	850	28	20	211.6
133	223	164	405.2	492	47	39	308.3	851	27	22	211.3
134	378	280	404.9	493	58	49	308.0	852	47	32	211.1
135	216	247	404.7	494	55	65	307.7	853	34	50	210.8
136	225	218	404.4	495	57	42	307.5	854	43	26	210.5
137	227	192	404.1	496	27	61	307.2	855	13	24	210.3
138	162	171	403.9	497	37	5	306.9	856	60	21	210.0
139	170	157	403.6	498	59	47	306.7	857	30	29	209.7
140	167	147	403.3	499	60	64	306.4	858	30	29	209.5
141	155	138	403.0	500	50	44	306.1	859	37	33	209.2
142	132	130	402.8	501	53	55	305.8	860	25	32	208.9
143	140	122	402.5	502	62	63	305.6	861	38	32	208.6
144	176	133	402.2	503	42	41	305.3	862	25	30	208.4
145	207	181	402.0	504	63	68	305.0	863	25	32	208.1
146	137	154	401.7	505	38	38	304.8	864	42	27	207.8
147	162	144	401.4	506	58	48	304.5	865	43	29	207.6
148	147	137	401.2	507	48	61	304.2	866	23	30	207.3
149	153	132	400.9	508	58	59	304.0	867	25	29	207.0
150	136	127	400.6	509	40	48	303.7	868	50	39	206.8
151	171	128	400.3	510	50	42	303.4	869	30	33	206.5
152	123	135	400.1	511	53	70	303.1	870	30	32	206.2
153	142	128	399.8	512	43	38	302.9	871	38	29	205.9
154	141	128	399.5	513	60	44	302.6	872	35	31	205.7
155	133	128	399.3	514	50	64	302.3	873	38	29	205.4
156	129	118	399.0	515	53	38	302.1	874	32	29	205.1
157	117	108	398.7	516	13	56	301.8	875	52	29	204.9
158	150	119	398.5	517	85	42	301.5	876	65	30	204.6
159	137	141	398.2	518	50	61	301.3	877	60	30	204.3
160	128	127	397.9	519	43	37	301.0	878	40	29	204.1
161	60	97	397.6	520	58	56	300.7	879	40	30	203.8
162	2	0	397.4	521	43	47	300.4	880	38	28	203.5
163	65	0	397.1	522	62	61	300.2	881	33	28	203.2
164	221	199	396.8	523	40	45	299.9	882	13	46	203.0
165	170	159	396.6	524	57	63	299.6	883	20	67	202.7
166	155	126	396.3	525	38	39	299.4	884	33	66	202.4
167	137	127	396.0	526	43	41	299.1	885	48	59	202.2
168	109	114	395.8	527	53	53	298.8	886	42	62	201.9
169	4	23	395.5	528	62	51	298.6	887	40	62	201.6
170	0	0	395.2	529	37	53	298.3	888	45	64	201.4
171	205	88	394.9	530	59	49	298.0	889	34	63	201.1
172	192	203	394.7	531	38	52	297.7	890	6	40	200.8

173	148	134	394.4	532	58	48	297.5	891	28	39	200.5
174	150	128	394.1	533	38	54	297.2	892	33	32	200.3
175	98	118	393.9	534	60	43	296.9	893	48	32	200.0
176	75	45	393.6	535	62	52	296.7	894	18	19	199.7
177	0	34	393.3	536	50	42	296.4	895	43	20	199.5
178	0	0	393.1	537	21	54	296.1	896	34	18	199.2
179	212	140	392.8	538	45	37	295.9	897	46	68	198.9
180	112	151	392.5	539	64	68	295.6	898	43	65	198.7
181	0	0	392.2	540	38	39	295.3	899	40	64	198.4
182	218	0	392.0	541	55	39	295.0	900	27	59	198.1
183	184	202	391.7	542	48	61	294.8	901	12	35	197.8
184	142	130	391.4	543	40	36	294.5	902	35	42	197.6
185	71	102	391.2	544	60	54	294.2	903	38	43	197.3
186	0	0	390.9	545	37	49	294.0	904	33	39	197.0
187	0	0	390.6	546	20	31	293.7	905	35	46	196.8
188	148	3	390.4	547	0	0	293.4	906	35	67	196.5
189	207	262	390.1	548	75	6	293.2	907	26	31	196.2
190	163	143	389.8	549	65	78	292.9	908	44	26	196.0
191	132	119	389.5	550	80	77	292.6	909	28	33	195.7
192	107	101	389.3	551	45	74	292.3	910	29	40	195.4
193	0	31	389.0	552	42	39	292.1	911	33	6	195.1
194	0	0	388.7	553	50	40	291.8	912	28	30	194.9
195	3	3	388.5	554	51	45	291.5	913	32	28	194.6
196	0	0	388.2	555	45	49	291.3	914	30	28	194.3
197	110	20	387.9	556	34	54	291.0	915	40	30	194.1
198	224	234	387.7	557	0	17	290.7	916	45	31	193.8
199	186	171	387.4	558	63	17	290.5	917	53	40	193.5
200	190	171	387.1	559	63	63	290.2	918	33	44	193.3
201	163	154	386.8	560	50	55	289.9	919	31	44	193.0
202	127	119	386.6	561	60	60	289.6	920	22	42	192.7
203	177	211	386.3	562	41	49	289.4	921	33	33	192.4
204	157	239	386.0	563	55	63	289.1	922	40	43	192.2
205	117	208	385.8	564	57	39	288.8	923	35	37	191.9
206	114	202	385.5	565	33	45	288.6	924	17	7	191.6
207	103	144	385.2	566	58	67	288.3	925	42	48	191.4
208	118	182	385.0	567	8	34	288.0	926	33	48	191.1
209	18	132	384.7	568	0	0	287.8	927	33	42	190.8
210	103	24	384.4	569	69	19	287.5	928	27	22	190.6
211	148	171	384.1	570	63	60	287.2	929	2	3	190.3
212	137	93	383.9	571	60	58	286.9	930	0	0	190.0
213	120	237	383.6	572	61	59	286.7	931	0	0	189.7
214	95	221	383.3	573	50	64	286.4	932	57	9	189.5
215	101	247	383.1	574	58	56	286.1	933	42	50	189.2
216	100	131	382.8	575	42	56	285.9	934	58	50	188.9
217	114	131	382.5	576	45	40	285.6	935	45	44	188.7

218	63	191	382.3	577	48	62	285.3	936	43	79	188.4
219	123	115	382.0	578	58	35	285.1	937	40	41	188.1
220	106	115	381.7	579	27	51	284.8	938	38	43	187.9
221	90	115	381.4	580	68	55	284.5	939	40	37	187.6
222	67	96	381.2	581	45	43	284.2	940	48	36	187.3
223	70	90	380.9	582	35	49	284.0	941	22	44	187.0
224	115	122	380.6	583	45	29	283.7	942	33	39	186.8
225	100	110	380.4	584	44	43	283.4	943	30	35	186.5
226	63	113	380.1	585	50	48	283.2	944	38	37	186.2
227	123	123	379.8	586	38	38	282.9	945	25	27	186.0
228	93	122	379.6	587	56	48	282.6	946	40	59	185.7
229	105	128	379.3	588	32	42	282.4	947	33	54	185.4
230	82	102	379.0	589	42	38	282.1	948	37	50	185.2
231	110	138	378.7	590	3	19	281.8	949	30	35	184.9
232	76	111	378.5	591	0	0	281.5	950	32	31	184.6
233	103	93	378.2	592	62	6	281.3	951	28	49	184.3
234	80	126	377.9	593	68	64	281.0	952	40	35	184.1
235	84	125	377.7	594	65	65	280.7	953	40	31	183.8
236	70	88	377.4	595	62	51	280.5	954	23	39	183.5
237	95	74	377.1	596	58	54	280.2	955	12	37	183.3
238	82	115	376.9	597	55	58	279.9	956	15	3	183.0
239	89	83	376.6	598	45	70	279.7	957	60	49	182.7
240	105	92	376.3	599	46	37	279.4	958	45	53	182.5
241	75	103	376.0	600	55	58	279.1	959	34	40	182.2
242	85	91	375.8	601	43	42	278.8	960	25	35	181.9
243	77	85	375.5	602	48	47	278.6	961	32	24	181.6
244	95	82	375.2	603	47	67	278.3	962	33	12	181.4
245	97	114	375.0	604	41	37	278.0	963	35	56	181.1
246	98	118	374.7	605	60	0	277.8	964	27	47	180.8
247	77	101	374.4	606	0	0	277.5	965	23	17	180.6
248	79	97	374.2	607	0	93	277.2	966	41	45	180.3
249	86	91	373.9	608	28	0	277.0	967	38	45	180.0
250	81	101	373.6	609	55	94	276.7	968	33	40	179.8
251	88	100	373.3	610	42	64	276.4	969	25	25	179.5
252	61	100	373.1	611	23	82	276.1	970	28	40	179.2
253	95	93	372.8	612	50	79	275.9	971	53	44	178.9
254	78	84	372.5	613	47	74	275.6	972	30	43	178.7
255	89	88	372.3	614	38	66	275.3	973	28	45	178.4
256	82	84	372.0	615	45	60	275.1	974	20	44	178.1
257	93	92	371.7	616	48	50	274.8	975	27	44	177.9
258	67	74	371.5	617	55	72	274.5	976	40	34	177.6
259	78	79	371.2	618	37	60	274.3	977	27	34	177.3
260	57	71	370.9	619	42	59	274.0	978	22	30	177.1
261	102	69	370.6	620	55	60	273.7	979	22	32	176.8
262	102	121	370.4	621	57	56	273.4	980	35	1	176.5

263	52	108	370.1	622	45	45	273.2	981	43	25	176.2
264	83	55	369.8	623	43	21	272.9	982	0	12	176.0
265	92	98	369.6	624	50	21	272.6	983	0	0	175.7
266	175	85	369.3	625	43	13	272.4	984	0	0	175.4
267	0	81	369.0	626	43	5	272.1	985	0	0	175.2
268	65	83	368.8	627	5	1	271.8	986	0	0	174.9
269	83	88	368.5	628	65	1	271.6	987	0	0	174.6
270	78	82	368.2	629	40	5	271.3	988	0	0	174.4
271	80	82	367.9	630	50	1	271.0	989	0	0	174.1
272	85	66	367.7	631	32	0	270.7	990	0	0	173.8
273	50	66	367.4	632	37	0	270.5	991	0	0	173.5
274	85	76	367.1	633	47	0	270.2	992	0	0	173.3
275	92	86	366.9	634	55	0	269.9	993	0	0	173.0
276	68	94	366.6	635	52	0	269.7	994	0	0	172.7
277	85	87	366.3	636	27	12	269.4	995	0	0	172.5
278	72	86	366.1	637	21	58	269.1	996	7	0	172.2
279	82	85	365.8	638	42	41	268.9	997	97	32	171.9
280	76	91	365.5	639	19	32	268.6	998	53	31	171.7
281	67	83	365.2	640	32	3	268.3	999	30	32	171.4
282	82	80	365.0	641	33	23	268.0	1000	20	35	171.1
283	55	86	364.7	642	25	26	267.8	1001	33	34	170.8
284	102	70	364.4	643	52	28	267.5	1002	80	30	170.6
285	77	91	364.2	644	19	32	267.2	1003	63	52	170.3
286	68	82	363.9	645	64	36	267.0	1004	50	32	170.0
287	78	83	363.6	646	52	58	266.7	1005	58	46	169.8
288	78	82	363.4	647	23	27	266.4	1006	62	46	169.5
289	75	83	363.1	648	37	30	266.2	1007	53	43	169.2
290	80	83	362.8	649	37	32	265.9	1008	37	43	169.0
291	77	80	362.5	650	65	50	265.6	1009	16	42	168.7
292	65	87	362.3	651	40	27	265.3	1010	27	40	168.4
293	65	81	362.0	652	43	33	265.1	1011	20	35	168.1
294	25	81	361.7	653	48	40	264.8	1012	48	27	167.9
295	68	54	361.5	654	38	43	264.5	1013	42	29	167.6
296	112	96	361.2	655	39	36	264.3	1014	43	41	167.3
297	92	85	360.9	656	37	32	264.0	1015	37	40	167.1
298	87	67	360.7	657	32	26	263.7	1016	47	34	166.8
299	73	101	360.4	658	38	27	263.5	1017	28	34	166.5
300	73	90	360.1	659	28	27	263.2	1018	30	28	166.3
301	47	75	359.8	660	0	3	262.9	1019	20	30	166.0
302	103	86	359.6	661	0	0	262.6	1020	35	20	165.7
303	67	79	359.3	662	0	0	262.4	1021	47	23	165.4
304	72	82	359.0	663	0	0	262.1	1022	53	21	165.2
305	90	88	358.8	664	70	7	261.8	1023	47	22	164.9
306	57	81	358.5	665	64	41	261.6	1024	33	22	164.6
307	65	79	358.2	666	65	40	261.3	1025	27	21	164.4

308	63	77	358.0	667	63	46	261.0	1026	28	20	164.1
309	78	79	357.7	668	55	47	260.8	1027	38	22	163.8
310	80	76	357.4	669	43	45	260.5	1028	43	19	163.6
311	63	77	357.1	670	42	43	260.2	1029	28	20	163.3
312	81	63	356.9	671	53	40	259.9	1030	40	32	163.0
313	47	78	356.6	672	40	39	259.7	1031	23	31	162.7
314	86	81	356.3	673	50	33	259.4	1032	20	30	162.5
315	62	80	356.1	674	47	40	259.1	1033	17	23	162.2
316	75	80	355.8	675	47	39	258.9	1034	27	16	161.9
317	33	73	355.5	676	38	38	258.6	1035	35	15	161.7
318	87	37	355.3	677	40	35	258.3	1036	43	15	161.4
319	55	37	355.0	678	42	37	258.1	1037	54	15	161.1
320	99	32	354.7	679	42	35	257.8	1038	28	40	160.9
321	75	126	354.4	680	48	36	257.5	1039	22	35	160.6
322	64	76	354.2	681	47	33	257.2	1040	30	43	160.3
323	78	78	353.9	682	32	40	257.0	1041	23	40	160.0
324	73	81	353.6	683	38	36	256.7	1042	22	43	159.8
325	62	78	353.4	684	48	36	256.4	1043	20	43	159.5
326	65	65	353.1	685	44	35	256.2	1044	33	31	159.2
327	22	60	352.8	686	45	28	255.9	1045	36	30	159.0
328	87	20	352.6	687	45	42	255.6	1046	33	30	158.7
329	83	99	352.3	688	33	35	255.4	1047	32	29	158.4
330	86	82	352.0	689	52	35	255.1	1048	23	30	158.2
331	60	80	351.7	690	40	36	254.8	1049	27	29	157.9
332	70	83	351.5	691	55	36	254.5	1050	30	30	157.6
333	72	77	351.2	692	47	34	254.3	1051	37	12	157.3
334	67	77	350.9	693	37	32	254.0	1052	44	15	157.1
335	68	76	350.7	694	27	36	253.7	1053	30	31	156.8
336	72	78	350.4	695	53	34	253.5	1054	28	27	156.5
337	66	74	350.1	696	37	34	253.2	1055	30	49	156.3
338	63	76	349.9	697	30	34	252.9	1056	37	74	156.0
339	73	71	349.6	698	52	34	252.7	1057	40	75	155.7
340	70	69	349.3	699	28	35	252.4	1058	32	75	155.5
341	55	84	349.0	700	60	35	252.1	1059	33	48	155.2
342	65	73	348.8	701	40	35	251.8	1060	28	30	154.9
343	67	76	348.5	702	43	39	251.6	1061	30	25	154.6
344	80	74	348.2	703	38	35	251.3	1062	0	0	154.4
345	63	76	348.0	704	37	36	251.0	1063	47	44	154.1
346	62	76	347.7	705	29	36	250.8	1064	48	31	153.8
347	70	71	347.4	706	40	33	250.5	1065	48	26	153.6
348	62	76	347.2	707	53	34	250.2	1066	43	27	153.3
349	62	73	346.9	708	42	29	250.0	1067	34	27	153.0
350	68	71	346.6	709	42	36	249.7	1068	38	31	152.7
351	64	73	346.3	710	25	36	249.4	1069	35	44	152.5
352	60	91	346.1	711	53	37	249.1	1070	23	24	152.2

353	70	61	345.8	712	42	34	248.9	1071	33	27	151.9
354	64	82	345.5	713	30	35	248.6	1072	30	24	151.7
355	62	74	345.3	714	47	32	248.3	1073	20	26	151.4
356	62	79	345.0	715	45	26	248.1	1074	23	29	151.1
357	65	69	344.7	716	40	36	247.8	1075	23	27	150.9
358	60	70	344.5	717	35	37	247.5	1076	26	26	150.6
359	74	70	344.2	718	43	33	247.3	1077	28	25	150.3

Appendix C: Figures

[If your thesis includes supplemental information not included in the previous sections, append it here. Create more appendices if necessary. If you are not including an appendix/appendices, delete this page.]

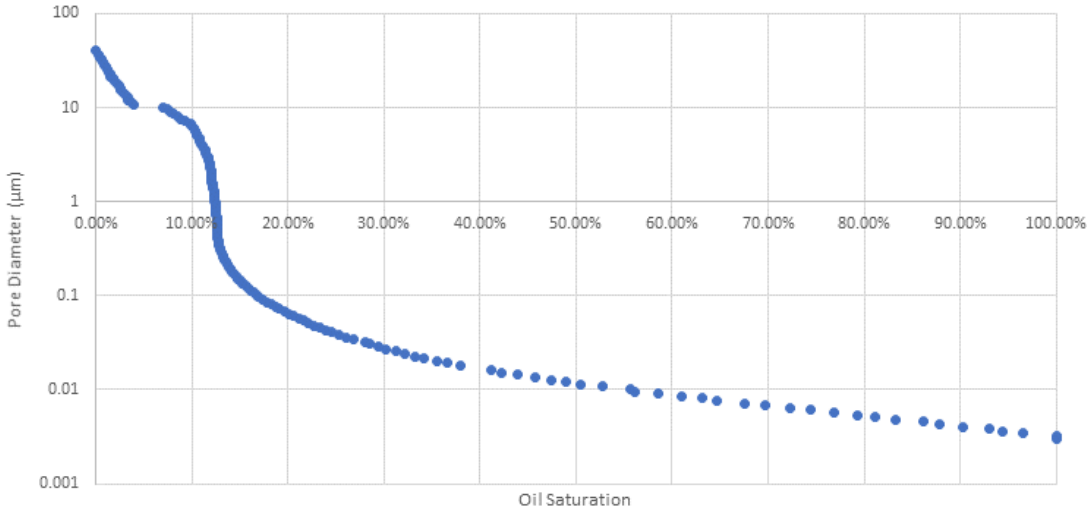

Figure C 1: Pore Size Distribution from IC^3 MICP Data

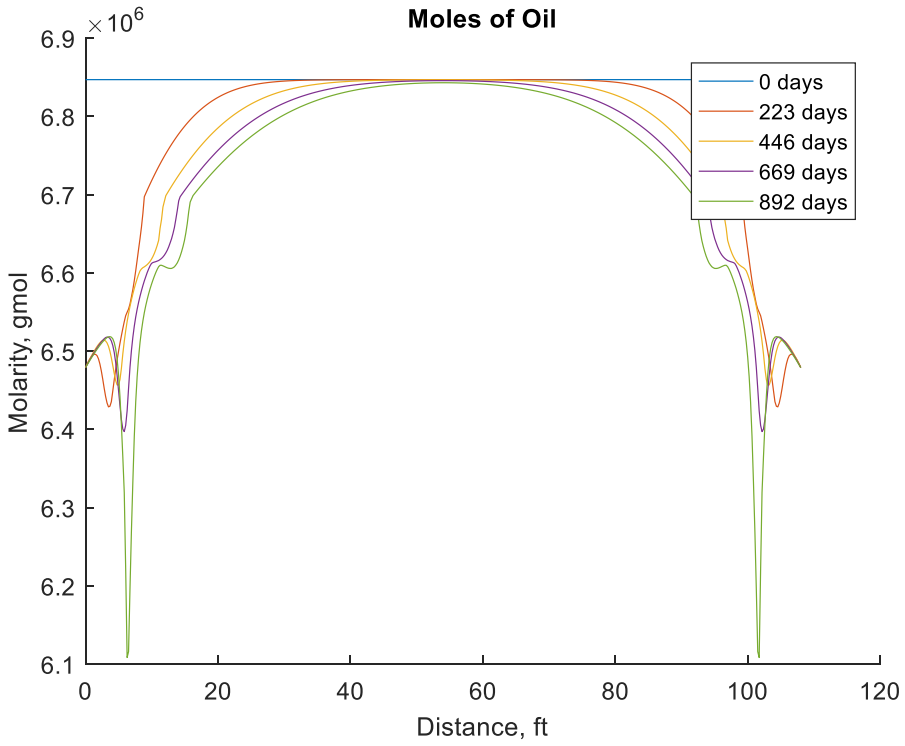

Figure C 2: Oil molarity beginning to destabilize

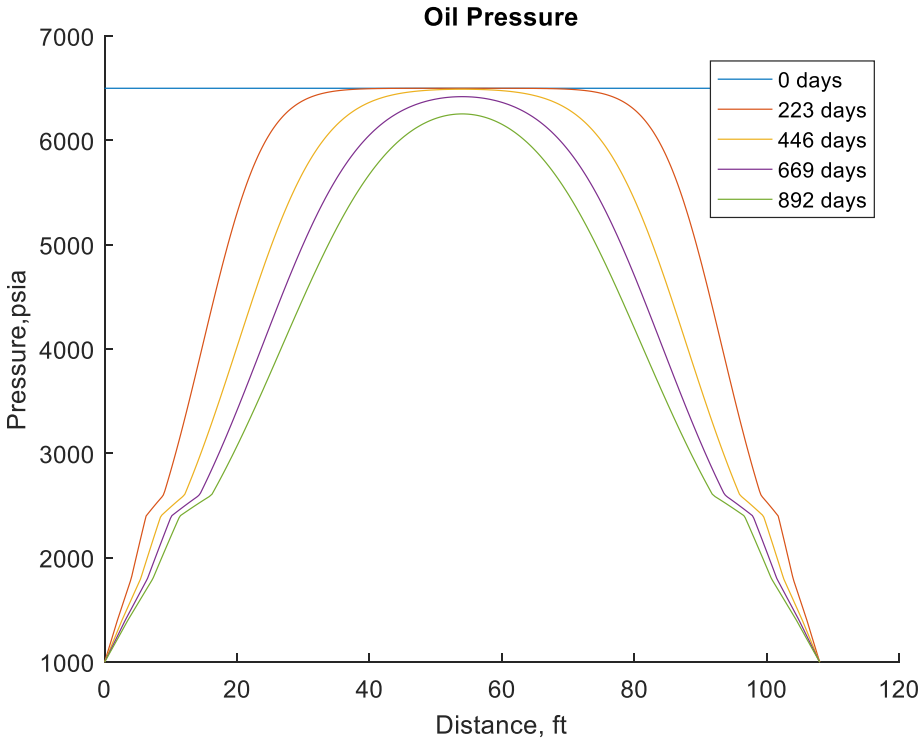

Figure C 3: Oil Pressure behaving as expected

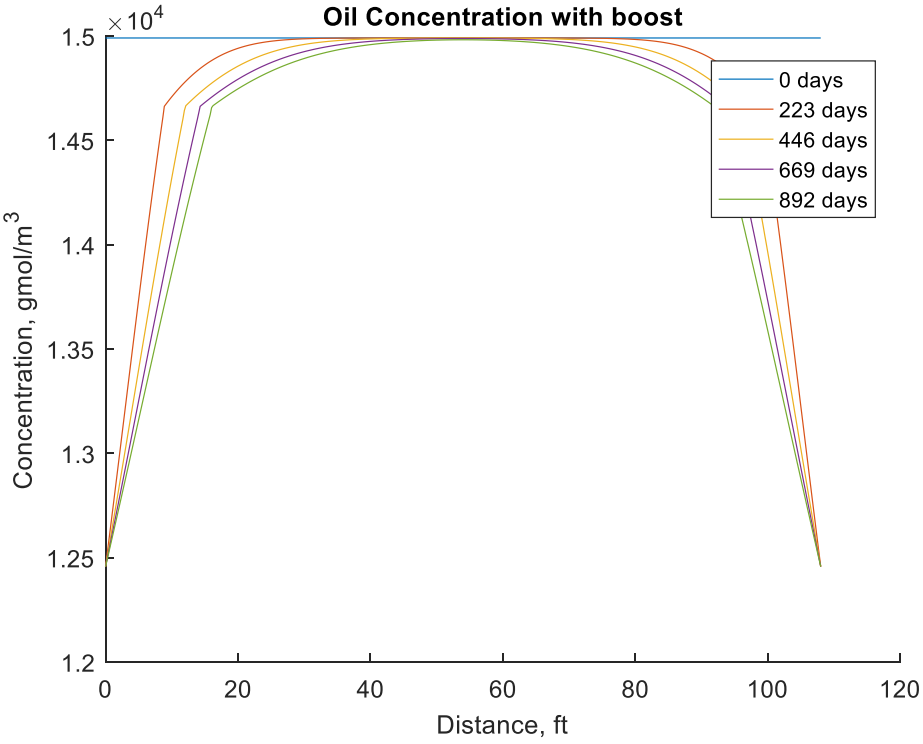

Figure C 4: Oil Concentration behaving as expected

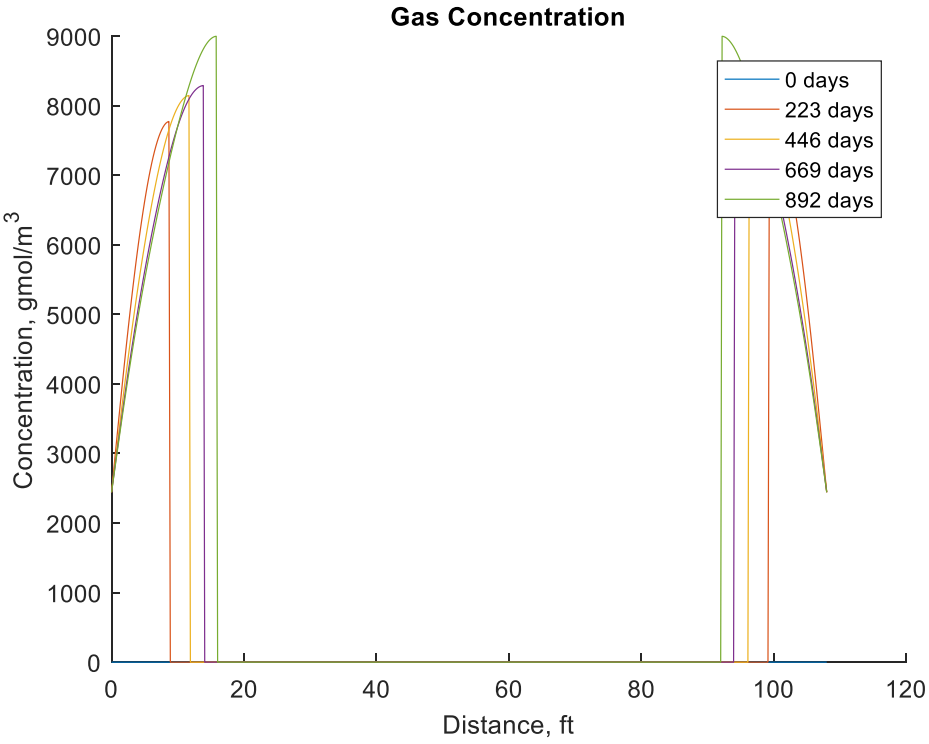

Figure C 5: Reasonable Gas Concentration behavior

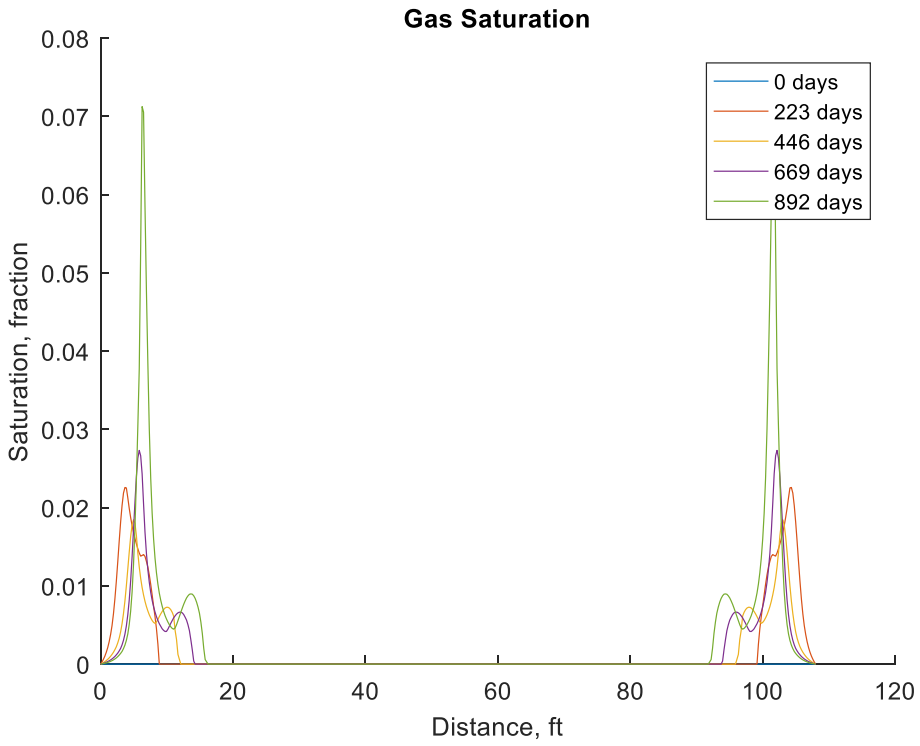

Figure C 6: Increasingly unstable saturation behavior

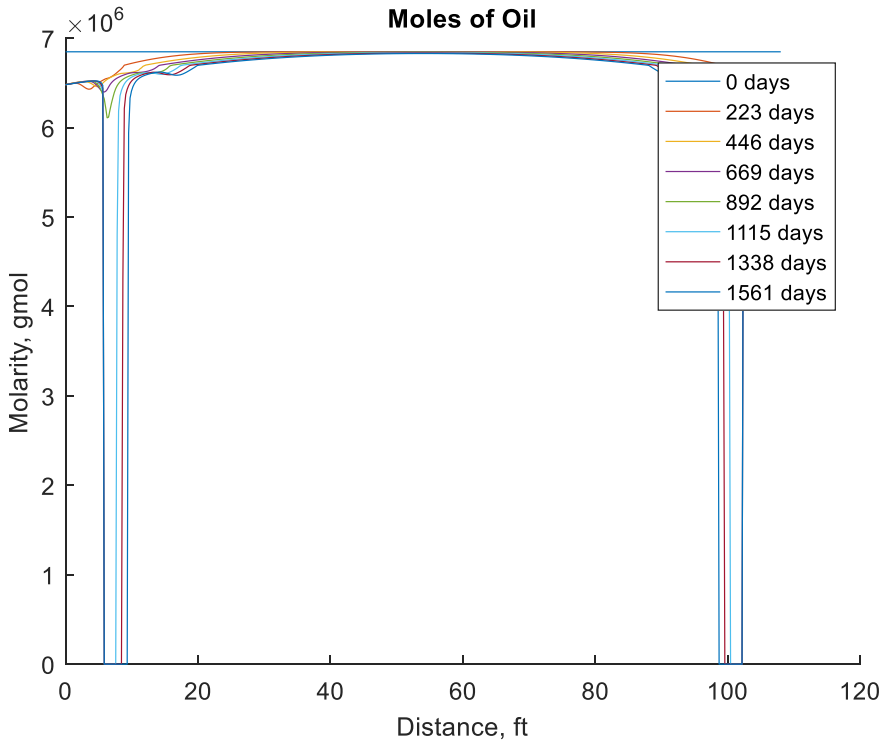

Figure C 7: Saturation behavior has destabilized molar values entirely

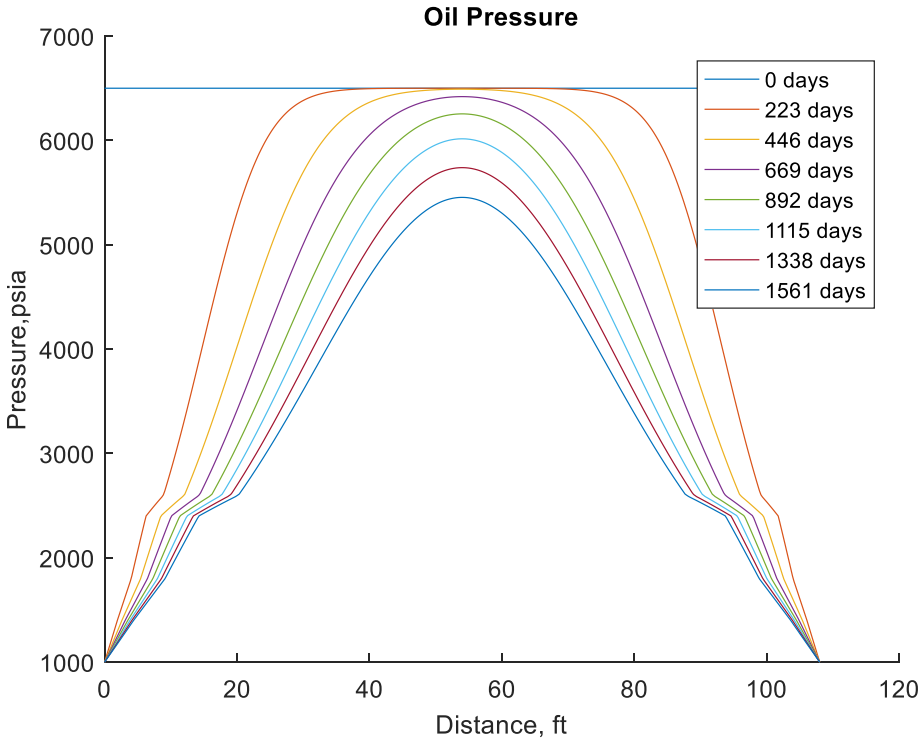

Figure C 8: Oil Pressure still behaving perfectly

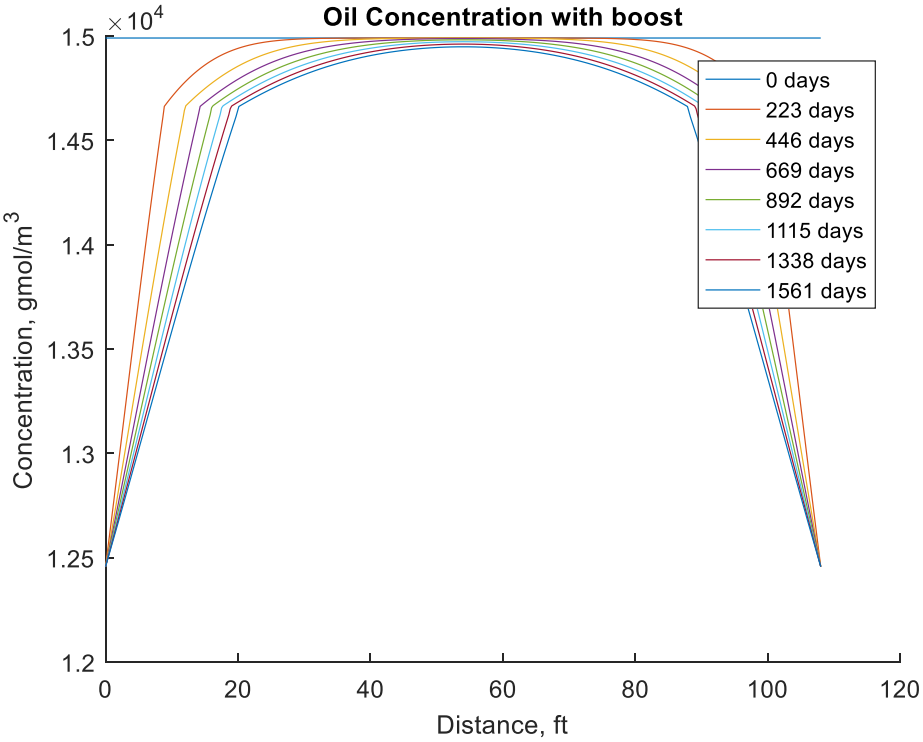

Figure C 9: Oil Concentration still behaving as expected

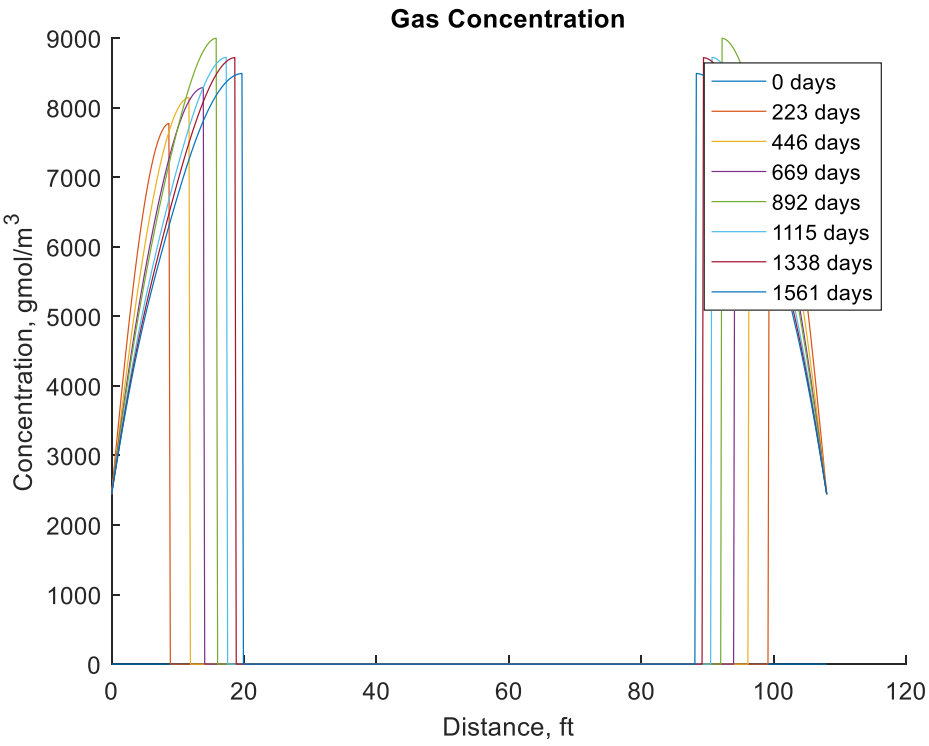

Figure C 10: Gas Concentration behaving as expected

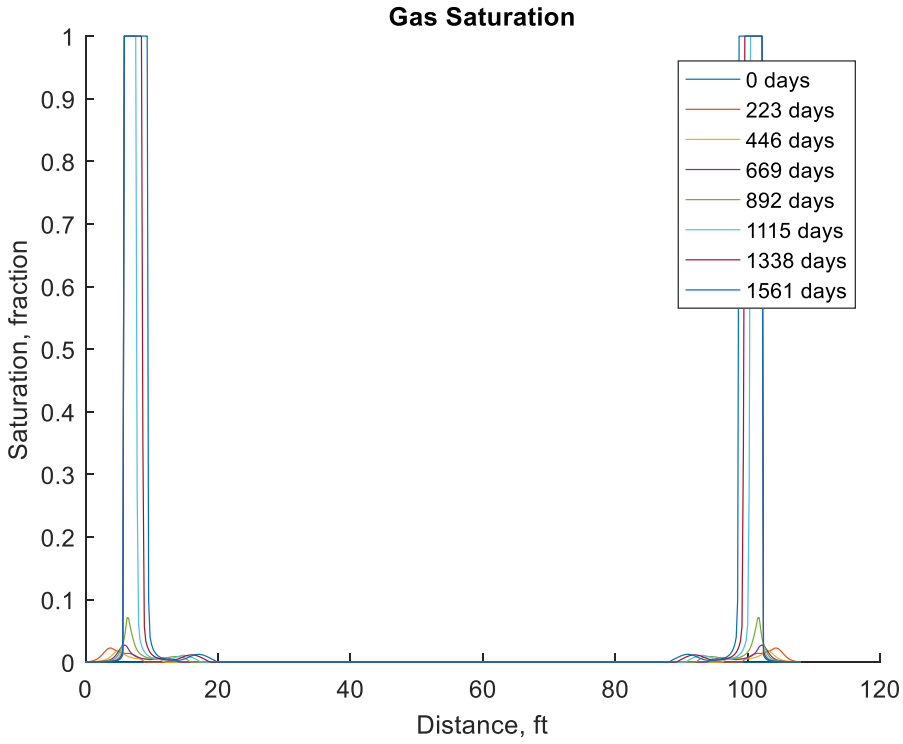

Figure C 11: Gas Saturation has destabilized entirely, beyond any reasonable result

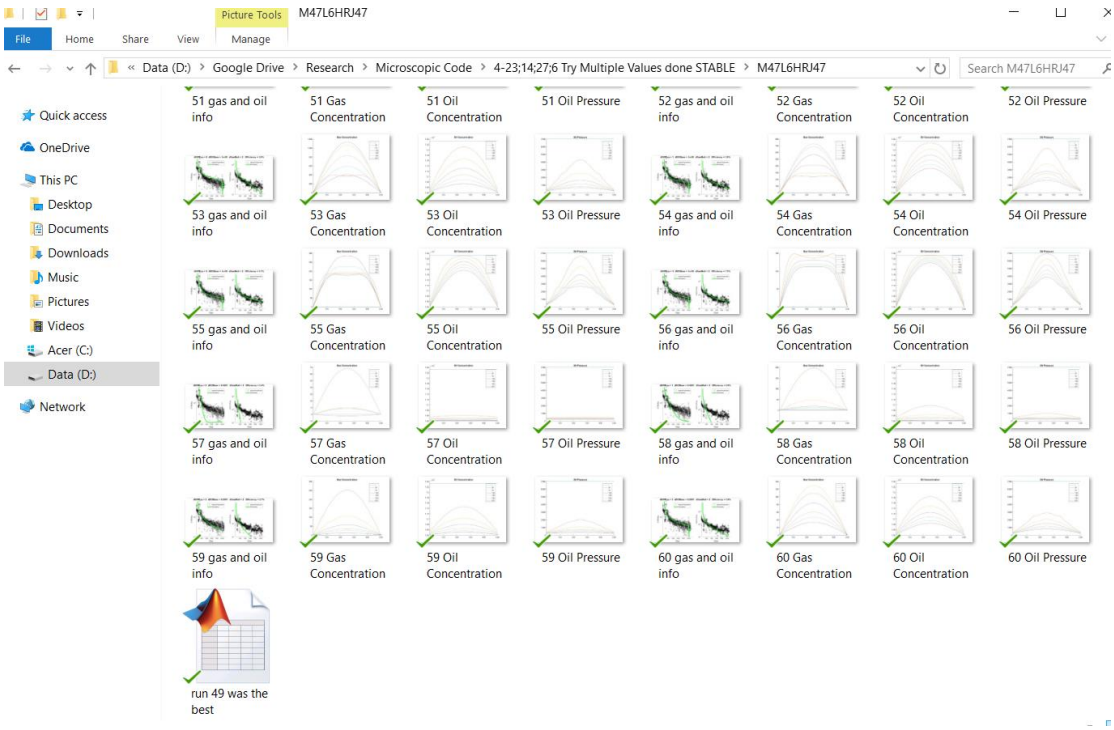

Figure C 12: Bulk Saving Output

Appendix D: Codes

Function 1: FVF Controller

```
function dFVF=FVF_Finder(dAPI,dGasSG,dTempK,adRSP,adRS,adP)
%adRSP and adRS values must be at p_bp
%adRSP and adP must be in psi, adRS must be scf/stb
%results in res volume/standard volume

dTempF=dTempK*9/5-459.67;

dFVF=zeros(1,length(adP));
dP_BP=adRSP(end-1); %I add an additional value for interpolation
reasons. The second to last pressure is the bubblepoint pressure
dFVF(adP<=dP_BP)=VB_Bo_sat(interp1(adRSP,adRS,adP(adP<=dP_BP)),dGasSG,
dTempF,dAPI);
c_o=VB_c_o(adRS(end),dTempF,dGasSG,dAPI,0,0,adP(adP>dP_BP));
dFVF(adP>dP_BP)=VB_Bo_unsat(VB_Bo_sat(adRS(end),dGasSG,dTempK*9/5-
459.67,dAPI),c_o,dP_BP,adP(adP>dP_BP));

%figure
%plot(adP,dFVF)
end
```

Function 2: FVF of saturated oil

```
function B_o=VB_Bo_sat(R_s,SG_g,T,API)
%FVF for saturated oil Reservoir Bbl/STB
%T in Farenheit, Rs in scf/stb, p in psia
if API<=30
    A1=4.677E-4;
    A2=1.751E-5;
    A3=-1.811E-8;
    C1=.0362;
    C2=1.0937;
    C3=25.7240;
elseif API>30
    A1=4.670E-4;
    A2=1.100E-5;
    A3=1.337E-9;
    C1=.0178;
    C2=1.187;
    C3=23.9310;
end

B_o=1+A1*R_s+A2*(T-60).*(API/SG_g)+A3.*R_s.*(T-60).*(API/SG_g);

end
```

Function 3: FVF of unsaturated oil

```
function B_o=VB_Bo_unsat(B_ob,c_o,p_b,p)
%FVF for undersaturated oil
```

```
B_o=B_ob.*exp(c_o.*(p_b-p));

end
```

Function 4: Saturated Oil Compressibility

```
function c_o=VB_c_o(R_sb,T,SG_g,API,Bg_Bo,dRs_Dp,p)
%compressibility of saturated oil. For undersaturated case, simply set
B_g,
%B_o, dR_s, or dp to 0.
if API<=30
    A1=4.677E-4;
    A2=1.751E-5;
    A3=-1.811E-8;
    C1=.0362;
    C2=1.0937;
    C3=25.7240;
elseif API>30
    A1=4.670E-4;
    A2=1.100E-5;
    A3=1.337E-9;
    C1=.0178;
    C2=1.187;
    C3=23.9310;
end

c_o=(-1433+5*R_sb+17.2*T-
1180*SG_g+12.61*API)./(10^5*p)+(Bg_Bo).*(dRs_Dp)./5.6145835;

end
```

Function 5: Z Factor Calculation

```
function Z=Z_Hall_Yarborough(P,T,spec_g,N2_frac,CO2_frac,H2S_frac)

num_ps=length(P);
num_ts=length(T);

%Solution and equations
T_pc=326+315.7*(spec_g-.5)-240*N2_frac-83.3*CO2_frac+133.3*H2S_frac;
P_pc=678-50*(spec_g-.5)-206.7*N2_frac+440*CO2_frac+606.7*H2S_frac;
T_pr=(T+459.67)./T_pc;
t_r=1./T_pr;
p_pr=P./P_pc;
A=.06125.*t_r.*exp(-1.2.*(1-t_r).^2);
B=t_r.*(14.76-9.76.*t_r+4.58.*t_r.^2);
C=t_r.*(90.7-242.2.*t_r+42.4.*t_r.^2);
D=2.18+2.82.*t_r;
syms Y
Z=zeros(num_ps,num_ts);
for cur_p=1:num_ps
    for cur_t=1:num_ts
        y_solved=vpasolve(0==(Y+Y.^2+Y.^3-Y.^4)./(1-Y).^3-
A(cur_t).*p_pr(cur_p)-B(cur_t).*Y.^2+C(cur_t).*Y.^D(cur_t),Y,[0,5]);
```

```
        Z(cur_p,cur_t)=A(cur_t).*p_pr(cur_p)./y_solved;
    end
end
end
```

Function 6: Efficient Function Controller

```
function dOutputs = EfficientFunction(sFunc,varargin)

sMasterPath=pwd;
sSavedRunsPath=[sMasterPath '\SavedFuncRuns'];

if ~isdir(sSavedRunsPath) %if the folder does not exist make it, else
continue
    mkdir(sSavedRunsPath)
end

sFileName = [sFunc '_outputs']; % Pattern for well files
sFullFilePath=[sSavedRunsPath '\' sFileName '.mat'];

if exist(sFullFilePath,'file') %if the file exists, check it for our
exact run

    load(sFullFilePath,'FuncRuns')

    [iNumRow,~]=size(FuncRuns);
    iNumCol=nargin;
    for iCurRow=1:iNumRow
        for iCurCol=2:iNumCol
            if ~isequal(varargin{iCurCol-
1},FuncRuns{iCurRow,iCurCol}{:})
                break %found an inconsistency, move to next row
            elseif iCurCol==iNumCol-1 %No match has failed, including
the last one
                %display(['The exact run of the ' sFunc ' function was
found, originally saved on ' datestr(FuncRuns{iCurRow,1})])
                dOutputs=FuncRuns{iCurRow,iNumCol}{:};
                return
            end
        end
    end
    %check for exact run
    %if exact run is here, return it and note timestamp in message
else
    FuncRuns=cell(0); %if the file does not exist create a blank
variable to add to
    iNumRow=0;
end
%if the file does not exist, or if it exists but the exact solution is
not
%found and returned, run the function, and save a copy of this exact
solution

fCurFun=str2func(sFunc);
dOutputs=fCurFun(varargin{:});
```

```
FuncRuns{iNumRow+1,nargin}={dOutputs};
for iCurCol=2:nargin-1 %note that one argument is just the function
name
    FuncRuns{iNumRow+1,iCurCol}=varargin(iCurCol-1);
end
FuncRuns{iNumRow+1,1}=clock;

save(sFullFilePath,'FuncRuns')
%everything below is unrelated, just having code around, likely delete

end
```